Kinetic Studies on Preparation Processes of Functional Ultrafine Particles Using Reverse Micellar Systems

HIROSHI SATO

Department of Chemical Engineering
Faculty of Engineering Science
Osaka University
1996

Kinetic Studies on Preparation Processes of Functional Ultrafine Particles Using Reverse Micellar Systems

HIROSHI SATO

Department of Chemical Engineering
Faculty of Engineering Science
Osaka University
1996

Preface

This dissertation work was carried out under the joint supervision of Professor Isao Komasawa and Dr. Takayuki Hirai at the Department of Chemical Engineering, Faculty of Engineering Science, Osaka University from 1991 to 1996.

The studies on the preparation of ultrafine particles in reverse micelles were initiated in 1989 in the Komasawa's group, and a research paper entitled "Preparation of Metal Oxide Ultrafine Particles by Hydrolysis of Metal Alkoxide in Reverse Micelles" was published in *Kagaku Kogaku Ronbunshu* (vol. 18, p. 296–302, 1992). Particle diameters were found to be controlled in the range of 2–8 nm by the number of successive and repeated operations to inject alkoxide solution of which the concentration was less than that of the solution used for the initial nucleation. The method was established by a trial and error, referring to several research papers published up to 1989. Several fragmentary findings on the kinetic behavior of particle formation had been found in the literature. But, a systematic knowledge of the formation process was quite insufficient at that time, since most of the works had been carried out to study the physical characteristics of ultrafine particles.

One of the most important missions of research staff and scholars in the field of chemical engineering is to establish new unit operations for the preparation processes of new materials and for the separation and purification processes. For these, two research streams have been running in the Komasawa's group. One is oriented mainly to the study on novel functions of composite ultrafine particles and stabilization of the particles when isolated from the reverse micelles. This subject has been tackled by Mr. Susumu Shiojiri who has published a research paper entitled "Preparation of Metal

Sulfide Ultrafine Particles in Reverse Micellar Systems and Their Photocatalytic Property" in *J. Chem. Eng. Japan* (vol. 27, p. 589-596, 1994). The other is oriented mainly to the study on the kinetics of the reactions in particle formation process, relating with the behavior of reverse micelles such as intermicellar interaction. The latter subject has been carried out by the present author and now summarized as this doctoral dissertation. In this, the application as photocatalysts of the particles prepared by the present gas injection method was carried out, referring to Mr. Susumu Shiojiri's work obtained with particles prepared by the solution mixing method.

The author hopes that this dissertation work would mark a milestone to the final goal, that is, the establishment of "Unit Operation for the Preparation of Ultrafine Particles".

Hiroshi Sato

Hiroshi Sato
Department of Chemical Engineering
Faculty of Engineering Science
Osaka University
Toyonaka, Osaka 560, Japan

CONTENTS

General Introduction 1

Chapter I Mechanism of Formation of Titanium Dioxide Ultrafine Particles Using Organic Solution Injection Method 10

Introduction 10

Experimental Section 11

1. Preparation of particles 11
2. Measurements 12

Results and Discussion 13

1. Spectral change during hydrolysis of TTB and particle formation 13
2. Kinetics of particle formation 16
3. Factors controlling particle formation 19
4. Model for particle formation 22
5. Application of the model for particle formation 25

Summary 31

Chapter II Mechanism of Formation of Metal Sulfide Ultrafine Particles Using Solution Mixing Method 33

Introduction 33

Experimental Section 34

1. Preparation of particles 34
2. Measurements 35

Results and Discussion 35

1. Spectral change during particle formation 35
2. Estimation of particle diameter 40
3. Effect of excess amount of reactant ions on particle formation 44
4. Analysis of kinetics for rapid coagulation process 47
5. Analysis of kinetics for reduced rate coagulation process 53

Summary 57

Chapter III Mechanism of Formation of Silver Halide Ultrafine Particles Using Solution Mixing Method 59

Introduction 59

Experimental Section 60

Results and Discussion 61

1. Spectral change during particle formation 61

2. Estimation of particle diameter 66
3. Analysis of kinetics for rapid coagulation process 68
4. Analysis of kinetics for reduced rate coagulation process 71
Summary **74**
Chapter IV Mechanism of Formation of Ultrafine Particles Using Gas Injection Method **75**
Introduction **75**
Experimental section **76**
1. Preparation of particles 76
2. Measurements 76
Results and Discussion **77**
1. Spectral change during particle formation 77
2. Analysis of kinetics for particle formation 82
3. Model for particle formation 85
4. Application of the model for simulation of particle formation 89
Summary **93**
Chapter V Preparation of Composite Ultrafine Particles and Application as Photocatalysts **95**
Introduction **95**
Experimental Section **97**
1. Preparation of particles 97
2. Photocatalytic reduction of water 98
Results and Discussion **99**
1. Absorption spectra of coprecipitated particles 99
2. Composition of coprecipitated particles 102
3. Analysis of coagulation kinetics of coprecipitated particles 105
4. Preparation of core-shell structure particles using gas injection method 110
5. Photocatalytic activity of ultrafine particles 112
Summary **116**
General Conclusions **118**
Suggestions for Future Work **122**
Nomenclature **125**
References **128**
List of Publications **135**
Acknowledgment **136**

General Introduction

Ultrafine particles have become increasingly important in recent years. This interest is directed to the size-dependent energy structure of ultrafine particles since the characteristics of ultrafine particles such as electric and optical properties and catalytic activities are primarily controlled by the size-dependent energy structure, and to the preparation and stabilization of uniform ultrafine particles. In the case of ultrafine semiconductor particles, the optical absorption thresholds are at higher energy levels than those of the bulk materials. One rationalization for this blue-shift with decreasing diameter is that since the excitations of a particle are spatially confined to its dimensions, an exciton on a particle which is smaller than a bulk exciton must be compressed, thus raising the transition energy and shifting the absorption threshold to a higher energy level. This size effect on energy structure of semiconductor is thus called quantum-size effect. The theoretical and quantitative treatments of the quantum-size effect have been proposed (Brus, 1984; Weller *et al.*, 1986; Wang *et al.*, 1987). Since the ultrafine particles are prone to aggregate into larger particles, it is necessary to prevent uncontrolled aggregation in the course of preparation.

Reverse micelles consist of self-organized extremely small water droplets stabilized in organic solvents by surfactant molecules. The microstructure of these systems leads to a number of interesting properties. For example, the size and number of reverse micelles are controlled by water to surfactant molar ratio of the solution (Zulauf and Eicke, 1979; Kuboi *et al.*, 1990). This may have considerable effects on the size of prepared particles and on the prevention of uncontrolled aggregation in the course of preparation. Although the micellar droplets are thermodynamically stable, they do exhibit a dynamic exchange of their contents by fusion of droplets and redispersion of dimer

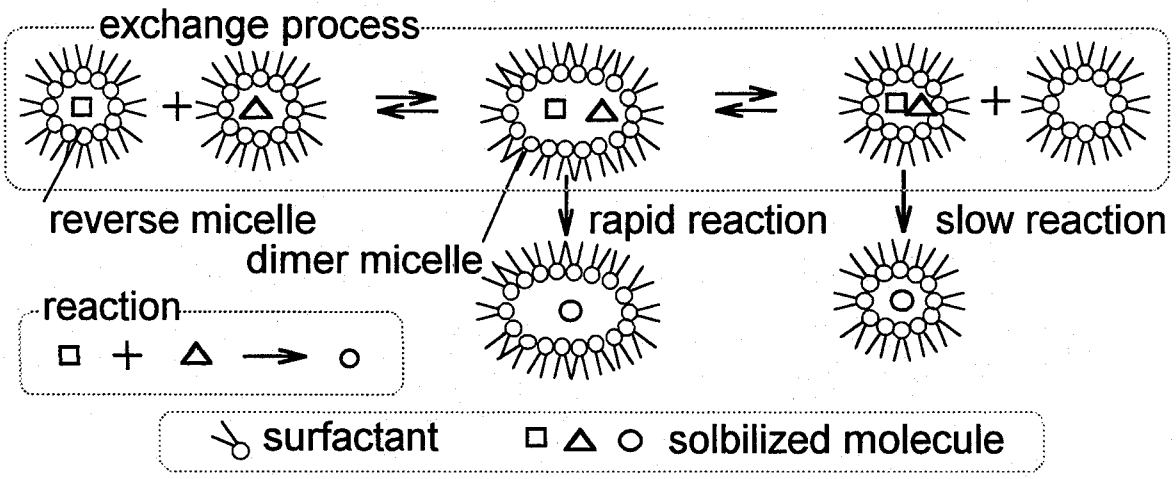

Figure 1 Intermicellar exchange process of contents in reverse micelles.

droplets as shown in **Figure 1.** The intermicellar exchange process facilitates reaction between reactants dissolved in different droplets and thus the kinetics of this reaction will be dominated by that of the exchange process. If the intrinsic rate of the reaction is faster than the rate of the exchange process, then when both reactants meet in a dimer micellar droplet, the reaction is complete before the redispersion of the dimer droplet. The reaction rate becomes identical to the exchange rate and thus the exchange kinetics can be investigated using such kind of reaction. The exchange rate constant has been reported to be 10^6–10^8 $M^{-1}s^{-1}$ for AOT (sodium bis(2-ethylhexyl) sulfosuccinate)/isooctane reverse micellar system (Fletcher *et al.*, 1987, Lang *et al.*, 1988). The exchange process occurs on a sub-millisecond time scale in this system. On the other hand, in the case of reaction slower than the exchange process, the reactants distribute among the micelles according to the same distribution as that in the case without any reaction. The reaction proceeds in micellar droplets containing both reactants. The reaction rate will be independent of the exchange rate and controlled by the concentration of the micellar droplets containing both reactants.

Ultrafine particles can be prepared in water cores in the reverse micelles

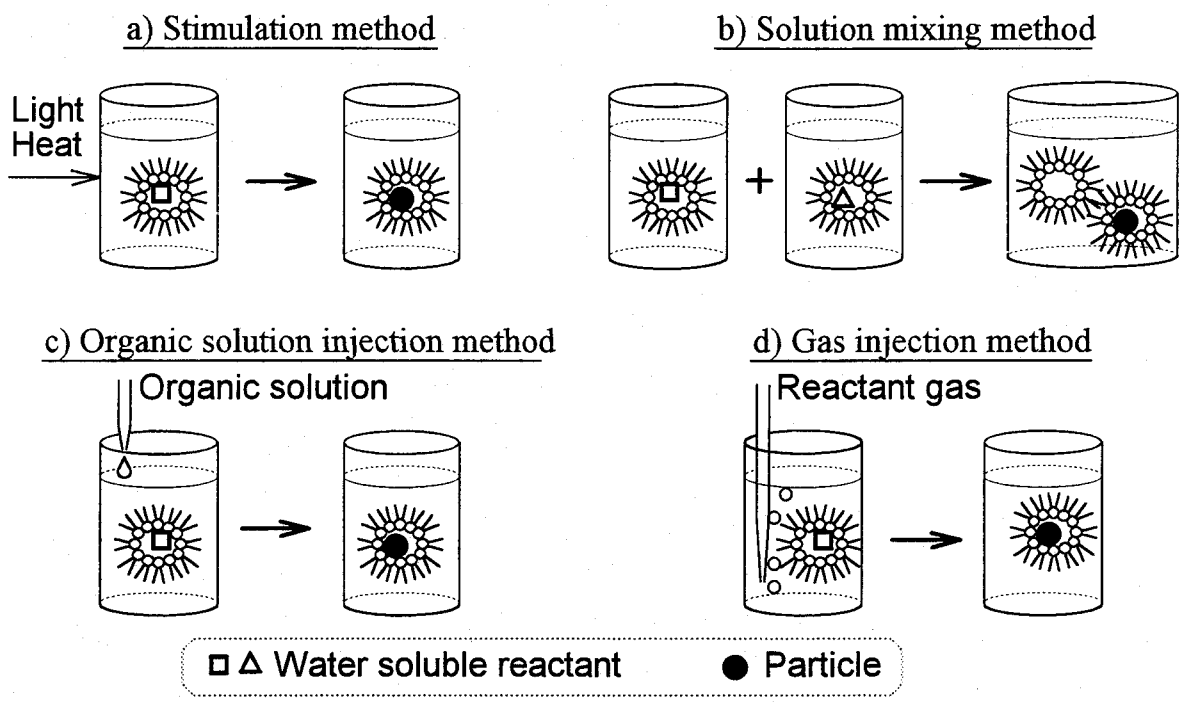

Figure 2 Schematic diagram of the feeding methods of reactants into reverse micelles.

using various methods. Numerous papers describing preparation methods of ultrafine particles in the reverse micelles have been published. A schematic diagram of these methods is shown in **Figure 2.** Although the case is much limited, a reaction in reverse micelles can be initiated by simple physical stimulation from the outside (stimulation method) as shown in Figure 2(a). Ultrafine Au particles were prepared by the reduction of $HAuCl_4$ in water cores initiated by laser pulse (Kurihara *et al.*, 1983). The particles can also be prepared using the intermicellar exchange process by mixing two reverse micellar solutions containing reactants separately (solution mixing method) as shown in Figure 2(b). Most studies have adopted this method. For example, CdS (Lianos and Thomas, 1987), Ni_2B and Co_2B (Ravet *et al.*, 1987), Ag (Barnickel *et al.*, 1992), and AgBr (Johansson *et al.*, 1992) particles were prepared by this method. The particles may also be prepared by the injection of an organic reactant solution into a reverse micellar solution containing the other reactants (organic solution injection method) as shown in Figure 2(c).

Preparation of CdSe (Steigerwald *et al.*, 1988) and SiO_2 (Arriagada and Osseo-Asare, 1992) particles has been reported. A reactant gas soluble in organic solvent can be used instead of an organic reactant solution. The reactant gas is injected into a reverse micellar solution containing the other reactants (gas injection method) as shown in Figure 2(d). This method was applied to the preparation of $CaCO_3$ (Kandori *et al.*, 1988), Cu (Lisiecki and Pileni, 1993), and Rh (Kishida *et al.*, 1995) particles.

Preparation of composite ultrafine particles is stimulating and fascinating since the composite ultrafine particles have interesting energy structure which may lead to remarkable optical characteristics. For example, Mn-doped ultrafine ZnS particles were reported to have an extraordinary strong photoemission (Bhargava *et al.*, 1994). Several attempts have been made to prepare the composite particles in reverse micelles. CdSe-coated ZnS (Kortan *et al.*, 1990), CdSe-coated ZnSe (Hoener *et al.*, 1992), and ZnS-coated CdS (Hirai *et al.*, 1994) particles were prepared by the subsequent growth of shell material on the core particles. Coprecipitated particles of Ni_2B and Co_2B (Ravet *et al.*, 1987) and CdS and ZnS (Hirai *et al.*, 1994; Cizeron and Pileni, 1995) were also prepared by the simultaneous precipitation of both materials. These works were carried out, in the majority of cases, to investigate the possibility of the preparation method or the characteristics of the prepared particles.

The mechanism of particle formation process must be investigated to prepare single component and composite ultrafine particles having desired size and controlled structure. The size and number of particles prepared in reverse micelles have been reported to be controlled by the concentration of reactants and water content of the solution (Ravet *et al.*, 1987; Lisiecki and Pileni, 1993). In addition to these generally recognized and apparent findings, several attempts have been made to present a model expressing the particle formation

process. For metal boride particles, a quantitative model based on the statistical distribution of metal ions to the reverse micelles has been presented to explain the number of formed metal boride particles (Ravet *et al.*, 1987). For SiO_2 particles, a qualitative model has been proposed to explain the variation of particle size with water content (Osseo-Asare and Arriagada, 1990). However, these works were much limited, since these were carried out based on the analysis of only the final size of formed particles without information obtainable during the course of particle formation.

A schematic diagram of the particle formation process in reverse micelles is illustrated in **Figure 3.** The overall particle formation process includes dissolution of reactants into the organic (continuous) phase in the solution, transfer of reactants into the water cores, chemical reaction in the water cores, nucleation from solute molecules, particle growth (addition of solute molecules to the particles), coagulation of particles, and Ostwald ripening (growth of larger particles accompanied by the dissolution of smaller particles) steps. A kinetic approach is of great importance in understanding the mechanism of formation of the ultrafine particles and in obtaining a quantitative model for the total process. This can lead to further development in the preparation of particles having special compositions and functions based on a control of the rates of the successive steps in the particle formation process. There have been only a few reports on the kinetic analysis of the particle formation process in the reverse micelles. For CdS particles produced by the solution mixing method, rapid coagulation in the reverse micelles has been found to explain a time-course change in absorbance at the initial stage of the particle formation (Towey *et al.*, 1990). However, the spectral change of CdS particles was not complete in this short period and thus their study may be applicable only to the very initial stage of particle formation process. Chew *et al.* (1990) reported a kinetic analysis of the formation process of AgBr particles in reverse micelles.

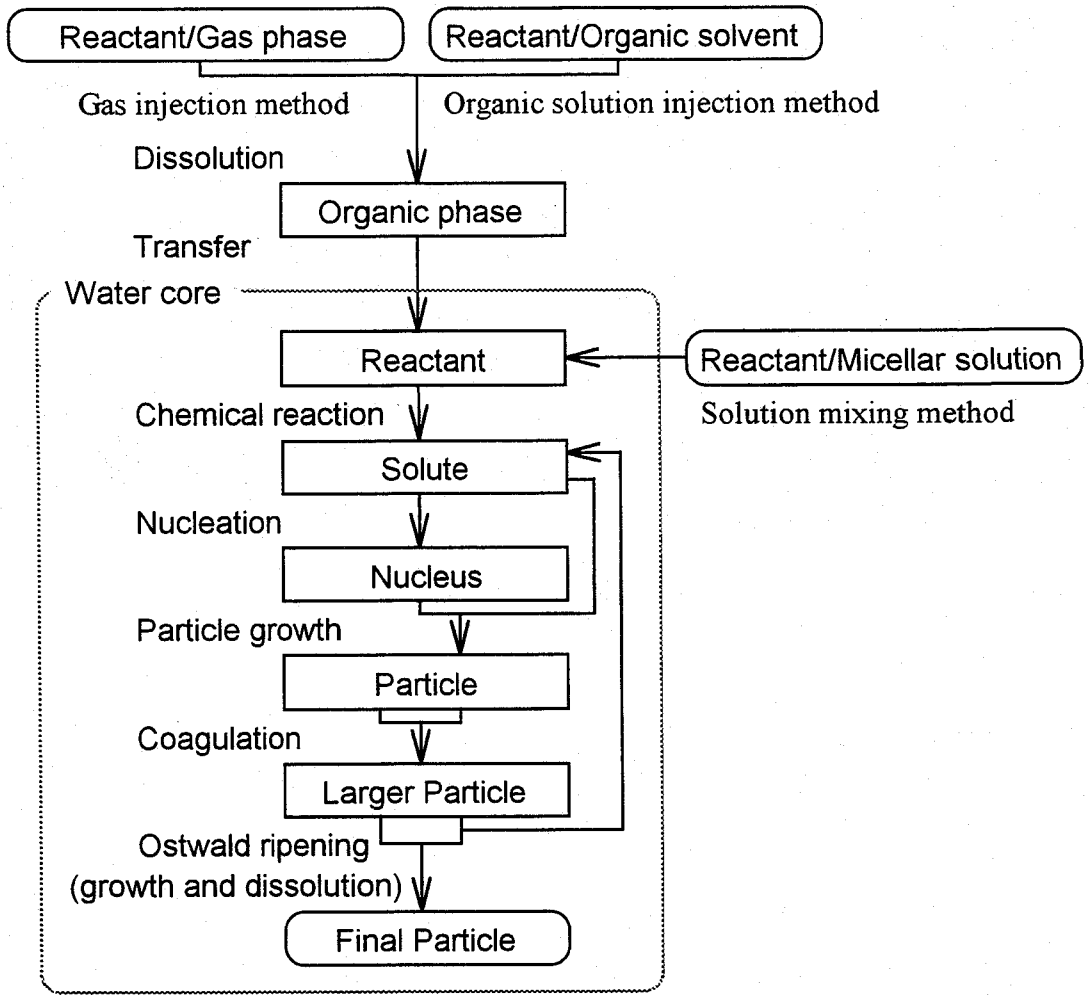

Figure 3 Schematic diagram of the particle formation process in reverse micelles.

Unfortunately, they measured the intensity of light scattering from particles that had already been out of ultrafine range.

A systematic study to obtain a quantitative and complete model for the whole stages during formation of ultrafine particles is now needed. This can lead to further development for the preparation of particles having special composition and functions, that is, to establishment of a "Unit Operation for the Preparation of Ultrafine Particles". In this work, the mechanism of formation of ultrafine particles in reverse micelles for several kinds of reactions having different reaction rates and various feeding methods of reactants has been systematically studied from a kinetic approach to establish a reasonably

complete model for the whole process. The analyses are focused on the variations in the size and number of formed particles during the process, followed by the continuous spectroscopic measurements. The effects of the feeding methods on the rate-determining step and on the size of resulting particles were also studied. AOT is employed as the surfactant throughout this work because AOT is widely known to form a well-defined spherical reverse micelle of which size is controlled only by the water content of the solution.

In Chapter I, the mechanism of formation of ultrafine particles formed by a slow reaction was studied. Preparation of TiO_2 ultrafine particles by slow hydrolysis of titanium tetrabutoxide (TTB) was employed. The rate of the hydrolysis is much slower than that of the micellar exchange process and the rate of particle formation is therefore expected to depend on the statistical distribution of reactants among the micelles. TTB was introduced using the organic solution injection method and then reacted with water in the core of the micelles. The kinetics of chemical reaction step or nucleation is possibly important in this case. A quantitative model for the particle formation processes was proposed from the kinetic analysis of the change in the absorption spectra.

In Chapter II, the mechanism of formation of ultrafine particles formed by a fast reaction was studied. Preparation of metal sulfide particles such as CdS, ZnS, and PbS was employed. The rate of reaction in the reverse micellar system will compete with that of the intermicellar exchange process. The reaction was initiated by the rapid mixing of two reverse micellar solutions containing metal nitrate or Na_2S and the particle formation process was thus followed by measuring the absorption spectra using a stopped-flow technique for the initial stage of the particle formation process. The spectral changes including the later stage as well as the initial stage were analyzed and an extended model for the whole process was presented. A special attention was

paid to the solubility of the materials in the form of ultrafine particles, since this solubility may be much different from that of bulk material.

In Chapter III, the study on the formation process of the ultrafine particles formed by a fast reaction was extended to the cases of particles other than the metal sulfide particles, in order to check the generality of the model. Silver halide particles such as AgBr, AgCl, and AgI were prepared using the solution mixing method and the formation process was also followed by the measurement of the absorption spectra. A special attention was paid to the purity of the reverse micellar systems, since the formed silver halide ultrafine particles are very sensitive to the presence of foreign materials.

In Chapter IV, the preceding kinetic studies for the solution mixing method were extended to the gas injection method. The gas injection method is important practically since the quantity and the injection rate of the reactants can be controlled over the wide range and further since the volume of the solution does not increase by the addition of the reactants. Preparation of metal sulfide particles such as CdS and ZnS by the injection of H_2S gas into the micelles containing metallic ions was studied. The whole process from the dissolution of H_2S into the organic phase (gas absorption), the transfer of H_2S from the organic phase to the water cores in the reverse micelles, and the formation of particles in the water cores was followed continuously using the absorption spectra. The time required for the gas injection is certainly much greater than that for the conversion of the ions to the particles in the micelles. A kinetic scheme for the steps in particle formation is proposed based on the statistical distribution of species and particles among the micelles.

In Chapter V, the results described in Chapters II and IV for the preparation of ultrafine particles composed of single components, CdS and ZnS, were extended to that of the composite ultrafine particles. The preparation of the composite particles of CdS and ZnS having mixed crystal or core-shell

structure was carried out by using both the solution mixing and gas injection methods. A kinetic model applicable to single component particles was also investigated on its applicability to the present case of composite particles. The composition of coprecipitated particles was also investigated, and then the effect of the difference in the solubility of both materials in the form of ultrafine particles on the composition was discussed.

The photocatalytic activity for the reduction of water to generate H_2 was studied for the single component and composite ultrafine particles of CdS and ZnS prepared in the reverse micelles. The study was done with emphasis on the structure and composition of the particles prepared using the gas injection method and the results were compared with those obtained for particles prepared using solution mixing method (Hirai *et al.*, 1994). The single component ultrafine PbS particles described in Chapter II were also studied for their photocatalytic activity due to the quantum-size effect.

The results obtained in this work are summarized in General Conclusions. Suggestions for Future Work are also described as an extension of the present work.

Chapter I
Mechanism of Formation of Titanium Dioxide Ultrafine Particles Using Organic Solution Injection Method

Introduction

Hydrolysis of metal alkoxide is a convenient and useful route to prepare highly pure metal oxide particles. The condition under which monodispersed particles are formed is, however, much confined in homogeneous solution and thus the control of particle size is much difficult (Ikemoto *et al.*, 1985; Mizutani, 1989). A few attempts to prepare metal oxide ultrafine particles in reverse micelles by the hydrolysis have been reported. SiO_2 particles were prepared using the injection of organic solution of silicon alkoxides into reverse micellar solution (organic solution injection method) by Yamauchi *et al.* (1989) and Osseo-Asare and Arriagada (1990). However, the prepared particles were much larger in size than the reverse micelles. Hirai *et al.* (1992) prepared TiO_2 and ZrO_2 ultrafine particles in the size range 2–8 nm by this method. The particles formed very slowly and the size of the particles was dependent on the concentration of alkoxide and water content of the reverse micellar solution.

Analysis of particle formation process is important to control the size of the particles. Osseo-Asare and Arriagada (1990) analyzed the variation of the size of SiO_2 particles with water content prepared in reverse micellar solution and proposed a qualitative model based on the numbers of the micellar droplets and the reactant molecules in the solution. However, there have been no reports on the quantitative kinetic analysis of the mechanism of particle formation process for this method.

In this chapter, the mechanism of formation of TiO_2 ultrafine particles by the hydrolysis of titanium tetrabutoxide (TTB) in AOT reverse micelles was

studied as a case study of the organic solution injection method. The whole process from the hydrolysis of TTB to form hydrolyzed TTB molecules to the formation of TiO_2 particles was continuously followed by the continuous measurement of UV-visible absorption spectra of the micellar solution. A kinetic scheme was then proposed, for the stagewise reactions including nucleation and particle growth in the micelles, based on the kinetic analysis of the spectra obtained with the micellar solution or a homogeneous organic solution.

Experimental Section

1. Preparation of particles

Sodium bis(2-ethylhexyl) sulfosuccinate (AOT) and titanium tetrabutoxide (TTB) supplied by Wako Pure Chemical Industries were used without further purification. Isooctane (2,2,4-trimethylpentane) supplied by Ishizu Seiyaku and 1-butanol supplied by Wako were dehydrated using molecular sieves 3A (Wako) and filtered using a 0.2-μm membrane filter, prior to use. Deionized water was distilled and filtered using a 0.45-μm membrane filter.

Reverse micellar solution was prepared by dissolving AOT in isooctane and filtered using a 0.2-μm membrane filter. The concentration of surfactant, [AOT] was 0.05 or 0.1 M. Water content of the reverse micellar solution (water to surfactant molar ratio, $W_o = [H_2O]/[AOT]$) was determined with a Karl-Fisher Titrator (Kyoto Electronics MKS-1) and was varied in the range 9-30 by injection of the filtered water. TTB/isooctane solution was prepared daily by injecting a 1 M TTB/1-butanol stock solution into the dehydrated isooctane. The TTB/1-butanol stock solution was stored with molecular sieves 3A.

The hydrolysis of TTB was carried out in a beaker-type reactor (10 m*l*) at 25 ℃. The reaction was initiated by injecting the TTB/isooctane solution

(0.1 m*l*) into the reverse micellar solution (5 m*l*) with mild stirring (300 min^{-1}) generated by a magnetic stirrer. The instant when the TTB solution was injected was defined as $t = 0$ s. The mixture was then shaken by hand and stored at 25 ℃ with continuous stirring. The formation of particles in a homogeneous organic solution was also carried out for comparison with the results in the micellar solutions. In this case, 1-butanol was employed as an organic solution instead of isooctane, since isooctane could dissolve only a very limited amount of water. A required amount of water was dissolved in the filtered 1-butanol to make the overall water concentration equal to that of the reverse micellar solution. The other operations were the same as those for the reverse micellar solutions. The concentrations of all materials are defined in terms of moles per liter of the micellar solution or the homogeneous solution.

2. Measurements

UV-visible absorption spectra of reverse micellar solution were recorded on a Shimadzu UV-265FW double-beam spectrophotometer. A reaction mixture of about 3 m*l* was poured into a quartz cell with a lid and the reaction was carried out in this cell for the measurement of the change in absorption spectra for periods up to 12 h. When the reaction time was greater than 1 day, the reaction was carried out in a capped reactor to reduce vaporization and leakage of isooctane. The solution was transferred to a quartz cell to measure the absorption spectra as required and then returned to the reactor.

The size distribution of the reverse micelles and the ultrafine particles was measured with a dynamic light scattering spectrophotometer (DLS, Otsuka Electronics DLS-700Ar). The samples were filtered using a 0.2-μm membrane filter, just before the measurement. The size of AOT reverse micelles has been reported to be independent of salt concentration (Aveyard *et al.*, 1986) and of the change in countercation of AOT (Dunn and Robinson,

1990). Therefore, the size of micelles seems to be independent of the concentration of reactant. The diameter of the particles was measured as follows. Ethanol (3 m*l*) was added to 5 m*l* of the reverse micellar solution of $W_o = 30$ containing the particles. The solution was separated into two phases and the particles suspended in the lower phase were measured with DLS.

Results and Discussion

1. Spectral change during hydrolysis of TTB and particle formation

The formation of metal oxide particles by hydrolysis of metal alkoxides involves a hydrolysis stage, a nucleation stage, and a particle growth stage. The first stage is the hydrolysis of the alkoxides and the formation of hydrolyzed molecules. In the case of TTB, the overall hydrolysis reaction is described as,

$$Ti(OC_4H_9)_4 + 4H_2O \rightarrow Ti(OH)_4 + 4C_4H_9OH \qquad (1-1)$$

TiO_2 is, then, formed by the condensation of the hydrolyzed molecules.

$$Ti(OH)_4 \rightarrow TiO_2 + 2H_2O \qquad (1-2)$$

In the nucleation stage, nuclei (the smallest particles in the solution) are formed from the hydrolyzed molecules (LaMer, 1952). Since a small particle has larger solubility than bulk material (Nielsen, 1964), a certain number of hydrolyzed molecules in the oversaturated solution are required in order to form a stable nucleus which grows to larger particle. In the growth stage, larger particles are formed by particle growth, coagulation, and Ostwald ripening. Particle growth, however, is the principal step and this occurs by addition of the hydrolyzed molecules to the particles. On the other hand, coagulation and Ostwald ripening are secondary steps and do not require

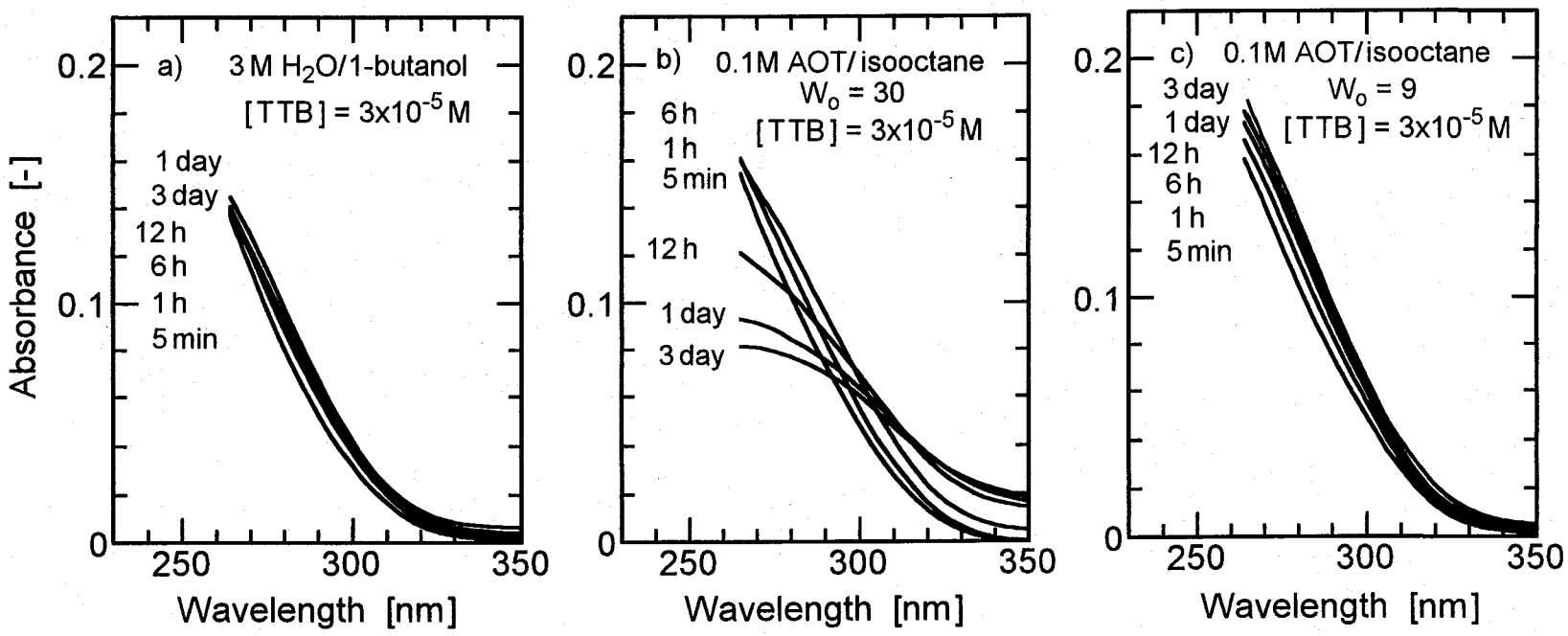

Figure 1–1 Change in absorption spectra during the hydrolysis of TTB at various systems. (a) 3 M H_2O/1–butanol (homogeneous) system; (b) $W_o = 30$ reverse micelles; (c) $W_o = 9$ reverse micelles.

hydrolyzed molecules. The former is the combination of the particles as a result of Brownian motion (Smoluchowski, 1916). The latter is via growth of larger particles accompanied by dissolution of smaller particles caused by the difference in solubility.

Figures 1-1(a), (b), and (c) show the UV-visible absorption spectra obtained during the hydrolysis of 3×10^{-5} M TTB for various systems. In the 3 M H_2O/1-butanol (homogeneous) system, the absorption increases slightly and monotonously in the period from $t = 5$ min to 12 h and no further spectral change is observed after $t = 12$ h, as shown in Figure 1-1(a). In the $W_o = 30$ reverse micellar system, where the overall water concentration is the same as that in the homogeneous system, different behavior patterns are observed, as shown in Figure 1-1(b). In this, the absorbance increases until 6 h and then decreases at wavelengths less than 300 nm. On the other hand, in the $W_o = 9$ reverse micellar system, the spectral changes are similar to those in the homogeneous system, as shown in Figure 1-1(c). However, when water is added to this micellar system at $t = 6$ h, 1 day, or 3 day, in order to increase W_o to 30, the absorbance decreases within 1 day, following the addition of water, as shown in **Figure 1-2.**

These results indicate that the particle formation process can be separated into two stages. The first stage proceeds in all systems within 12 h, but the second stage occurs only in the $W_o = 30$ reverse micellar system. Because of the large excess amount of water (more than 10^4-fold), the hydrolysis of TTB is likely to proceed in all cases. The subsequent nucleation requires a certain number of hydrolyzed molecules and proceeds only under specific conditions. The difference in the spectral changes can, therefore, be attributed to nucleation and particle formation. Only the hydrolysis of TTB occurred in the $W_o = 9$ reverse micellar system and in the homogeneous solution system. In

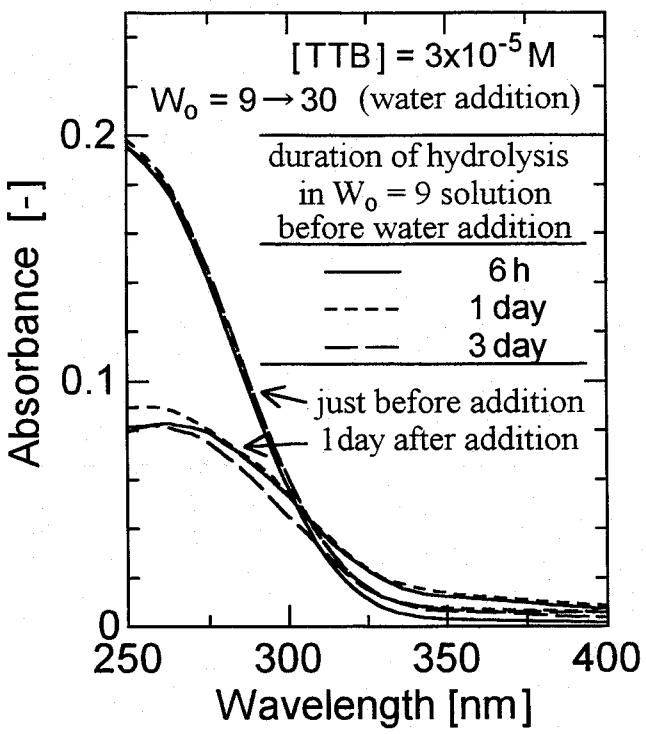

Figure 1–2 Change in absorption spectra by increase in water content of micellar solution during hydrolysis of TTB.

these systems, the stable spectra observed after $t = 12$ h can be ascribed to hydrolyzed molecules. On the other hand, both hydrolysis and particle formation have occurred in the $W_o = 30$ reverse micellar system, and the spectrum observed at $t = 3$ day is attributable to TiO_2 particles.

2. Kinetics of particle formation

The kinetics of the overall hydrolysis reaction of alkoxides in the particle formation process has been studied by the measurement of the induction period, namely, the time between the mixing of the reactants and the first observation of particles. The kinetics of the hydrolysis of titanium alkoxides in water/alcohol homogeneous solution was reported by Harris and Byers (1988). In their study, titanium tetraethoxide was diluted with 1-butanol to obtain titanium butoxide using alkoxy group exchange reaction between alkoxide and

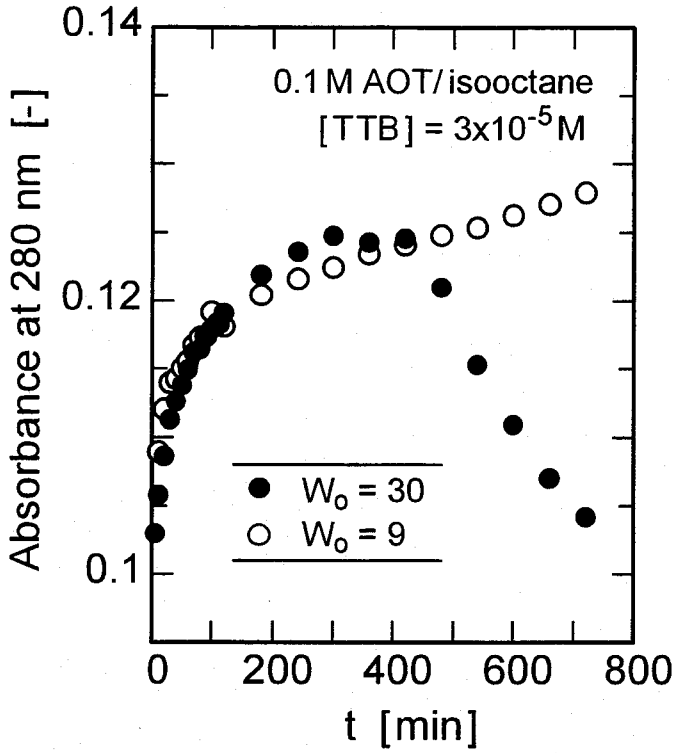

Figure 1–3 Time-course change in absorbance at 280 nm during hydrolysis of TTB.

alcohol. Then the alkoxide solution was injected into water/alcohol solution and particles were formed. The induction period obtained in 1-butanol was much longer than that in ethanol and was 120 min when the alkoxide and water concentrations were 0.016 and 0.38 M, respectively. This result indicates that the overall hydrolysis reaction of TTB is slower than that of titanium tetraethoxide. Furthermore, the induction period varied inversely with alkoxide concentration in 1-butanol, thus indicating that the kinetics of the overall hydrolysis of TTB was first-order with respect to TTB.

The particle formation was followed by taking the absorption spectra of the reaction solution. **Figure 1–3** shows the absorbance at 280 nm obtained during the hydrolysis of TTB in the reverse micellar solutions. In the $W_o = 30$ system, the absorbance increases to a maximum value and then decreases. In the $W_o = 9$ system where particle formation is not observed, the absorbance

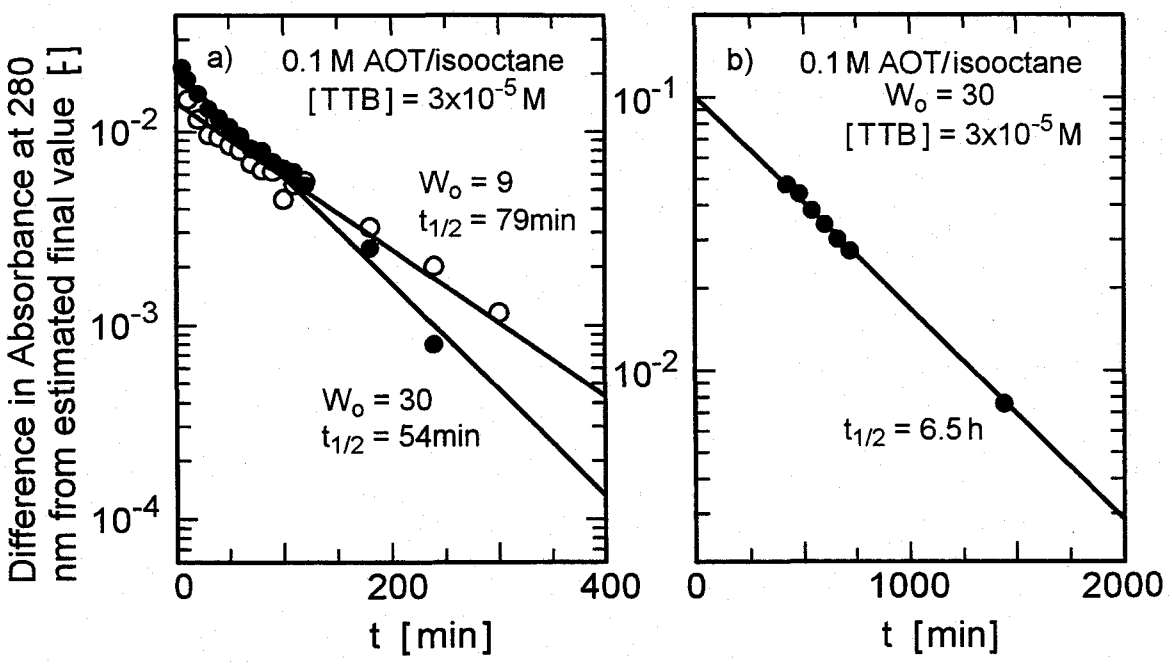

Figure 1–4 First-order kinetic analysis of change in absorbance at 280 nm. (a) Initial part; (b) later part.

increases together with that of the $W_o = 30$ solution at the initial part of the reaction and then increased slightly. The slight increase may be due to the vaporization of isooctane and the increase in concentration of AOT in the solution. This vaporization was confirmed by a reduction in the volume of solution. The increase and decrease in absorbance are related to the hydrolysis of TTB and particle formation, respectively. To study the rate of the hydrolysis reaction in the reverse micelles, the initial part of the kinetic transient up to $t = 120$ min in the absorbance was analyzed in terms of first-order kinetics. **Figure 1–4(a)** shows the results for the $W_o = 30$ and $W_o = 9$ systems. The half period ($t_{1/2}$) of the hydrolysis of 3 x 10^{-5} M TTB in the reverse micellar system is about 1 h. The later part of the absorbance change was also analyzed in terms of first-order kinetics. **Figure 1–4(b)** shows the result for the system of [TTB] = 3 x 10^{-5} M and $W_o = 30$, indicating that $t_{1/2}$ is about 6.5 h. This later part may correspond to the consumption of hydrolyzed molecules for particle formation. These values of half period will

be used to determine the rate constants.

3. Factors controlling particle formation

In homogeneous solution, both the alkoxide concentration and the water concentration are known to affect particle formation and the size distribution of the particles (Ogihara *et al.*, 1989). In the reverse micellar system, the overall water concentration is controlled by the water content ($[H_2O]/[AOT]$) and by the surfactant concentration ([AOT]). The effects of water content, TTB concentration, and surfactant concentration on particle formation were investigated. **Figures 1-5(a), (b), and (c)** show the absorption spectra measured after 3 day of hydrolysis at various TTB concentrations and various water contents. The result for 3×10^{-5} M TTB is shown in Figure 1-5(a). In the $W_o = 30$ system, TiO_2 particles are formed as mentioned above. When the water content is less than 30, however, the spectral features are similar to that of the hydrolyzed molecules, showing that no particles are formed in these systems. The increase in the water content thus facilitates the particle formation.

The absorbance in the system where $[TTB] = 9 \times 10^{-5}$ M and $W_o = 30$ shown in Figure 1-5(c) increases by three times compared to that obtained with 3×10^{-5} M TTB shown in Figure 1-5(a). This indicates that the absorption of formed particles is proportional to the initial TTB concentration. In this TTB concentration, the particles are formed except for the case of $W_o = 9$ system. In the case of $W_o = 15$ and $[TTB] = 6 \times 10^{-5}$ M, the spectrum lies between that of the hydrolyzed molecules and that of the particles, as shown in Figure 1-5(b), indicating that the conversion of hydrolyzed molecules to the particles is not complete in 3 day. In this water content, the particles are formed with $[TTB] = 9 \times 10^{-5}$ M, while these are not formed with $[TTB] = 3 \times 10^{-5}$ M. The increase in TTB concentration also facilitates particle formation. Furthermore, the decrease in surfactant concentration

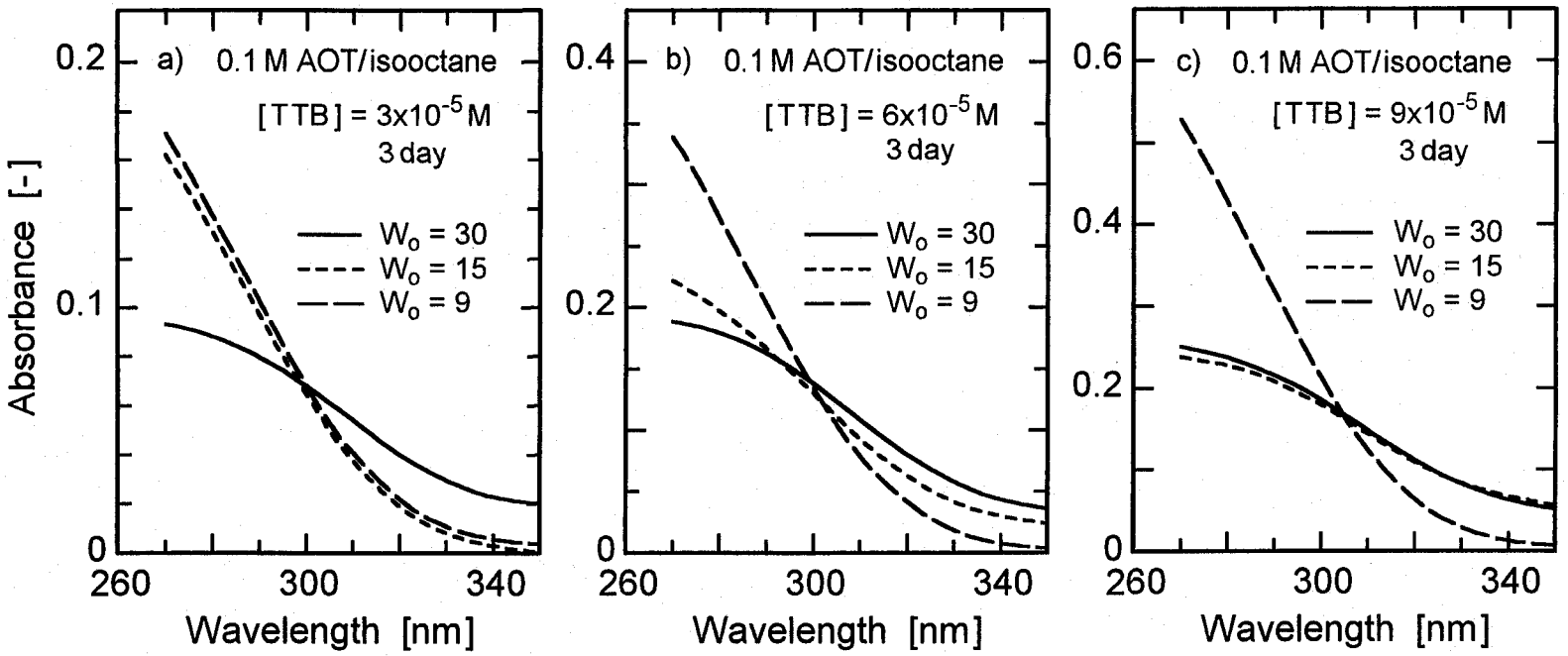

Figure 1–5 Effect of water content on absorption spectra at various initial TTB concentrations. (a) [TTB] = 3 x 10^{-5} M; (b) [TTB] = 6 x 10^{-5} M; (c) [TTB] = 9 x 10^{-5} M.

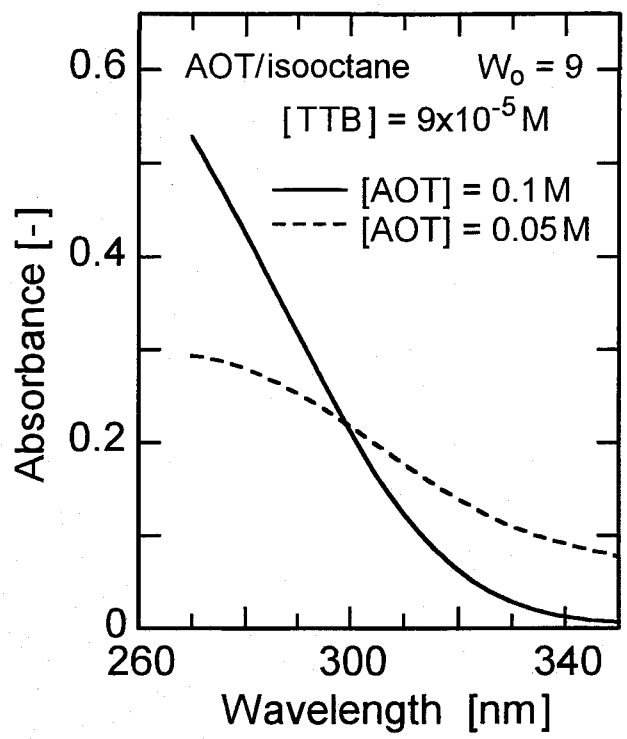

Figure 1–6 Effect of surfactant concentration on absorption spectra.

facilitates the particle formation. In the case of [TTB] = 9 x 10^{-5} M and W_o = 9, the particle formation occurred in the [AOT] = 0.05 M system, but not in the [AOT] = 0.1 M system, as shown in **Figure 1–6.**

Both the increase in water content and the decrease in surfactant concentration are found to facilitate the particle formation. The former increases the overall water concentration of the reverse micellar solution, while the latter causes a decrease. The overall water concentration does not seem to be a controlling factor for the particle formation in the reverse micelles. This problem is reconciled from a viewpoint taken from the concentration of micellar droplets (the number of micellar droplets in the solution expressed in the concentration unit). The concentration of micellar droplets, C_m, was calculated from the size of water cores in the micelles and total volume of the water cores in the solution in the same manner as reported by Kuboi *et al.* (1990). **Table 1–1** shows the average outer diameter of micelles, d_m, and the

Table 1-1 Reverse micellar systems used for preparation of TiO_2 particles.

[AOT] [M]	W_o [-]	d_m [nm]	σ_m [-]	$N_m/10^{19}$ [l^{-1}]	$C_m/10^{-5}$ [M]
0.1	30	19.30	0.267	1.42	2.36
0.1	15	10.72	0.188	7.20	11.97
0.1	9	8.97	0.206	9.56	15.88
0.05	9	8.98	0.206	4.75	7.90

standard deviation, σ_m, measured with DLS for present systems. The calculated values of N_m (number of micellar sroplets) and C_m are also shown in this table. These values decrease with increasing water content and decreasing surfactant concentration. The average number of the hydrolyzed molecules per micelle increases with decreasing concentration of micellar droplets. This facilitates the formation of the nuclei of the particles, since a certain number of hydrolyzed molecules are required to form a stable nucleus. Thus the concentration of micelles controls the particle formation in the reverse micelles.

The diameter of formed ultrafine particles was measured with DLS. **Figure 1-7** shows the effect of TTB concentration on the diameter (d_p) of particles formed in the $W_o = 30$ reverse micellar solutions measured at $t = 3$ day. The diameters are slightly affected by TTB concentration. Since the ultrafine particles have rather weak scattering characteristics, the DLS measurement is not very reproducible. The circles represent the average of four to six separate runs, and the arrows indicate the degree of scatter of the data.

4. Model for particle formation

Reverse micelles can exchange their contents in water cores via fusion of the micellar droplets and redispersion of the dimer droplets (Fletcher *et al.*, 1987). The rate constant for the exchange process has been reported to be

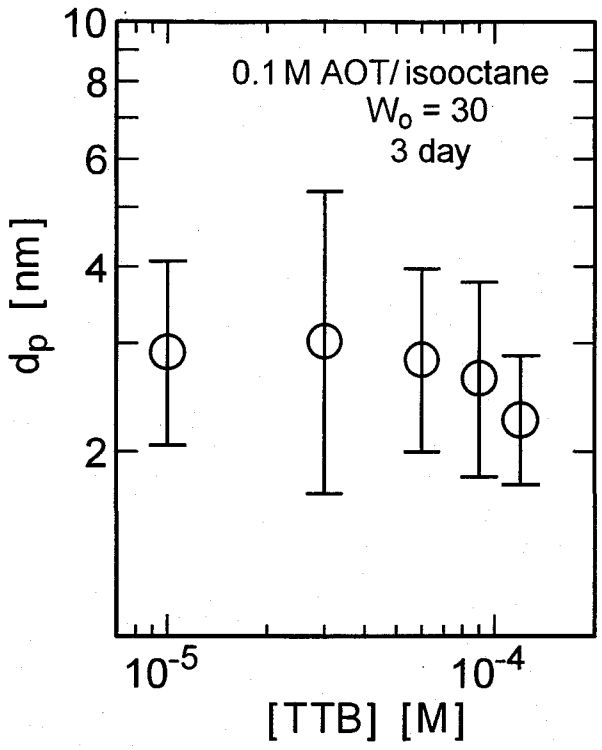

Figure 1–7 Effect of TTB concentration on diameter of particles measured with DLS.

10^6–10^8 M^{-1} s^{-1} for the AOT/isooctane system (Fletcher *et al.*, 1987, Lang *et al.*, 1988). Thus, the rearrangement of micelles occurs on a millisecond time scale, since the concentration of micelles is in the range of 10^{-5}–10^{-4} M^{-1} (Table 1–1). The reactions in the present particle formation process are much slower than the intermicellar exchange process. The reaction is considered to occur in micelles containing all required reactant molecules, and thus the rate of the reaction is controlled by the concentration of the micellar containing all required reactant molecules. Water-soluble molecules are considered to distribute among the reverse micelles according to a Poisson distribution (Atik and Thomas, 1981). The probability to have i molecules in a micelle, p_i, is given by,

$$p_i = \lambda^i \exp(-\lambda)/i! \qquad (1\text{–}3)$$

where λ is the average number of molecules per micelle.

The rate of hydrolysis follows a first-order kinetics as shown in Figure 1-4(a). Hence,

$$- dC_{TTB}/dt = k_H C_{TTB} \qquad (1-4)$$

where k_H and C_{TTB} are the first-order rate constant for hydrolysis and the concentration of TTB, respectively. The second step of the particle formation process is nucleation. The nucleation rate is considered to be proportional to the concentration of micellar droplets containing a sufficient number of hydrolyzed molecules for the nucleation, $C_{m,n}$. Thus,

$$dC_p/dt = k_N C_{m,n} \qquad (1-5)$$

where k_N and C_p are the first-order rate constant for nucleation and the concentration of formed nuclei, respectively. Assuming that nucleation requires n molecules of hydrolyzed TTB and using Eq. 1-3, $C_{m,n}$ is expressed as,

$$C_{m,n} = C_m \sum_{i=n}^{\infty} \left(\frac{C_h}{C_m}\right)^i \frac{\exp(-C_h / C_m)}{i!} = C_m \left\{1 - \sum_{i=0}^{n-1} \left(\frac{C_h}{C_m}\right)^i \frac{\exp(-C_h / C_m)}{i!}\right\} \qquad (1-6)$$

where N_p is the concentration of hydrolyzed molecules.

Particle growth can occur in micelles containing a nucleus or a particle, in addition to hydrolyzed molecules. By assuming that the rate of consumption of the hydrolyzed molecules by particle growth is proportional to the concentration of such pregnant micelles and is independent of the particle size, balance equation of the hydrolyzed molecule can be expressed by,

$$dC_h/dt = - \text{n}\, dC_p/dt - k_G C_h C_p / C_m + k_H C_{TTB} \qquad (1-7)$$

where k_G is the first-order rate constant taking into account the probability of particle growth. The concentration of micellar droplets containing both a particle and a hydrolyzed molecule is represented by C_hC_p/C_m. Each term of Eq. 1-7 represents the consumption rate of hydrolyzed molecules for

nucleation, the consumption rate of hydrolyzed molecules for particle growth, and the rate for the formation of hydrolyzed molecules by hydrolysis. In the case of TiO_2 particles, both particle growth and particle coagulation proceed through the condensation reaction shown by Eq. 1-2. The diameter of particles formed is about 3.0 nm as shown in Figure 1-7, the concentration of the particles is calculated as 6.6×10^{-8} M. The number of the particle is much less than that of TTB, the rate of coagulation is thus much less than that of particle growth. Ostwald ripening can also be negligible, since this requires dissolution of TiO_2 particles which hardly occur in the neutral pH. Assuming that no ripening and coagulation occur, that is, the number of particles is identical to the number of nuclei formed, one can simulate the variations with time of the concentrations of TTB molecules (C_{TTB}), hydrolyzed molecules (C_h), and particles (C_p) by solving Eqs. 1-4, 1-5, and 1-7.

5. Application of the model for particle formation

The proposed model contains four parameters to be determined such as the first-order hydrolysis rate constant (k_H), the first-order particle growth reaction rate constant (k_N), the first-order nucleation rate constant (k_G), and the number of hydrolyzed molecules required to form a stable nucleus (n). The value of k_H can be determined by the value of $t_{1/2}$ of the initial part of the absorbance change at 280 nm shown in Figure 1-4(a). This is determined to be 1.9×10^{-4} s^{-1} using 1 h as $t_{1/2}$.

The later part of the absorbance change in the time period after t = 500 min represents the consumption of hydrolyzed molecules for nucleation and particle growth. In this part, the hydrolysis of TTB is almost finished, and the consumption of hydrolyzed molecules by nucleation is much less than that by particle growth. The first and third terms of Eq. 1-7 are, thus, negligible after t = 500 min, and this equation is now simplified as,

$$-dC_h/dt = (k_G C_p/C_m)\, C_h \qquad (1\text{-}8)$$

Generally, nucleation proceeds mainly in the initial part of particle formation process (LaMer, 1952), C_p is thus assumed to be constant after $t = 500$ min. This assumption should be checked by the results of simulation. The observed first-order rate constant ($k_G C_p/C_m$) is calculated to be 3.0×10^{-5} s^{-1} using the value of $t_{1/2}$ (6.5 h) shown in Figure 1-4(b). For the present case, the concentration of micelles, C_m, is 2.36×10^{-5} M as shown in Table 1-1. The concentration of particles (C_p) is calculated by the diameter of formed particles (d_p) with assuming that the particles are spherical and the density of particles is independent of the particle size. Since d_p is about 3.0 nm as shown in Figure 1-7, C_p is calculated to be 6.6×10^{-8} M. The value of k_G is now estimated as 1.1×10^{-2} s^{-1}.

For the estimation of the nucleation rate constant, k_N, in Eq. 1-5, the value of n expressing the number of hydrolyzed molecules to form a stable nucleus, is first needed, since the value of $C_{m,n}$ is dependent on the value of n. The diameter of formed particles calculated from the simulated value of C_p is very sensitive to the ratio of k_G and k_N. The value of k_N is determined in each case for integer n greater than 1 using the observed diameter, 3.0 nm, at the case of $W_o = 30$ and [TTB] = 3×10^{-5} M shown in Figure 1-7. The variation of particle diameter with initial TTB concentration is then calculated for each n and k_N pair. The results are shown in **Figure 1-8.** The value of n is determined to be 5 to produce the best correlation with the observed data. The nucleation rate constant, k_N, on the basis of $n = 5$ is now estimated as 1.9×10^{-5} s^{-1}. Nucleation is generally taken to occur in the size range of 1-10 nm (Everett, 1988). In the reverse micelles, however, it must occur at much smaller sizes as suggested by Towey *et al.* (1990). Actually, Ravet *et al.* (1987) obtained the value of $n = 2$ for metal boride particles from the analysis of variation of the number of formed particles with the number of feed metal ions.

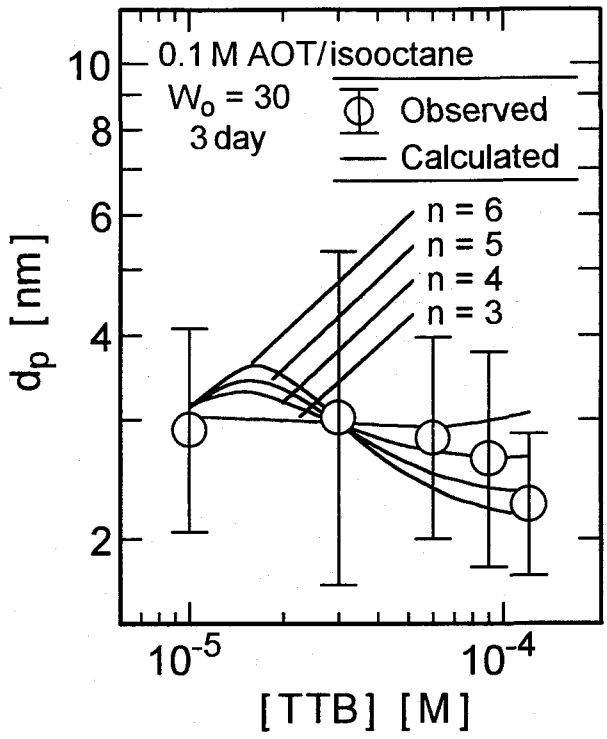

Figure 1–8 Calculated variation of diameter with initial TTB concentration for various *n* values.

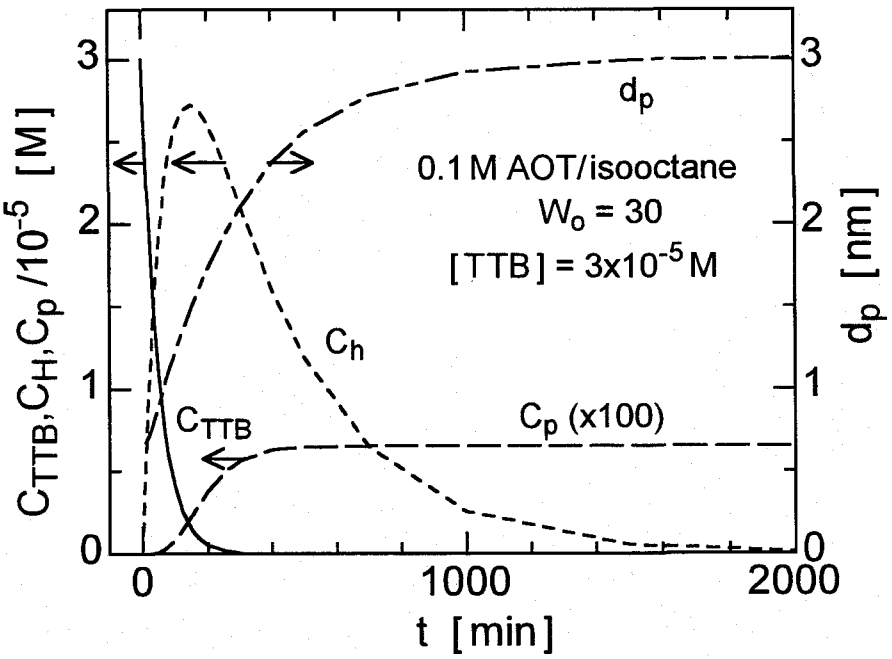

Figure 1–9 Calculated time-course variations of the concentrations of TTB, hydrolysis molecules, and particles and the particle diameter.

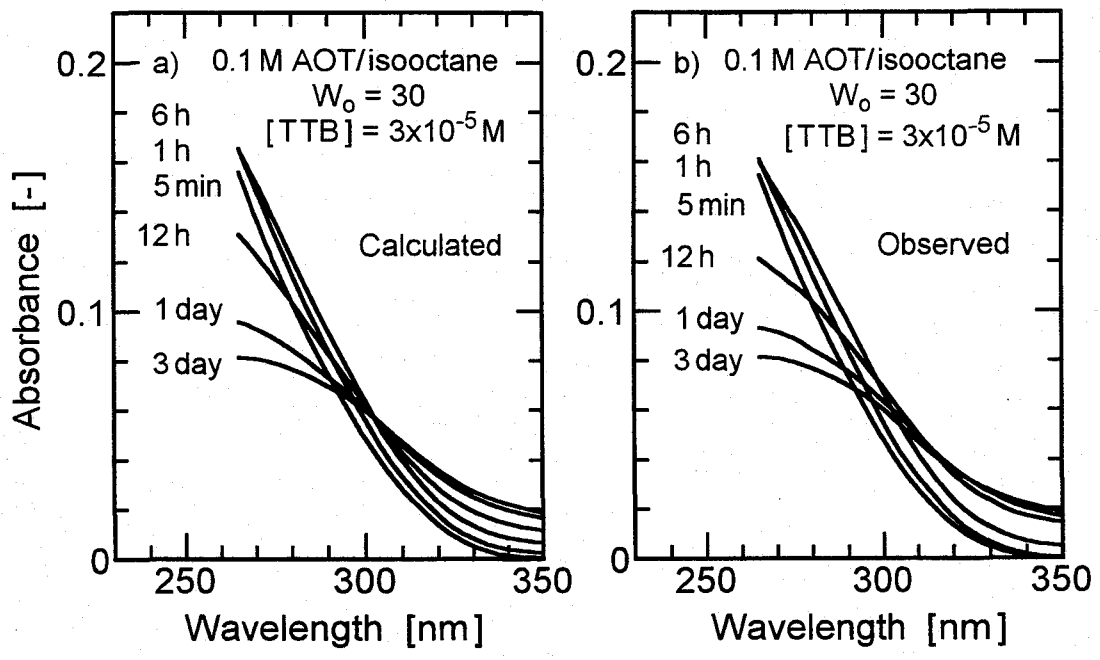

Figure 1–10 Change in absorption spectra during hydrolysis of TTB. (a) Calculated; (b) observed.

The changes in the concentrations of TTB, hydrolyzed molecules, and particles can now be calculated using Eqs. 1–4, 1–5, and 1–7 and the four parameters (k_H, k_N, k_G, and n). The calculated time-course variations of the concentrations and particle diameter in the case of [TTB] = 3 x 10^{-5} M and W_o = 30 are shown in **Figure 1–9.** The concentration of the particles is almost constant after t = 250 min, indicating that nucleation is complete in this period. **Figure 1–10(a)** shows the calculated change in the spectra of the solution using the calculated time-course variations of the concentrations and the observed absorption spectra of TTB, hydrolyzed molecules, and TiO_2 particles. These spectra show a good agreement with the observed data shown in **Figure 1–10(b).** The calculated time-course variation of absorbance at 280 nm is shown in **Figure 1–11.** The data obtained at the maximum absorbance are not used in determination of parameters. However, the calculated time-course variation of absorbance shows a good agreement with the observed data.

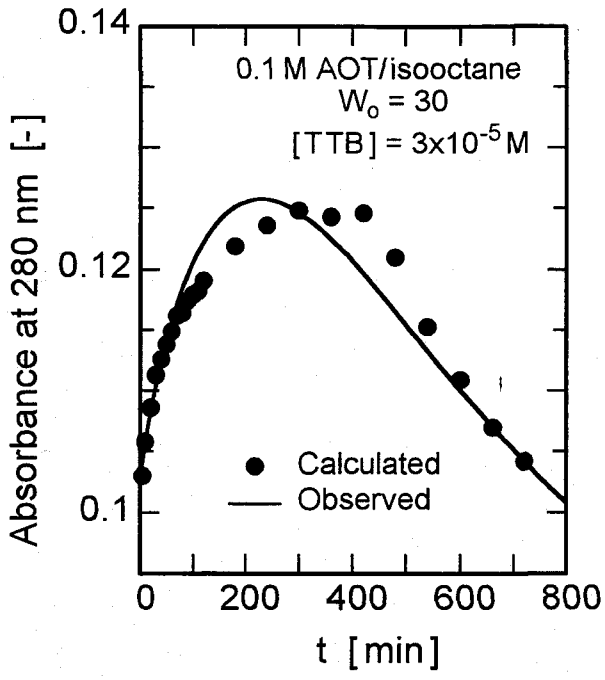

Figure 1−11 Comparison of change in absorbance at 280 nm during hydrolysis of TTB for calculated and for observed.

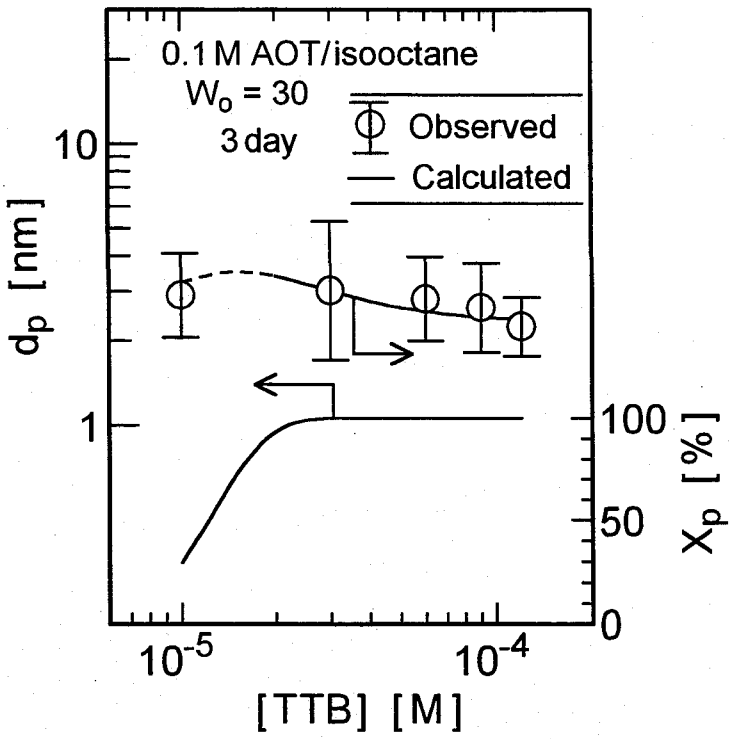

Figure 1−12 Effect of initial TTB concentration on calculated particle diameter and conversion of TTB molecules to particles.

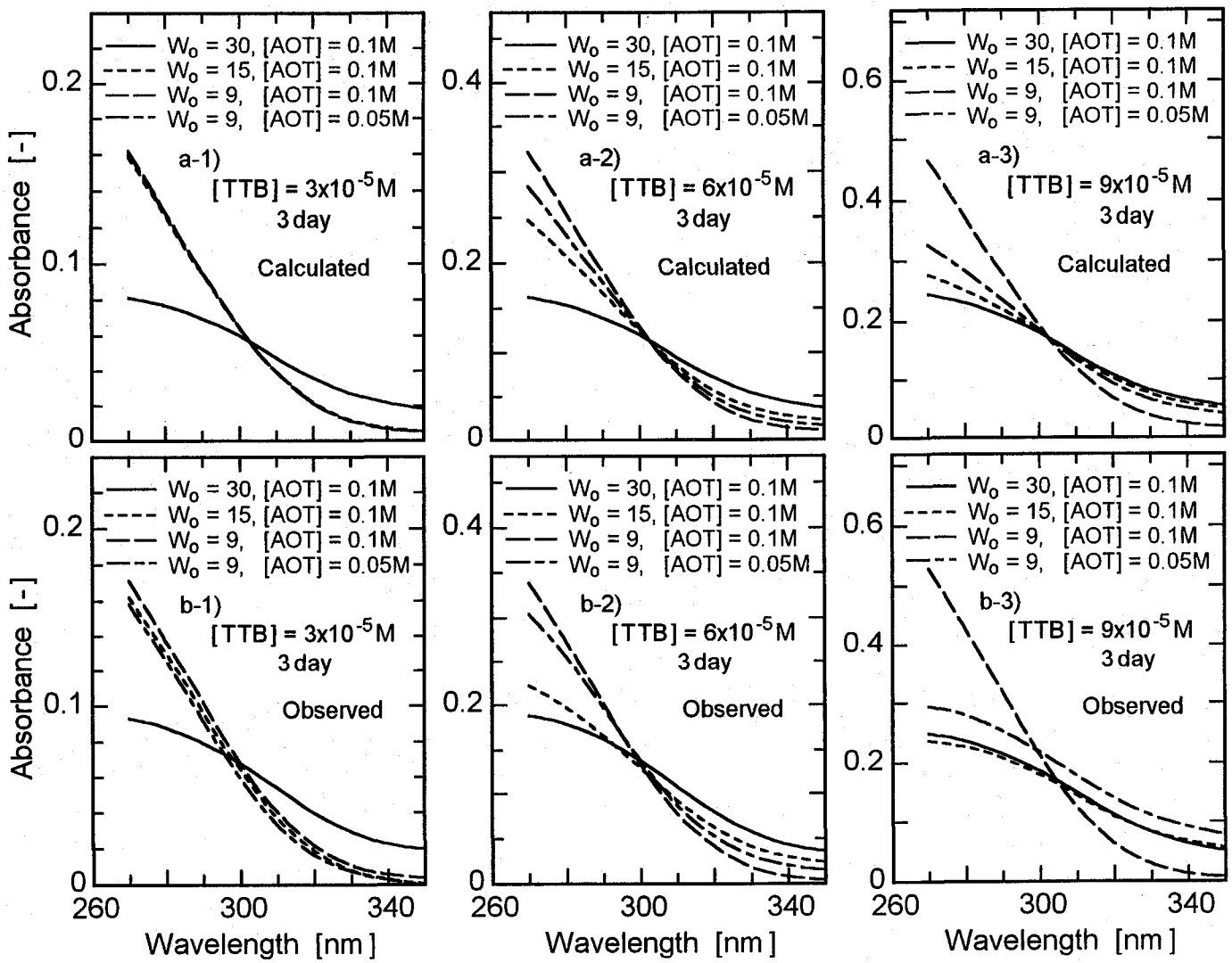

Figure 1–13 Absorption spectra after hydrolysis of TTB for 3 day in various reverse micellar systems. (a) Calculated; (b) observed.

The solid lines in **Figure 1-12** show the calculated diameter of particles and the conversion of TTB to the particles (X_p) at $t = 3$ day as functions of the initial TTB concentration. The calculated diameters show a good agreement with the observed data. This is to be expected, since the value of n is estimated based on the observed data of particle diameters. In the range of TTB concentration less than 2×10^{-5} M, the calculation suggests that the conversion of hydrolyzed molecules to the particles is not complete in 3 day. The particles could grow larger after 3 day in this low concentration range. However, the experiment is not plausible due to the inevitable vaporization and leakage of isooctane and a large absorption due to AOT compared to that due to particles.

The spectra of reverse micellar solutions after hydrolysis of TTB for 3 day at various water contents and various surfactant concentrations are calculated using the four parameters determined at the $W_o = 30$ reverse micelles. Typical results are shown in **Figure 1-13(a).** These spectra show good agreement with the corresponding observed data shown in **Figure 1-13(b).** The presented reaction scheme gives a satisfactory description of the slow particle formation process by hydrolysis of TTB in reverse micelles from the hydrolysis to particle growth.

Summary

The mechanism of formation of TiO_2 ultrafine particles in AOT/isooctane reverse micelles by hydrolysis of titanium tetrabutoxide (TTB) was studied. The particle formation process was followed by the UV-visible absorption spectra. The following results were obtained:

1. Different spectral changes are observed between an organic homogeneous solution containing 3×10^{-5} M TTB and 3 M water and a reverse micellar solution containing identical amounts of TTB and water. The

difference is caused by the formation of particles. The particles are formed in reverse micelles, but not in homogeneous organic solution under the relevant conditions.

2. The effects of water content, TTB concentration, and surfactant concentration on the particle formation were investigated. The increases in TTB concentration and water content and the decrease in surfactant concentration are found to facilitate the particle formation. The particle formation is controlled by the average number of TTB molecules per micellar droplet, since a certain number of hydrolyzed molecules are required to form a stable nucleus.

3. A reaction scheme for the particle formation was proposed. The rate of nucleation is assumed to be first-order with respect to the concentration of micellar droplets containing five or more hydrolyzed TTB molecules. The rate of consumption of the hydrolyzed molecules for particle growth is assumed to be first-order with respect to the concentration of micelles containing a particle and a hydrolyzed molecule, and to be independent of particle size. Coagulation and Ostwald ripening of the particles are neglected in the present particles. The scheme can explain the observed data for the spectral change during particle formation process successfully.

Chapter II
Mechanism of Formation of Metal Sulfide Ultrafine Particles Using Solution Mixing Method

Introduction

The particles can be prepared by either slow or fast chemical reaction in the reverse micelles. The rate for the reaction in reverse micellar system competes with that for the intermicellar exchange process. The particle formation by the reaction slower than the exchange process was studied in Chapter I and it was found that the formation was controlled by the statistical distribution of reactants among the micelles. In the case of the reaction faster than the exchange process, the reaction rate is considered to be controlled by the rate of the exchange process (Fletcher *et al.*, 1987). The particle formation via fast reaction was thus investigated in this chapter.

A few studies for the kinetic analysis of the particle formation process via the reactions faster than the exchange process have been reported. Towey *et al.* (1990) proposed a model for the particle coagulation by replacing the diffusion-controlled coagulation rate constant of the Smoluchowski rapid coagulation model (1916) by the rate constant for the intermicellar exchange process. They analyzed coagulation of CdS particles, and Petit *et al.* (1993) also analyzed that of Ag particles using this model. For CdS particles, the change in absorbance at 280 nm in the initial period up to 0.5 s was reasonably explained by this model. The spectrum, however, continued to change after 0.5 s. A study for a longer period is thus needed to obtain a complete picture of the particle formation process. Another question is how the particle material affects particle coagulation. While the coagulation rate is expected to be independent of the material in their model, this has not been confirmed experimentally.

In this chapter, the formation process of metal sulfide particles such as CdS, ZnS, and PbS was studied as a case study of the reaction faster than the exchange process. The particles were prepared by the mixing of two reverse micellar solutions (solution mixing method). The particle formation process in the period from 0.01 s to 1 h was followed by the change of UV–visible absorption spectra, using the stopped-flow technique for the initial stage. The coagulation kinetics was analyzed from the change in the particle diameter estimated from the spectra.

Experimental Section

1. Preparation of particles

Sodium bis(2-ethylhexyl) sulfosuccinate (AOT), sodium sulfide, cadmium nitrate, zinc nitrate, and lead nitrate were supplied by Wako Pure Chemical Industry. Isooctane (2,2,4-trimethylpentane) was supplied by Ishizu Seiyaku. All reagents were used without further purification. Distilled water was filtered with a 0.45-μm membrane filter and any dissolved oxygen was purged by argon bubbling, prior to use. Aqueous solutions containing $Cd(NO_3)_2$, $Zn(NO_3)_2$, $Pb(NO_3)_2$, or Na_2S were prepared daily. Reverse micellar solutions containing these reactants were prepared by injection of the required amount of aqueous solution into filtered AOT/isooctane solution and were then used within a few minutes. The water content of the reverse micellar solution, W_o, was varied in the range 3–10.

Ultrafine CdS particles were prepared by rapid mixing of a reverse micellar solution (1.2 m*l*) containing $Cd(NO_3)_2$ and an equal volume of a reverse micellar solution containing Na_2S. This was done at 25 ℃, using the mixing unit of a stopped-flow spectrophotometer. The water content and surfactant concentration of both reverse micellar solutions were identical. The instant when two solutions were mixed was defined as $t = 0$ s. $Zn(NO_3)_2$ or $Pb(NO_3)_2$,

were employed instead of $Cd(NO_3)_2$, for the preparation of ZnS or PbS ultrafine particles. Otherwise, the operations were the same as those for CdS particles.

2. Measurements

A stopped-flow spectrophotometer (Otsuka Electronics RA-401) equipped with a diode array detector (Otsuka Electronics RA-415) was used for measurement of the UV–visible absorption spectra for the period up to $t = 1$ s. For measurement for the period from 1 s to 1 min, the reverse micellar solutions were injected into a quartz flow cell (0.4 m*l*) by using the mixing unit and the resulting spectral change following injection was recorded on a Hewlett-Packard 8452A diode array spectrophotometer. With the reaction times greater than 10 min, the mixed reverse micellar solution (2.4 m*l*) was injected into a beaker-type glass reactor (10 m*l*) and was kept in the dark with mild stirring (300 min^{-1}) generated by a magnetic stirrer. The solution was transferred to a quartz cell in order to measure the absorption spectra as required and then returned to the reactor.

The concentration of reverse micellar droplets (C_m) was estimated from the average diameter (d_m) and the standard deviation of the diameter (σ_m) of micelles in the same manner as Chapter I. The results for the present systems are shown in **Table 2–1.**

Results and Discussion

1. Spectral change during particle formation

Semiconductor particles absorb the UV–visible light having greater energy than the band gap energy (E_g). The electric parameters of metal sulfides are shown in **Table 2–2.** These parameters are obtained from Landolt-Börnstein New Series III 17 (1982) and references therein. With a reduction in particle

Table 2-1 Reverse micellar systems used for preparation of metal sulfide particles ([AOT] = 0.1 M).

W_o [-]	d_m [nm]	σ_m [-]	$N_m/10^{20}$ [-]	$C_m/10^{-4}$ [M]
3	3.62	0.154	35.5	58.9
6	5.45	0.165	5.58	9.27
10	7.07	0.175	2.59	4.31

Table 2-2 Parameters for metal sulfide semiconductor particles.

	$E_{g,bulk}$ [eV]	m_e/m_0 [-]	m_h/m_0 [-]	$\varepsilon/\varepsilon_0$ [-]	d [g/cm^3]	s [g/l]	a [nm]	b [nm]
CdS	2.5	0.19	0.8	5.7		$2.11\text{x}10^{-8}$	0.4136	0.6714
ZnS	3.7	0.25	0.59	5.2		$1.43\text{x}10^{-7}$	0.3820	0.6260
PbS	0.41	0.080	0.075	17.2	7.59	$1\text{x}10^{-3}$		

size, the band gap energy of the semiconductor particles becomes larger and there is a concomitant blue-shift in the absorption spectra (Brus *et al.*, 1984). This size-dependent optical property provides a very convenient and useful way to monitor the growth of the semiconductor particles.

CdS ultrafine particles were prepared from $Cd(NO_3)_2$ and Na_2S by following reaction.

$$Cd(NO_3)_2 + Na_2S \rightarrow CdS + 2NaNO_3 \qquad (2\text{-}1)$$

Figure 2-1 shows the UV-visible absorption spectra obtained during the reaction between 1×10^{-4} M $Cd(NO_3)_2$ and 1×10^{-4} M Na_2S in the $W_o = 6$ reverse micellar solution. Since $Cd(NO_3)_2$ and Na_2S have very weak absorption characteristics, the observed absorption is attributable to the formed CdS semiconductor particles. The arrows on the spectra indicate the absorption threshold of the spectra determined using a method described in the next section. A continuous red-shift in the absorption threshold is observed.

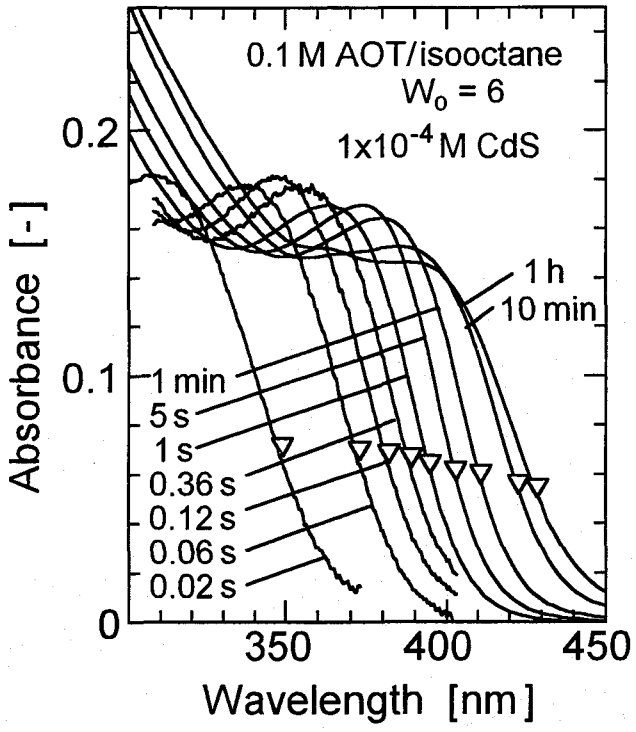

Figure 2−1 Change in absorption spectra during formation of CdS particles.

This indicates the decrease in band gap energy caused by the continuous increase in particle diameter.

The magnitude of the absorption indicates the quantity of formed particles. After $t = 0.02$ s, the peak absorbance is almost constant, indicating that the consumption of the ions for nucleation and particle growth is complete within 0.02 s. This is caused by the fast formation reaction (Eq. 2−1) and the low solubility of CdS (Towey *et al.*, 1990). The increase in particle diameter in this period, without consumption of ions, can occur by particle coagulation or Ostwald ripening. Ostwald ripening, however, may be considered to proceed over a much longer time scale in this case, since CdS has a very low solubility. The observed increase in particle diameter following $t = 0.02$ s can, therefore, be attributed to particle coagulation.

ZnS particles were prepared by following reaction.

$$Zn(NO_3)_2 + Na_2S \rightarrow ZnS + 2NaNO_3 \qquad (2-2)$$

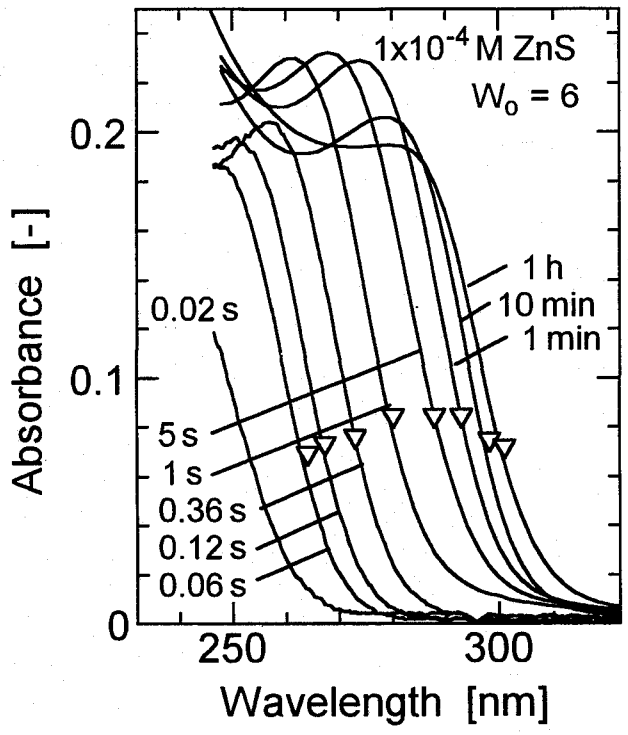

Figure 2–2 Change in absorption spectra during formation of ZnS particles.

Figure 2–2 shows the UV–visible absorption spectra obtained during the reaction at a reactant concentration of 1×10^{-4} M in the $W_o = 6$ reverse micellar solution. The absorption threshold of ZnS particles is observed at a shorter wavelength than that of CdS particles. This indicates that the band gap energy (E_g) of ultrafine ZnS particles is larger than that of CdS particles as in the case of the bulk material shown in Table 2–2. A similar spectral change to the case of CdS particles is observed, indicating the completion of nucleation and particle growth within 0.02 s after mixing and the succeeding coagulation of particles.

PbS particles were also prepared using following reaction.

$$Pb(NO_3)_2 + Na_2S \rightarrow PbS + 2NaNO_3 \qquad (2\text{–}3)$$

Figure 2–3(a) shows the UV–visible absorption spectra obtained during the reaction between 2.5×10^{-4} M $Pb(NO_3)_2$ and 2.5×10^{-4} M Na_2S in the $W_o = 3$ reverse micellar solution. The spectrum indicating the formation of PbS

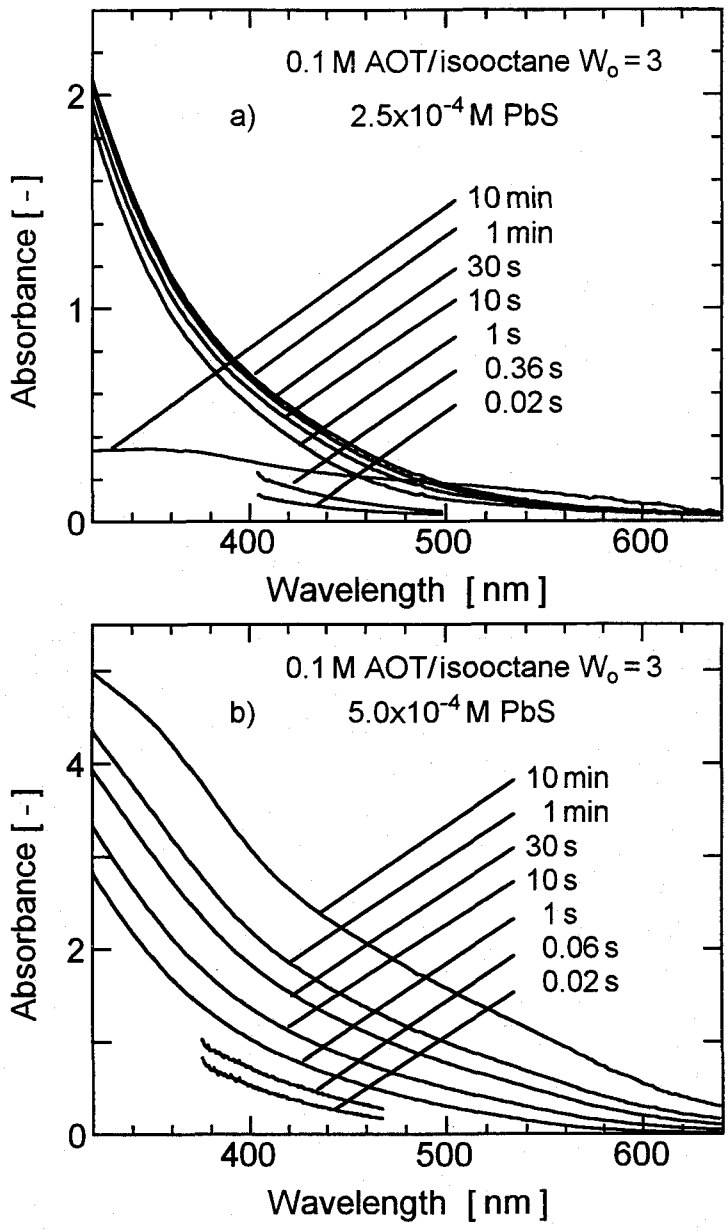

Figure 2–3 Change in absorption spectra during formation of PbS particles. (a) [PbS] = 2.5×10^{-4} M; (b) [PbS] = 5×10^{-4} M.

particles is observed at $t = 0.02$ s. The spectrum observed at $t = 1$ s is similar to that of 2–3 nm PbS colloids obtained by Nozik *et al.* (1985). A continuous red-shift in the absorption threshold indicating particle coagulation is observed after $t = 1$ s. In this case, large visible particles are, however, observed in the solution at $t = 10$ min. The particles are unstable and tend to grow larger. This may occur by Ostwald ripening, since PbS has a relative large solubility (s) as

shown in Table 2-2. **Figure 2-3(b)** shows the absorption spectra at a reactant concentration of 5×10^{-4} M. The characteristics of light scattering are not observed in the spectrum measured at $t = 10$ min and visible particles are not observed in this solution. These results indicate that the formed ultrafine particles can be stabilized in this condition. When W_o is greater than 3 or reactant concentration is less than 5×10^{-4} M, the particles are not stable for long period.

2. Estimation of particle diameter

The size of the formed semiconductor particles was estimated from band gap energy of the particles. Brus (1984) proposed the following equation about band gap energy (E_g) of ultrafine particles and particle diameter (d_p).

$$E_g = E_{g,bulk} + \frac{h^2}{2{d_p}^2}\left(\frac{1}{m_e} + \frac{1}{m_h}\right) - \frac{3.6e^2}{4\pi\varepsilon d_p} \qquad (2\text{-}4)$$

where $E_{g,bulk}$ is the bulk band gap energy, h is the Planck constant, m_e is the effective mass of electron, m_h is the effective mass of hole, e is the charge of electron, and ε is the dielectric constant of semiconductor at optical frequencies. These parameters of the present particles are shown in Table 2-2. However, in the case of PbS particles, where effective masses of electron and hole are very small, the estimated band gap energy from this equation becomes larger than the experimental value (Wang *et al.*, 1987). They proposed another equation to express the band gap energy for this case.

$$E_g = \left[{E_{g,bulk}}^2 + 2h^2 E_{g,bulk}\left(\frac{1}{d_p}\right)^2\left(\frac{1}{m_e} + \frac{1}{m_h}\right)\right]^{1/2} \qquad (2\text{-}5)$$

The diameters were thus estimated from Eq. 2-4 for CdS and ZnS particles and from Eq. 2-5 for PbS particles.

The band gap energy of the semiconductor can be estimated from the absorption spectrum. For the direct allowed transitions, the dependence of the

absorption coefficient (σ) on the photon energy ($h\nu$) near the band gap energy is given by (Ravich *et al.*, 1970; Wang *et al.*, 1987),

$$\sigma h\nu = K\,(h\nu - E_g)^{1/2} \qquad (2\text{-}6)$$

where K is the proportional factor. Since CdS, ZnS, and PbS are the direct gap semiconductors, the values of $(\sigma h\nu)^2$ were plotted versus $h\nu$ and then x-axis section of a straight line through the observed data was defined as E_g.

In the case of PbS particles, however, this plot sometimes gives unreasonable values for band gap of PbS ultrafine particles. Indirect allowed transition, in which a phonon is absorbed, should satisfy the following relationship near the absorption edge (Ravich *et al.*, 1970),

$$\sigma h\nu = K'\,(h\nu - E_g')^2 \qquad (2\text{-}7)$$

where K' and E_g' are the proportional factor and the indirect transition threshold, respectively. The difference between E_g and E_g' was found to be 0.04 eV for the case of bulk PbS (Ravich *et al.*, 1970). This indicates that indirect transitions involve the absorption of the long-wavelength optical phonons. The absorption spectra of prepared ultrafine PbS particles were also fitted to Eq. 2-7. In this, the values of $(\sigma h\nu)^{1/2}$ were plotted versus $h\nu$ to determine indirect transition threshold. This plot gives better straight lines than the plot using Eq. 2-6. The values of E_g for PbS particles were thus calculated by adding 0.04 eV to E_g'.

Figure 2-4(a) shows the time-course variations of the estimated diameters of CdS and ZnS particles at various reactant concentrations in the $W_o = 6$ reverse micellar solution. The diameter increases with time and with increasing reactant concentration. The diameter of CdS particles is greater than that of ZnS particles at the same conditions. The results for PbS particles in the $W_o = 3$ reverse micelles are shown in **Figure 2-4(b),** also showing the increase in d_p with increasing reactant concentration. The effect of water

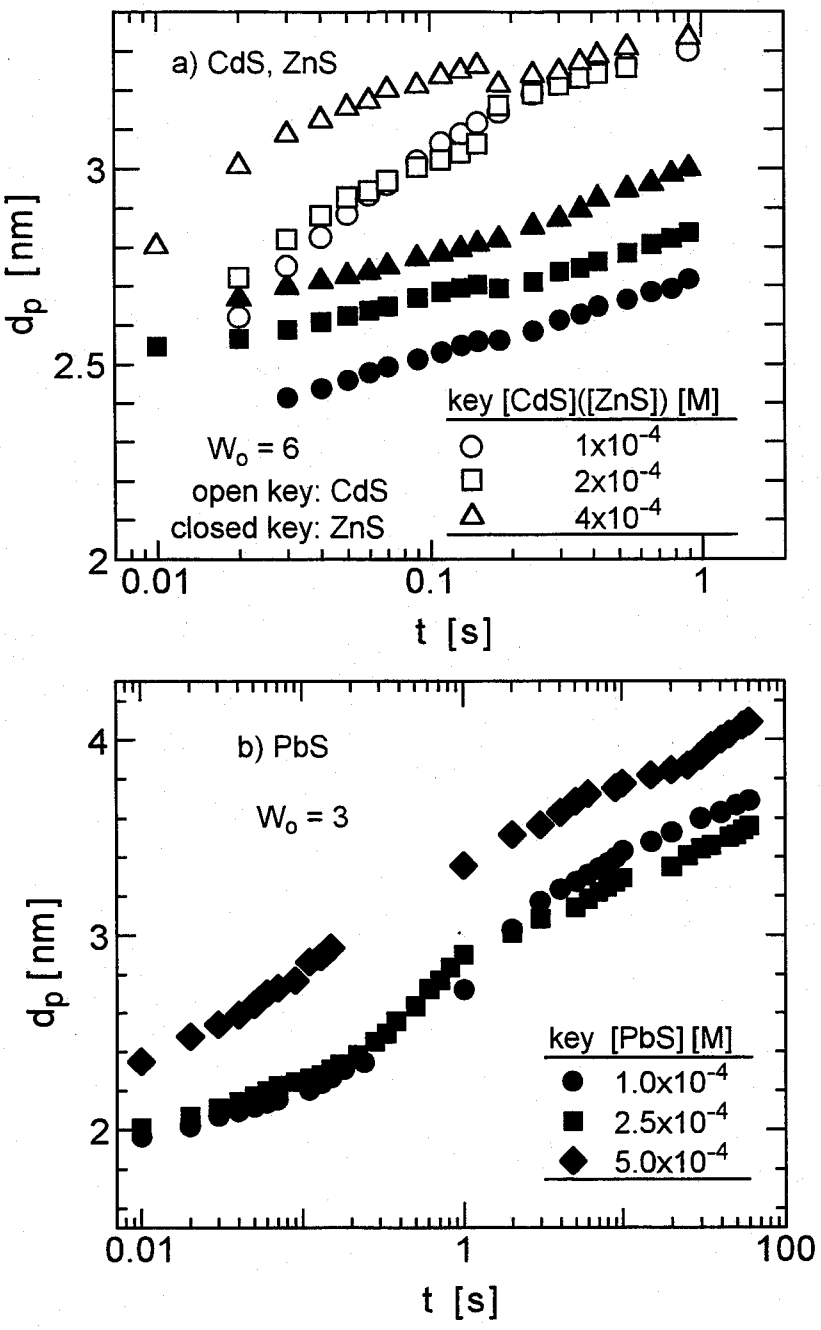

Figure 2-4 Effect of reactant concentration on time-course variation of particle diameter. (a) CdS and ZnS particles; (b) PbS particles.

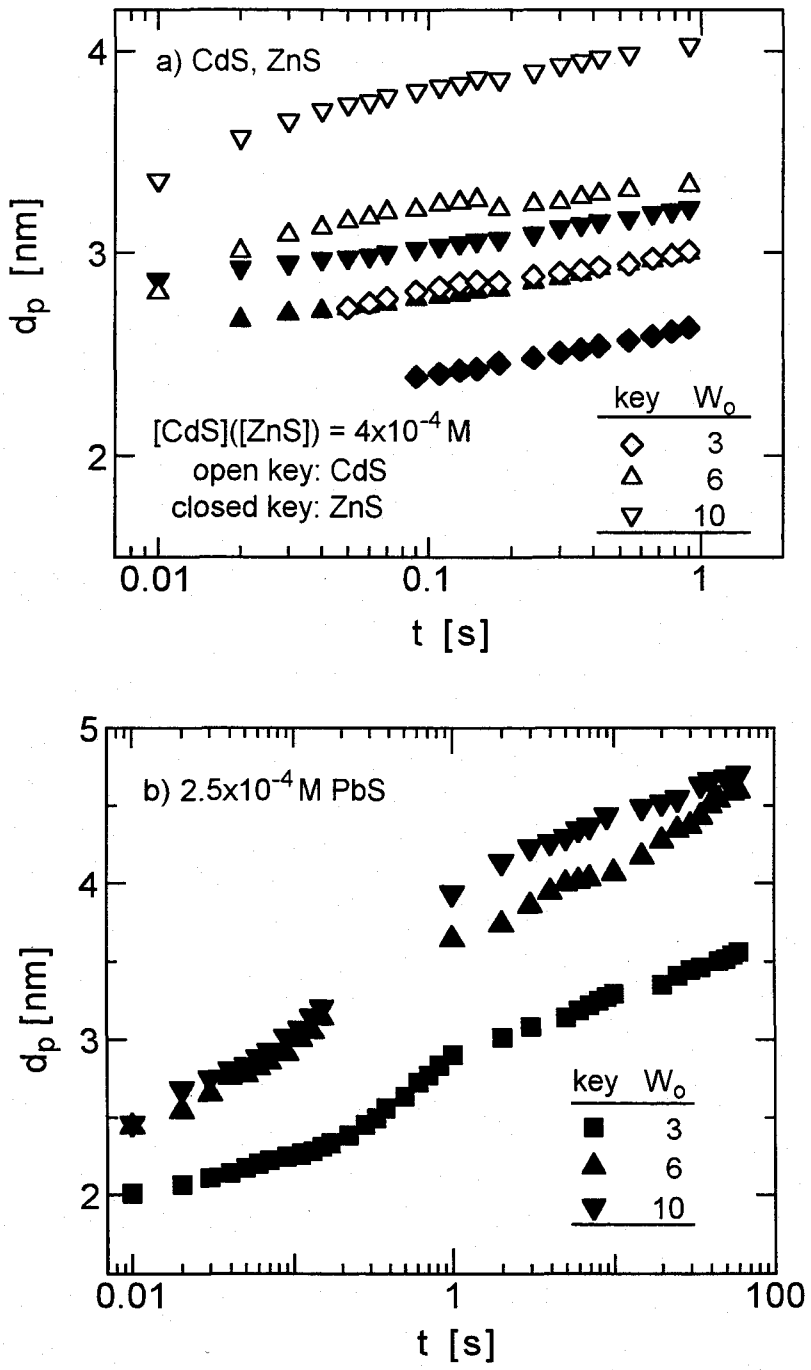

Figure 2–5 Effect of water content on time-course variation of particle diameter. (a) CdS and ZnS particles; (b) PbS particles.

content of the reverse micellar solution on d_p is shown in **Figure 2–5(a)** for CdS and ZnS particles and in **Figure 2–5(b)** for PbS particles. The values of d_p increased with increasing W_o in all cases.

3. Effect of excess amount of reactant ions on particle formation

The effect of excess amount of reactant ion on the spectra of particles was investigated. The molar ratio of S^{2-} ion to metallic ion in feed solution is expressed in y as follows,

$$y = [S^{2-}]/[M^{2+}] \qquad (2-8)$$

$$(M^{2+} = Cd^{2+}, Zn^{2+}, \text{or } Pb^{2+})$$

A series of experiments were carried out in which the feed concentration of one of S^{2-} ion and metallic ion was continuously increased from 1×10^{-4} M, while the concentration of the other ion was maintained constant at a value of 1×10^{-4} M. The effects of y on the spectra of CdS and ZnS particles are shown in **Figures 2–6(a) and (b)**, respectively. A red-shift in the absorption threshold with increasing values of y is observed. The change in the shape of absorption spectra may be due to the change in the energy band structure of semiconductor particles caused by the change in composition of particles.

The absorbance at peak wavelength for CdS and ZnS particles with various y values is shown in **Figure 2–7.** The absorbance increases with decreasing y, except at near $y = 1$. This increase is also possibly caused by the change in the energy band structure. The absorbance at $y = 1$ is less than that expected from the data for both sides. This is due to the unconverted precursor ions in the solution which have very weak absorption characteristics. Since the concentration of the residual ions in solution is controlled by the solubility product of the particle material (K_{sp}) as shown in the following equation, the concentration of residual ions can be reduced by the excess

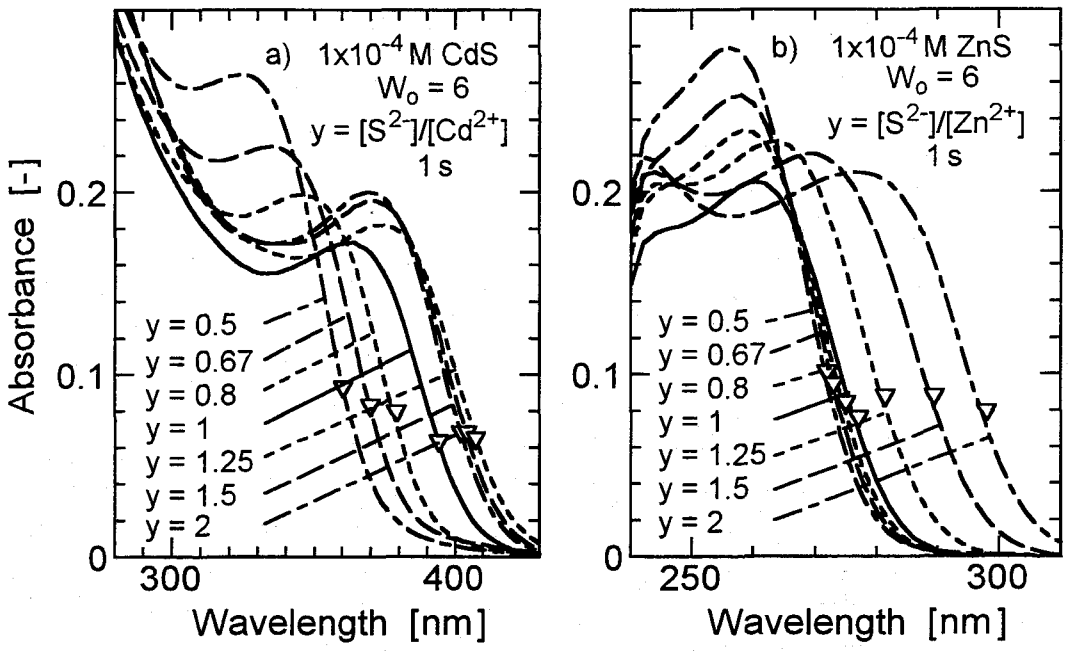

Figure 2–6 Effect of ratio of concentration of sulfide and metallic ions (y) on absorption spectra. (a) CdS; (b) ZnS.

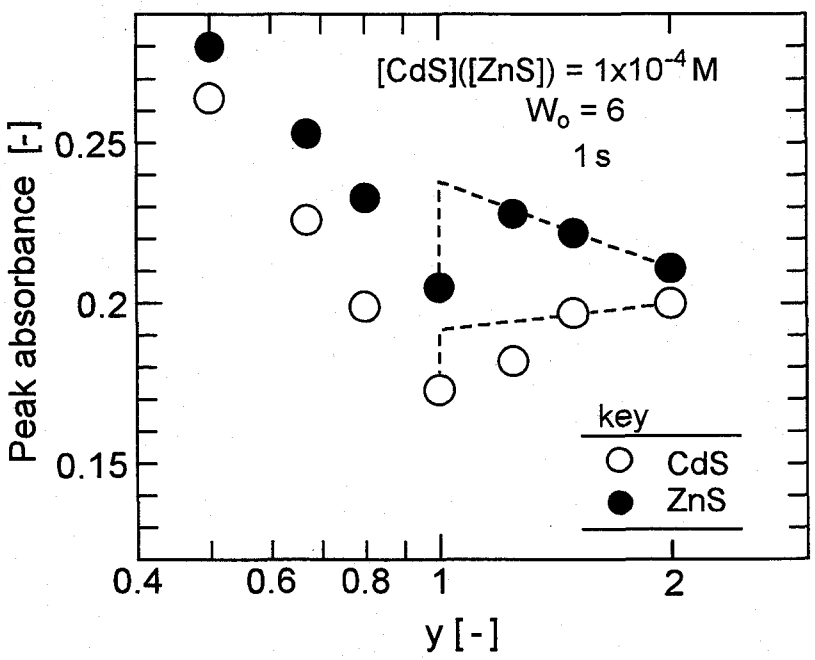

Figure 2–7 Effect of ratio of concentration of metallic and sulfide ions (y) on the peak absorbance.

amount of another reactant ion.

$$K_{sp} = [M^{2+}][S^{2-}] / M^2 \qquad (2\text{-}9)$$

The values of K_{sp} for bulk CdS and ZnS are 1.4×10^{-29} and 1×10^{-23}, respectively (Youn *et al.*, 1988). One problem encountered is that the solubility of the particles in the size range of ultrafine particles increases with decreasing particle size (Nielsen, 1964). Thus, the actual solubility values for ultrafine CdS and ZnS particles were estimated from the change in the conversion of the ions induced by the excess S^{2-} or metallic ions shown in Figure 2-7. The observed peak absorbance of the formed particles at $y = 1$ ($[Cd^{2+}] = [S^{2-}] = 1 \times 10^{-4}$ M) is at about 10 % below the extrapolated value from the data for $y = 1.5$ and 2 as shown with dotted line. Hence, since about 10 % of the supplied ions may reside in the solution in this case, the solubility for the ultrafine CdS particles can be estimated as 1×10^{-5} M. Similarly the solubility of ultrafine ZnS particles can be estimated as 2×10^{-5} M. Hence, the values of K_{sp} for CdS and ZnS particles, employed in the present study, are estimated to be 1×10^{-10} and 4×10^{-10}, respectively. These values are much larger than the values for bulk materials.

Figure 2-8 shows the absorption spectra of PbS particles prepared with a 5-fold excess amount of Pb^{2+} ion. The spectra are almost unchanged after $t = 10$ min, indicating that the particles can be stabilized for long time by the excess amount of Pb^{2+} ion compared with the result for the stoichiometric amount shown in Figure 2-3(a). The stable spectra are also obtained with the excess amount of S^{2-} ion in the solution. The excess amount of ion in the solution depresses the dissolution of particles since the dissolution is controlled by the solubility product. This will restrain Ostwald ripening. However, the solubility product of PbS particles can not be estimated, since no peaks are observed in the absorption spectrum. As expected from Eq. 2-9, an excess

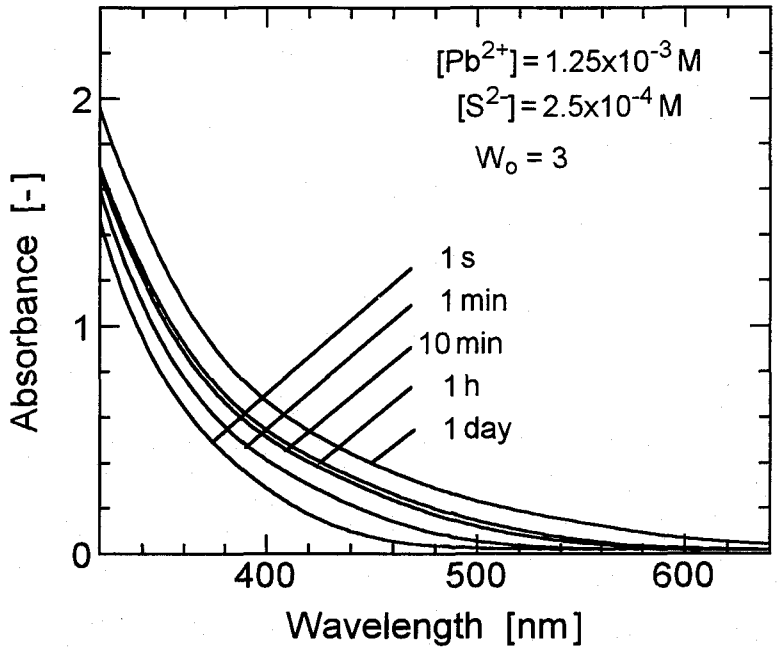

Figure 2–8 Change in absorption spectra of PbS particles prepared with excess amount of Pb^{2+} ion.

amount of S^{2-} ion (Hirai *et al.*, 1994) or the accompanying increases in the concentrations of both Pb^{2+} and S^{2-} ions can increase the conversion of the metallic ions to particles. The stable spectra of PbS particles are also obtained by the accompanying increases in concentrations of both reactants as shown in Figure 2–3(b).

4. Analysis of kinetics for rapid coagulation process

To study the mechanism of coagulation, the concentration of formed particles was calculated from the particle size data, and the amount of converted ions was estimated from the solubility product of the ultrafine particles. It was assumed that the lattice constants and density of particles were independent of particle diameter and that the formed particles were spherical and monodispersed. **Figure 2–9(a)** shows the results for CdS and ZnS particles. The results for PbS particles are shown in **Figure 2–9(b),** assuming that all supplied ions are converted to the particles. The

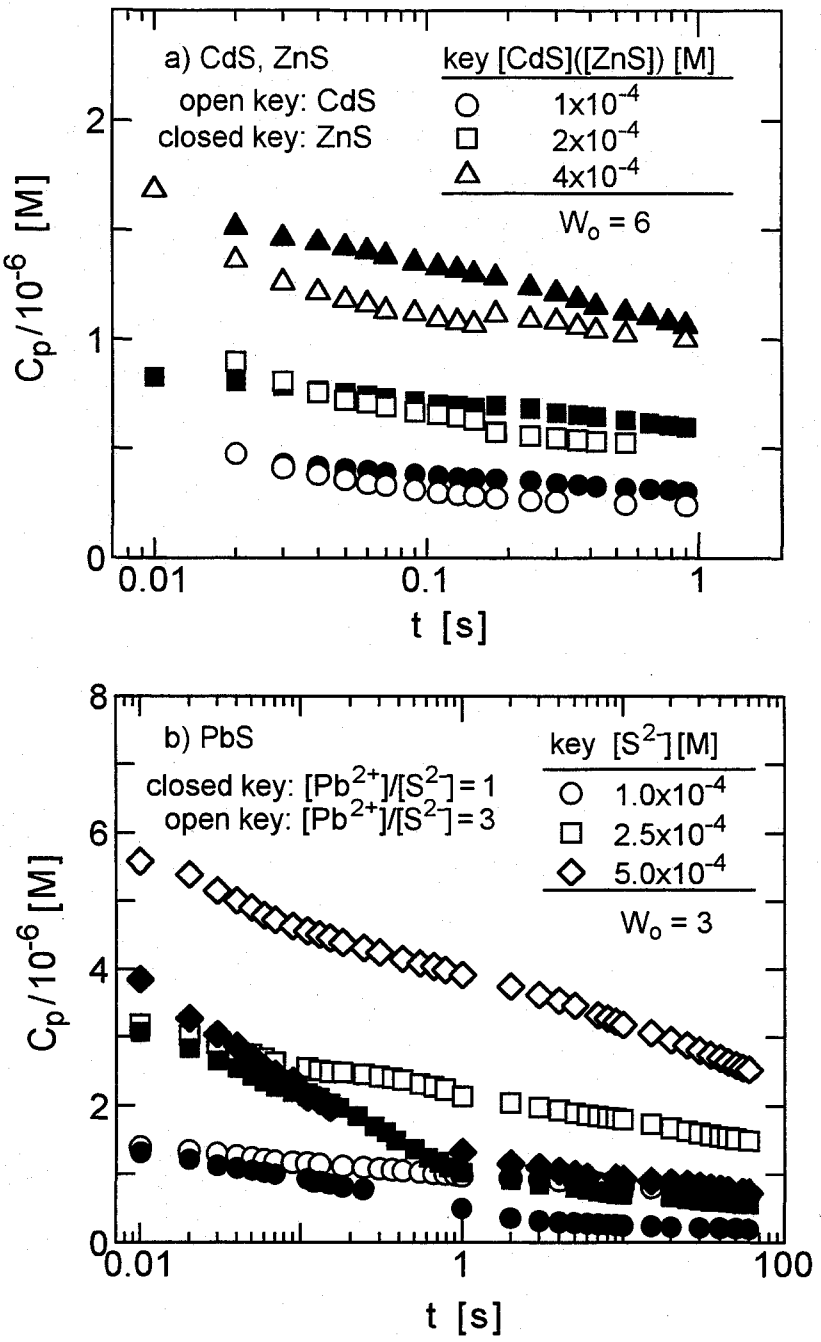

Figure 2–9 Time-course variation of concentration of particles. (a) CdS and ZnS particles; (b) PbS particles.

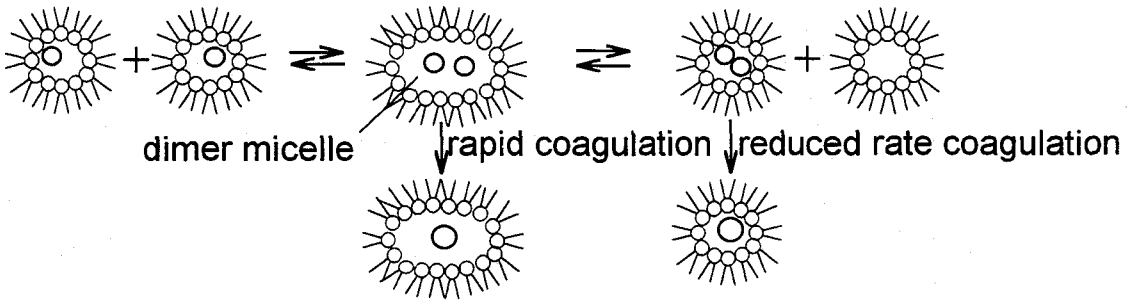

Figure 2–10 Coagulation process in reverse micelle.

concentration of particles is much less than that of the micelles shown in Table 2–1, decreases with time, and increases with increasing reactant concentration. Since the average number of particles per micelle is much less than unity, coagulation proceeds via an intermicellar process and it is therefore necessary to consider the rate for the intermicellar exchange process of reverse micelles.

The colloidal particles coagulate via the collision of particles. In the homogeneous system, when no barrier exists in the collision, the particles coagulate via a second-order kinetics and the rate constant (k_c) is identical to that of the diffusion-controlled rate constant (Smoluchowski, 1916) as follows,

$$- dC_p/dt = k_c C_p^2 \qquad (2\text{–}10)$$

When a barrier exists, the coagulation rate constant is restricted.

In the reverse micellar system, if coagulation is rapid and the concentration of particles is much less than that of the micelles, coagulation occurs via the fusion of two micelles containing particles as schematically shown in **Figure 2–10.** In this case, once a dimer micelle containing two or more particles is formed, the particles coagulate into a particle before the redispersion of the dimer micelle (rapid coagulation). The coagulation, therefore, proceeds via second-order kinetics and the rate constant is identical to the rate constant of the intermicellar exchange process. This rapid coagulation model has been presented by Towey *et al.* (1990). They analyzed

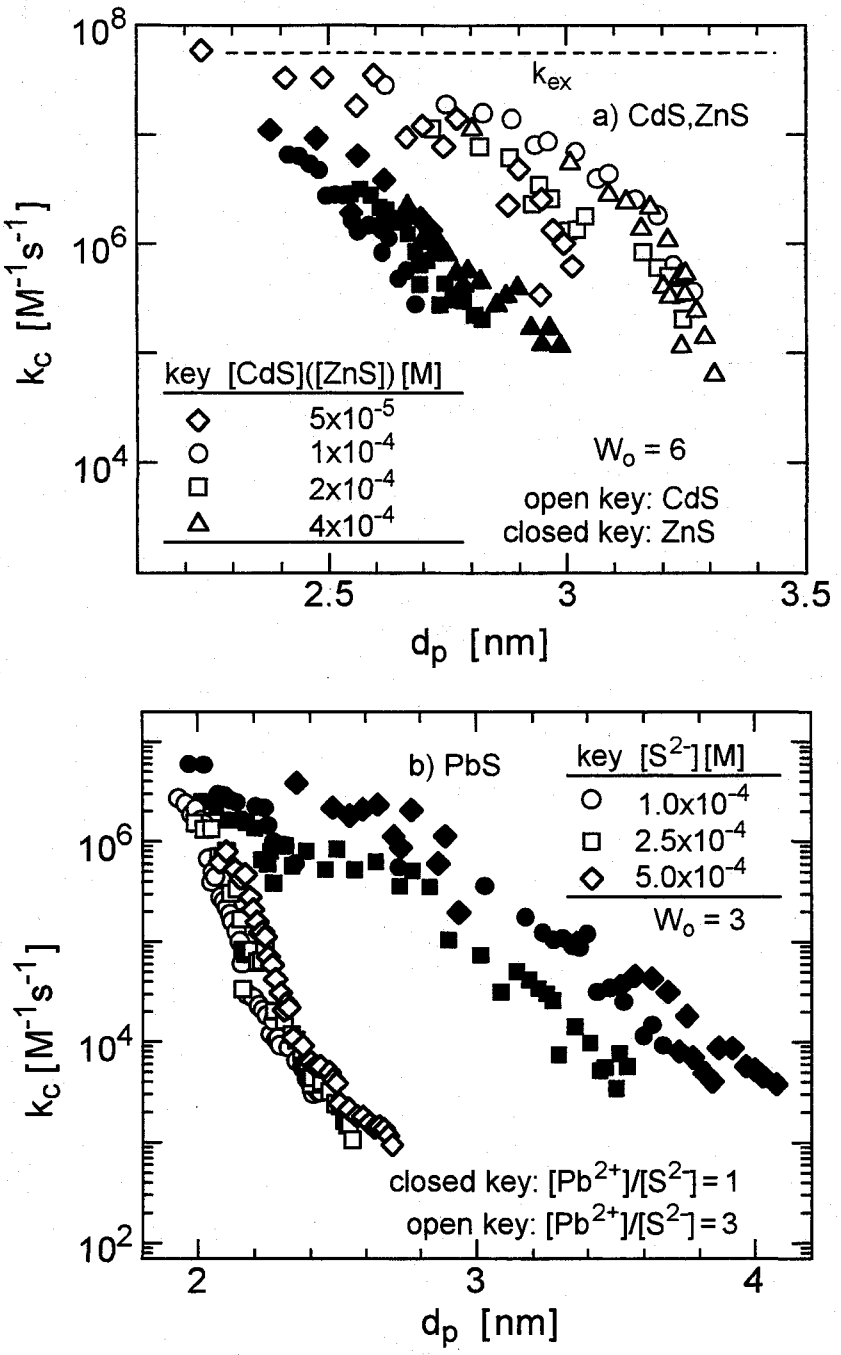

Figure 2−11 Relationship between second-order coagulation rate constants and particle diameter. (a) With various reactant concentrations (CdS, ZnS); (b) with various reactant concentrations (PbS); (c) with various water contents (CdS, ZnS); (d) with various water contents (PbS).

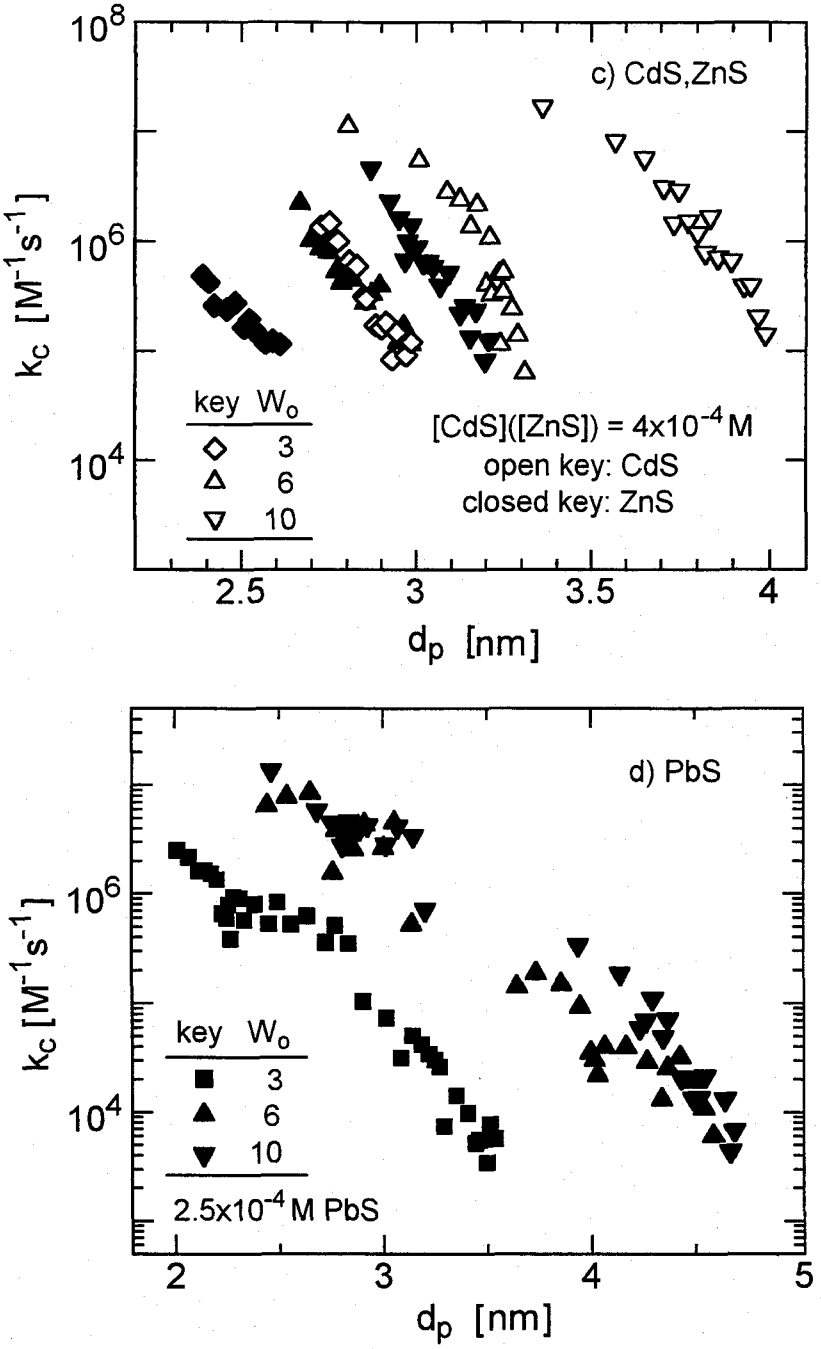

Figure 2–11 (continued)

the absorbance change at 280 nm in the initial stage up to 0.5 s using this rapid coagulation model and showed that the coagulation rate was controlled by the intermicellar exchange rate.

The results in the present study were analyzed in terms of second-order kinetics (Eq. 2-10). The coagulation rate constant, k_c, was calculated by dividing the rate of decrease in the concentration of particles ($-dC_p/dt$) by the square of the concentration (C_p^2). **Figures 2-11(a) and (b)** show the effect of reactant concentration on k_c for CdS and ZnS particles, and that for PbS particles, respectively. At the smallest limit of particle diameter, the values of k_c are seen to converge to a maximum value, which may correspond to the rate constant for the intermicellar exchange process (k_{ex}). The converged value is estimated as about 5.6×10^7 $M^{-1}s^{-1}$, for the $W_o = 6$ reverse micelles, which is between two reported values for k_{ex} for the AOT/isooctane reverse micelles (Fletcher *et al.*, 1987; Lang *et al.*, 1988). The effect of W_o on the coagulation rate constant is shown in **Figures 2-11(c) and (d),** with the coagulation rate constant increasing with increasing W_o.

The coagulation rate constant decreases with increasing particle diameter. Moreover, the value of k_c of CdS is greater than that of ZnS particles, for the same diameter. CdS particles coagulate faster than ZnS and accordingly the concentration of CdS particles is less than that of ZnS. Furthermore, the values of k_c of PbS particles decrease rapidly with increasing particle diameter when the 3-fold excess amount of Pb^{2+} ions are existing in the solution as shown in Figure 2-11(b). The rapid coagulation model of Towey *et al.* (1990) can be applicable only to the initial stage of the coagulation process, that is, to particles smaller than around 2.4 nm for CdS and ZnS particles and around 2.0 nm for PbS particles. The average diameter of the particles from mixing of the solutions was calculated from the rapid coagulation model by assuming an exchange rate constant of 5.6×10^7 $M^{-1}s^{-1}$, for the $W_o = 6$ reverse micellar

system. The calculation shows that the diameter of CdS particles increases up to 2.2 nm at $t = 0.02$ s, for the case of $[Cd(NO_3)_2] = [Na_2S] = 1 \times 10^{-4}$ M. This is smaller than the observed diameter of 2.6 nm shown in Figure 2-4(a). This difference may be caused by the problem in estimating the intermicellar exchange rate constant and by the effect of dead time in the stopped-flow measurement.

5. Analysis of kinetics for reduced rate coagulation process

When the particles achieve diameters greater than about 2.0-2.4 nm, the coagulation rate then decreases with particle size. Since the rate for the intermicellar exchange process is now greater than that for coagulation, the particles distribute among the micelles according to the same distribution as that of particles without coagulation, as a result of intermicellar exchange. In this case, coagulation occurs in micelles containing two or more particles as schematically shown in Figure 2-10. Since the average number of particles per micelle is less than unity, the coagulation rate is considered to be proportional to the concentration of such pregnant micelles (C_{mc}). Thus,

$$-dC_p/dt = k_{mc}\, C_{mc} \qquad (2\text{-}11)$$

where k_{mc} is the first-order rate constant for the reduced rate coagulation process taking into account the probability of coagulation. Assuming that the particles distribute according to a Poisson distribution (Atik and Thomas, 1981), the value of C_{mc} is given by,

$$C_{mc} = C_m \sum_{i=2}^{\infty} \left(\frac{C_p}{C_m}\right)^i \frac{\exp\left(-C_p / C_m\right)}{i!} = C_m \left\{1 - \sum_{i=0}^{1} \left(\frac{C_p}{C_m}\right)^i \frac{\exp\left(-C_p / C_m\right)}{i!}\right\} \qquad (2\text{-}12)$$

where C_m is the total concentration of micelles in the solution. The first-order coagulation rate constant, k_{mc}, was calculated by dividing the rate of decrease in the particle concentration ($-dC_p/dt$) by the concentration of micelles containing two or more particles (C_{mc}).

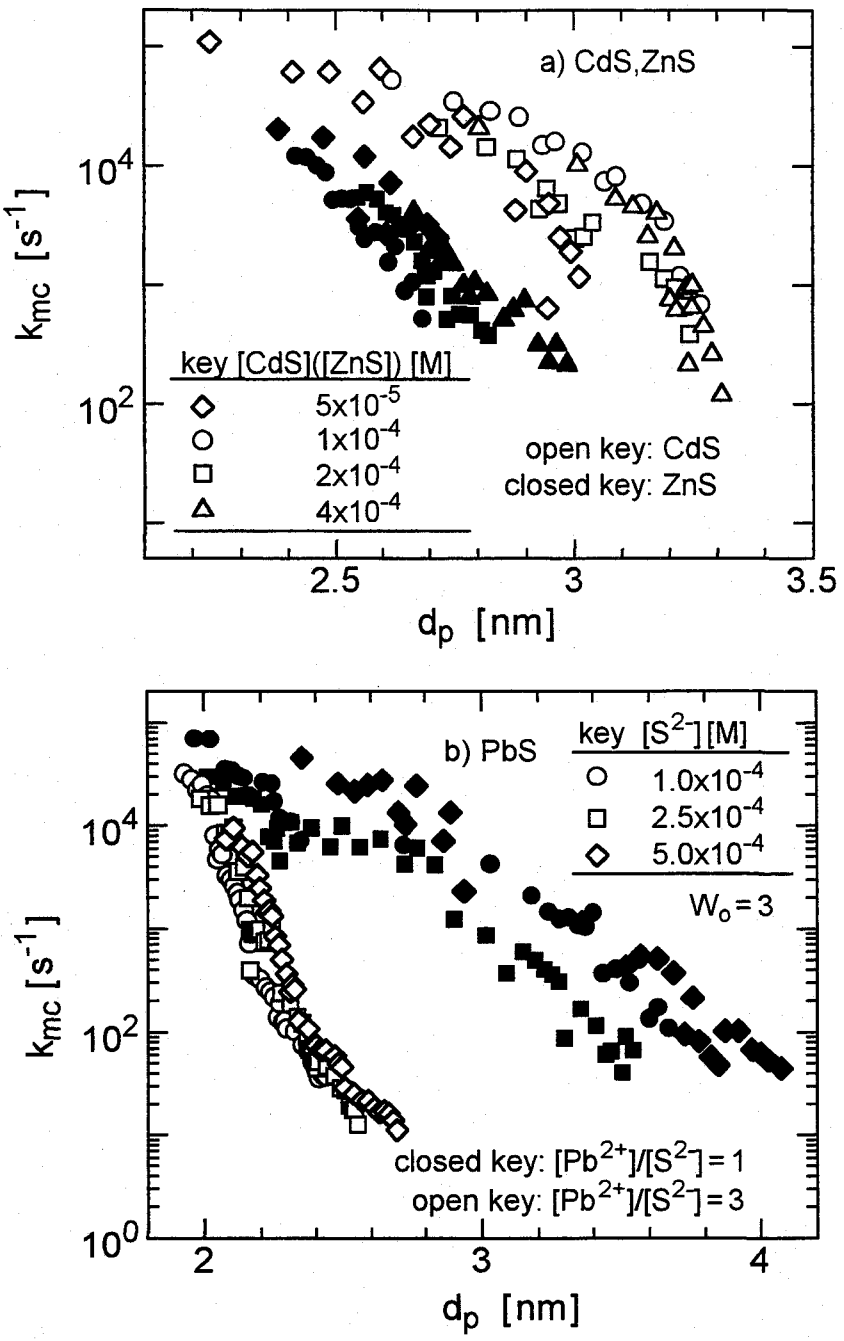

Figure 2−12 Relationship between first-order coagulation rate constants and particle diameter. (a) With various reactant concentrations (CdS, ZnS); (b) with various reactant concentrations (PbS); (c) with various water contents (CdS, ZnS); (d) with various water contents (PbS).

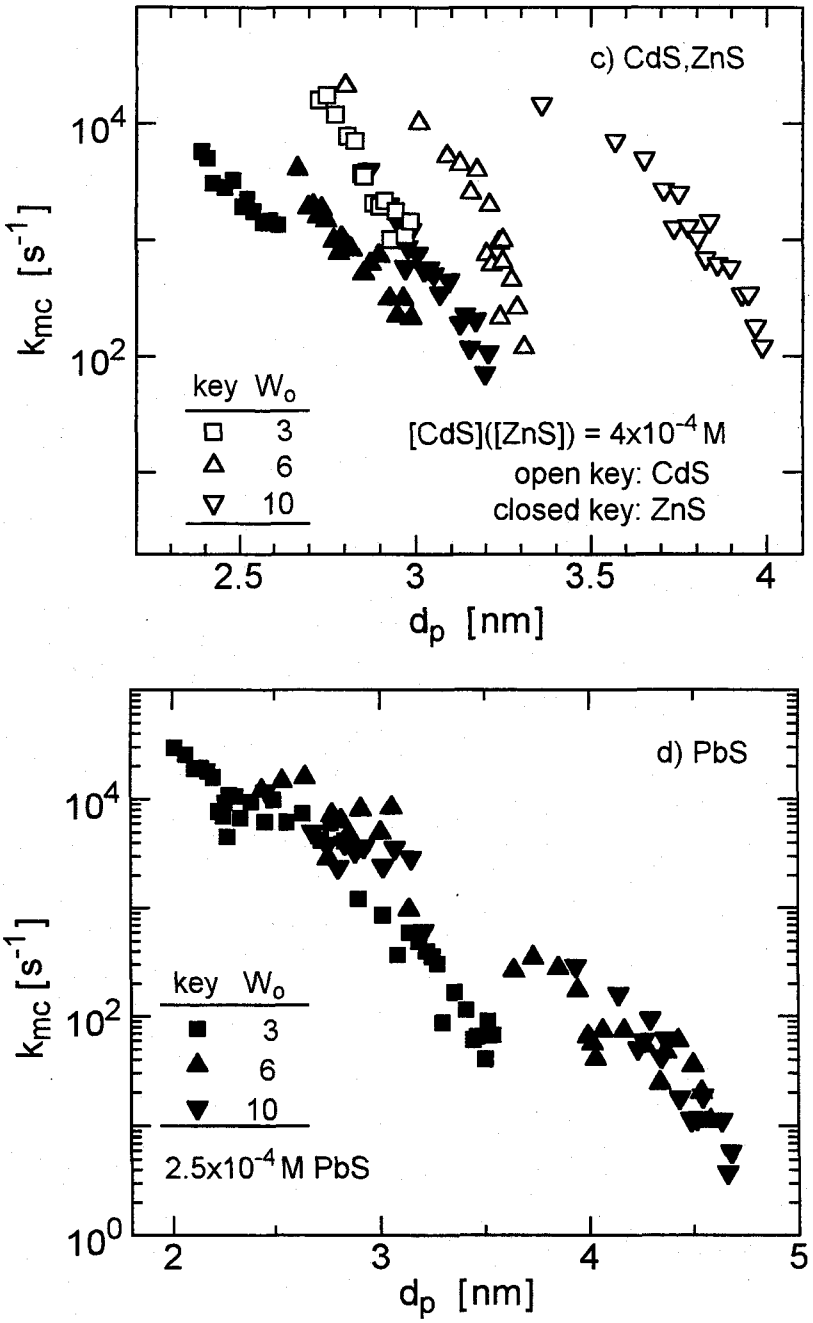

Figure 2–12 (continued)

The results are shown in **Figures 2-12(a), (b), (c), and (d).** The dependence of k_{mc} on W_o in Figures 2-12(c) and (d) is insignificant compared with that of k_c shown in Figures 2-11(c) and (d). This indicates that the kinetics of the reduced rate coagulation process can be expressed by Eq. 2-11 rather than Eq. 2-10 when d_p reaches the value (2.0-2.4 nm). The decrease in k_{mc} with increasing particle diameter is explained as follows. Assuming that the surface potential of the particles is independent of the particle diameter, the potential barrier between two particles will increase with increasing particle diameter (McCartney and Levine, 1969) and the coagulation rate will decrease. In the case of PbS particles, the coagulation rate constants of the particles prepared with excess Pb^{2-} ion decrease with increasing particle diameter more rapidly than those of the particles without any excess ions. This is possibly caused by the increase in the surface potential of particles due to the excess ion at the surface of the particles.

However, k_{mc} depends on the water content and the dependency for CdS particles is larger than that for ZnS particles as shown in Figure 2-12(c). The average diameter of CdS particles is larger than that of ZnS particles as shown in Figure 2-9 and approaches that of the micelles (Table 2-1). In the case of PbS particles, k_{mc} is almost independent of W_o when d_p is less than 2.7 nm. These results indicate an effect of the ratio of the sizes of the micelles and the particles on the coagulation rate. When the diameter of the particles approaches to that of the micelles, two effects on particle coagulation may appear. Firstly, a difficulty arises in the containment of two particles in any given micelle. This causes the decrease in the number of micelles containing two or more particles. Secondly, when the diameter of particle reaches that of the water core in the host micelle, the particle is surrounded by AOT molecules. Surfactant molecules at the surface of particle may then act as a protective

agent. Both effects possibly interfere with the coagulation of the particles. Therefore, the first-order coagulation rate constant decreases with decreasing micellar size, namely, decreasing water content.

Summary

The mechanism of formation of CdS, ZnS, and PbS ultrafine particles in AOT/isooctane reverse micelles by the reaction between $Cd(NO_3)_2$, $Zn(CO_3)_2$, or $Pb(NO_3)_2$ and Na_2S was studied. The particle formation process was followed by UV–visible absorption spectra. The following results were obtained:

1. In the cases of CdS and ZnS particles, the increase in absorbance caused by nucleation and particle growth occurs very rapidly and is complete within 0.02 s. A red-shift in the absorption threshold is observed after this period, expressing an increase in the particle diameter. This is caused by coagulation of particles. An increase in the reactant concentration or water content is found to increase the particle diameter. The diameter of ZnS particles is less than that of CdS particles.

2. The formation of PbS particles is also observed at 0.02 s after mixing. The stability of PbS particles is less than that of the other particles because of Ostwald ripening due to the relative large solubility of PbS. Stable PbS ultrafine particles can be prepared in the $W_o = 3$ reverse micellar solution with reactant concentration of 5×10^{-4} M. Ostwald ripening is depressed by the addition of the excess amount of Pb^{2+} or S^{2-} ions.

3. The coagulation rate was estimated by the rate of decrease in the concentration of particles. In the initial stage for times up to about 0.02 s, particle coagulation for all particles is controlled only by the rate for the intermicellar exchange process as shown by Towey *et al.* (1990). When the particles achieve diameters greater than about 2.0–2.4 nm, the coagulation rate

constant decreases with the particle size and becomes dependent on particle material. In this region, the coagulation kinetics is controlled by the statistical distribution of the particles among the micelles. When the particles have grown to be as large as the micelles, coagulation becomes restricted also by the micellar size.

Chapter III
Mechanism of Formation of Silver Halide Ultrafine Particles Using Solution Mixing Method

Introduction

In the previous chapter, a quantitative model for the formation of metal sulfide particles through fast reaction was proposed. To check the generality of this model, the analysis was extended to the case of the particles other than metal sulfide. Formation process of silver halide particles such as AgBr, AgCl, and AgI were studied in this chapter. Silver halides are important semiconductors and widely used in the photographic industry. Whereas AgI is a direct gap semiconductor, AgBr and AgCl are indirect gap semiconductors. A theoretical study about the size-dependent energy band structure of AgI ultrafine particles was reported by Rosseti *et al.* (1985). The spectral changes during particle formation were measured for AgI (Saijo *et al.*, 1982; Henglein *et al.*, 1989) and for AgBr (Tanaka *et al.*, 1985, Nedeljković *et al.*, 1991). In the case of AgI particles, a complicated spectral change was observed, which was related to the changes in the crystal structure and crystal shape (Saijo *et al.*, 1982).

Preparation of ultrafine AgBr particles in reverse micelles has been reported by Chew *et al.* (1990) and Johansson *et al.* (1992). Chew *et al.* (1990) reported also a kinetic analysis of the formation process, however, they measured the intensity of light scattering from particles that had already been out of ultrafine range. There have been no reports for the quantitative analysis of the formation process of silver halide particles in the ultrafine range performed in the reverse micelles. In this chapter, formation process of ultrafine AgBr, AgCl, and AgI was analyzed from the change in the UV-visible absorption spectra. The effects of water content of the system and

the reactant concentration on the process were also studied.

Experimental Section

Silver nitrate, sodium bromide, sodium chloride, and sodium iodide were supplied by Wako Pure Chemical Industries and isooctane (2,2,4-trimethylpentane) was supplied by Ishizu Seiyaku. These reagents were used without further purification. Distilled water was filtered with a 0.45-μm membrane filter and any dissolved oxygen was purged by Ar gas bubbling, prior to use. Sodium bis(2-ethylhexyl) sulfosuccinate (AOT) supplied by Tokyo Chemical Industry was purified following the method presented by Williams *et al.* (1957). In this work, 60 g of AOT was dissolved in 50 m*l* of methanol and treated with 20 g of activated carbon (Darco G-60) two times. This solution was then filtered and evaporated using a rotary evaporator. The AOT thus treated was stored under vacuum. The purification of AOT is essentially needed, since silver halides are known to form water soluble complexes with ligands such as alkali halide and thiosulfate ions (Sofen and Norland, 1986). In preliminary runs for the preparation of AgCl particles using AOT as received, a blue-shift in absorption threshold and a decrease in absorption intensity with time were observed after reaction for only 0.05 s. This suggests the dissolution of new-born ultrafine particles. This dissolution is possibly caused by some impurities in AOT. By using treated AOT, AgCl particles were found to grow at least for 1 s.

Preparation of silver halide particles, AgBr, AgCl, and AgI, was initiated by rapid mixing of a reverse micellar solution (1.2 m*l*) containing $AgNO_3$ and an equal volume of a reverse micellar solution containing NaBr, NaCl, or NaI. The other operations were the same as those for the metal sulfide particles described in Chapter II. The concentration of AOT was 0.1 M and the water content of the reverse micellar solution, W_o, was varied over the range 3-30.

Table 3−1 Reverse micellar systems used for preparation of silver halide particles ([AOT] = 0.1 M).

W_o [−]	d_m [nm]	σ_m [−]	$N_m/10^{20}$ [−]	$C_m/10^{-4}$ [M]
3	3.62	0.154	35.5	58.9
6	5.45	0.165	5.58	9.27
10	7.07	0.175	2.59	4.31
15	10.72	0.188	0.720	1.20
30	19.30	0.267	0.142	0.236

The size and concentration of the micelles are shown in **Table 3−1,** which are taken from Tables 1−1 and 2−1.

A stopped-flow spectrophotometer (Otsuka Electronics RA-401) equipped with a diode array detector (Otsuka Electronics RA-415) or a Hewlett-Packard 8452A diode array spectrophotometer was used to record the change in UV−visible absorption spectra of the solution, in the same manner as that performed in Chapter II. The band gap energy of semiconductor particles was estimated from the absorption spectra in the same manner as that used for the metal sulfide particles. Since AgI is a direct gap semiconductor, Eq. 2−6 is used for the estimation. On the other hand, AgBr and AgCl are indirect gap semiconductors and thus Eq. 2−7 is used.

Results and Discussion

1. Spectral change during particle formation

Figure 3−1 shows the UV−visible absorption spectra of AgBr particles measured during the reaction between 1 x 10^{-4} M $AgNO_3$ and 1 x 10^{-4} M NaBr in the $W_o = 6$ reverse micellar solution following the mixing of the solutions. The positions of the absorption threshold estimated using Eq. 2−7 are indicated

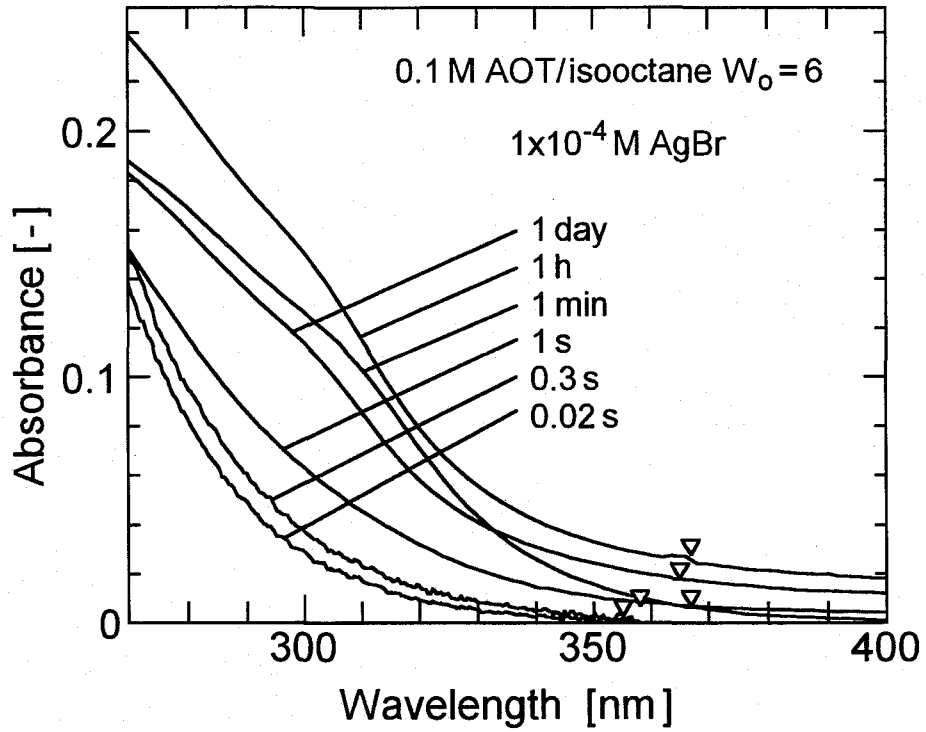

Figure 3-1 Change in absorption spectra during formation of AgBr particles .

with arrows on the corresponding spectra. Small drift of the base line of the spectra is seen. In such a case, the corrected values of absorbance based on the observed base line were used for the estimation. The absorption spectra showed characteristics of indirect gap semiconductors. The absorption of the formed particles appears at 0.02 s after mixing, indicating that the formation of particles by nucleation and particle growth proceed very rapidly. A red-shift in the absorption threshold with time up to 1 h is also seen. This indicates the decrease in band gap energy of AgBr particles caused by the increase in particle diameter. A continuous increase in absorbance up to 1 h is also observed. The magnitude of absorption of particles is related to the quantity of formed particles, but the observed increase in absorbance seems to be caused by the red-shift in the absorption threshold. On the other hand, a blue-shift in absorption threshold and a decrease in absorption magnitude are observed at 1 day after mixing. These changes are possibly attributed to the dissolution of

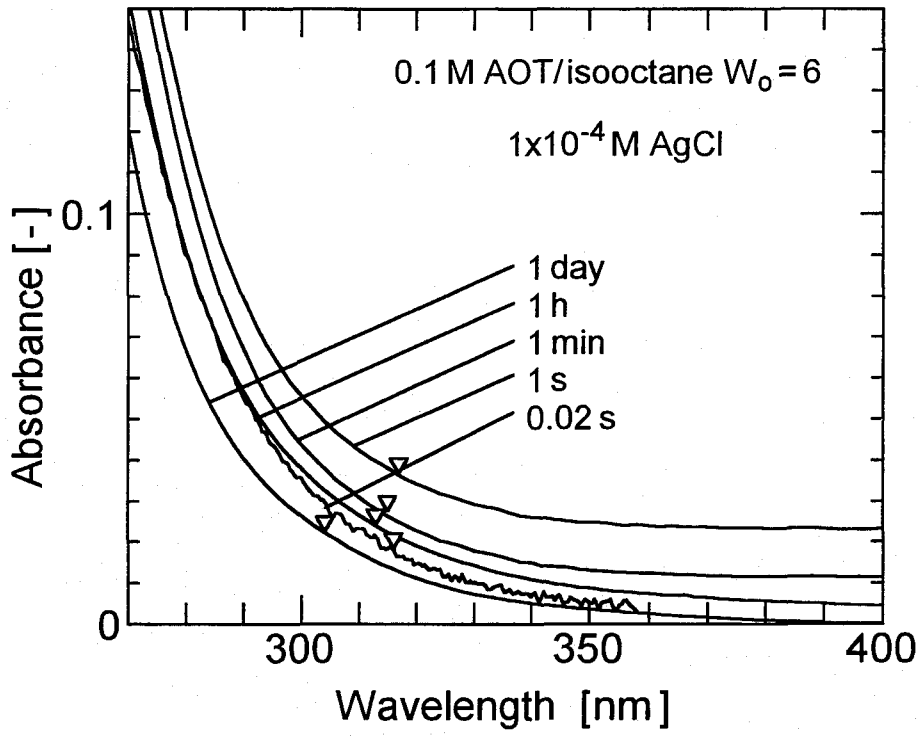

Figure 3–2 Change in absorption spectra during formation of AgCl particles .

particles. This dissolution becomes marked with increasing water content of the system.

Figure 3–2 shows the spectral change of AgCl particles measured during the reaction between 1 x 10^{-4} M $AgNO_3$ and 1 x 10^{-4} M NaCl in the $W_o = 6$ reverse micellar solution. The absorption threshold of AgCl particles is observed at a wavelength shorter than that of AgBr particles since the bulk band gap ($E_{g,bulk}$) of AgCl is greater than that of AgBr as shown in **Table 3–2.** The parameters in this table are obtained from Landolt-Börnstein New Series III 17b (1982) and references therein. Although small drift of base line of the spectra is seen, the increases in the absorption intensity and wavelength at absorption threshold are observed to be complete within 1 s after mixing. This suggests that the process of particle formation is complete within 1 s. The decrease in magnitude of absorption observed after this period is possibly caused by the dissolution of particles. The dissolution of AgCl particles is

Table 3-2 Parameters for silver halides.

Material	$E_{g,bulk}$ [eV]	$E'_{g,,bulk}$ [eV]	$\varepsilon/\varepsilon_0$ [-]	m_e/m_0 [-]	m_h/m_0 [-]	m^*/m_0 [-]	d [g/cm^3]
AgBr		2.5	4.62	0.215	0.645		6.4753
AgCl		3.0	3.02	3.92			5.5667
AgI	2.83		4.91			0.20	5.68

observed at a shorter reaction time than that of AgBr particles, indicating that the dissolution of AgCl particles is more marked than that of AgBr particles. The dissolution becomes marked with increasing water content as the case of AgBr.

Figures 3-3(a) and (b) show the spectral change of AgI particles in the $W_o = 6$ and $W_o = 30$ reverse micellar solutions, respectively. The absorption spectra show the characteristics of direct gap semiconductors. A peak is seen at around 425 nm in both cases at 1-10 min after mixing, which is attributed to an exciton transition in AgI particles. The exciton transition is not observed in the spectrum of ultrafine AgI particles smaller than the size of exciton (Berry, 1967). This suggests that the particles have grown as large as exciton diameter at this reaction time. After 1 h of reaction in the $W_o = 6$ reverse micellar solution, the absorption spectrum in Figure 3-3(a) shows the absorption towards wavelengths longer than bulk band gap position (438 nm). Both the light scattering from large particles and some visible particles are observed in this solution. At a reaction time of 1 day, the absorption of particles is almost diminished, and the settled particles are observed at the bottom of the reactor. These results indicate that the formed AgI particles are not stable at the ultrafine state in this condition. On the other hand, in the case of $W_o = 30$ solution, the intensity of light scattering at 1 h is small (Figure 3-3(b)) and no visible particles are observed. This shows that the stability of AgI ultrafine

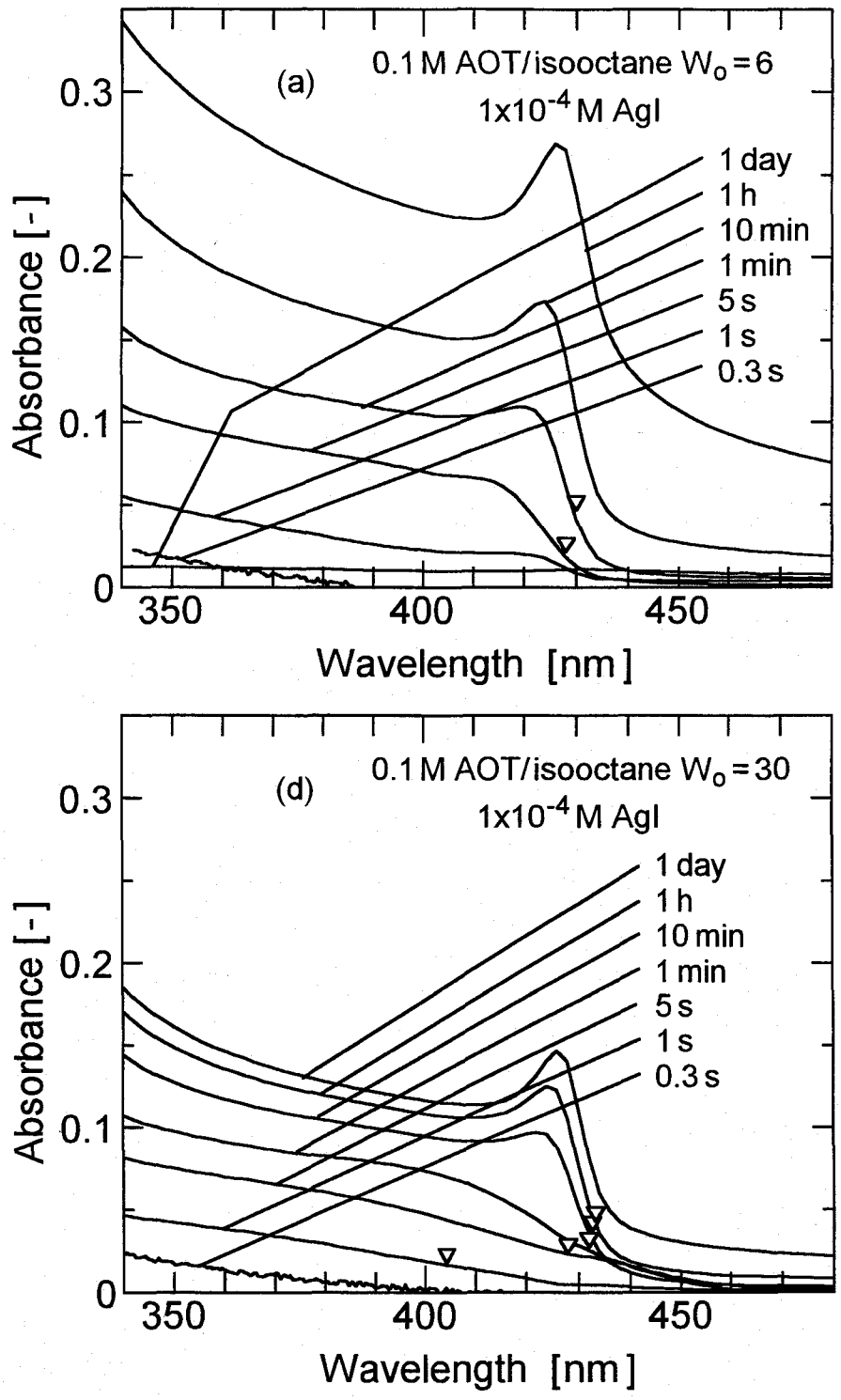

Figure 3–3 Changes in absorption spectra during formation of AgI particles in reverse micelles. (a) $W_o = 6$; (b) $W_o = 30$.

particles increases with increasing water content. The cause of this result will be discussed in the later section.

2. Estimation of particle diameter

The diameter of silver halide particles was estimated using Eq. 2-4 by the band gap energy in the same manner as that used for the CdS and ZnS particles. Rosetti *et al.* (1985) found that the dependence of band gap energy on particle diameter of ultrafine AgI particles satisfied this equation. The electric parameters shown in Table 3-2 were used for the estimation. Since the effective mass of hole in AgCl has not been reported, the size of AgCl particles can not be estimated from the absorption spectrum.

Figures 3-4(a) and (b) show the estimated diameters of AgBr and AgI particles, respectively, at various reaction times. The diameters of AgBr particles are seen to increase with increasing reaction time, concentrations of reactants, and water content. These are the similar results as observed in the cases of metal sulfide particles. The diameter of AgI particles is greater than that of AgBr particles when prepared under the same conditions. Until the diameter achieves about 4.5 nm, the diameter increases with increasing reactant concentration as in the case of AgBr particles. In this region, the diameter also increases with increasing water content up to 10, and then decreases.

The effect of water content on the size of AgCl particles was also investigated. Since the size of AgCl particles could not be estimated by the band gap energy, it was studied from the absorption spectra shown in **Figure 3-5.** The wavelength of absorption threshold slightly decreases with increasing water content. This tendency is opposite to the cases of AgBr and metal sulfide particles. This is possibly caused by the dissolution of AgCl particles since it becomes marked with increasing water content.

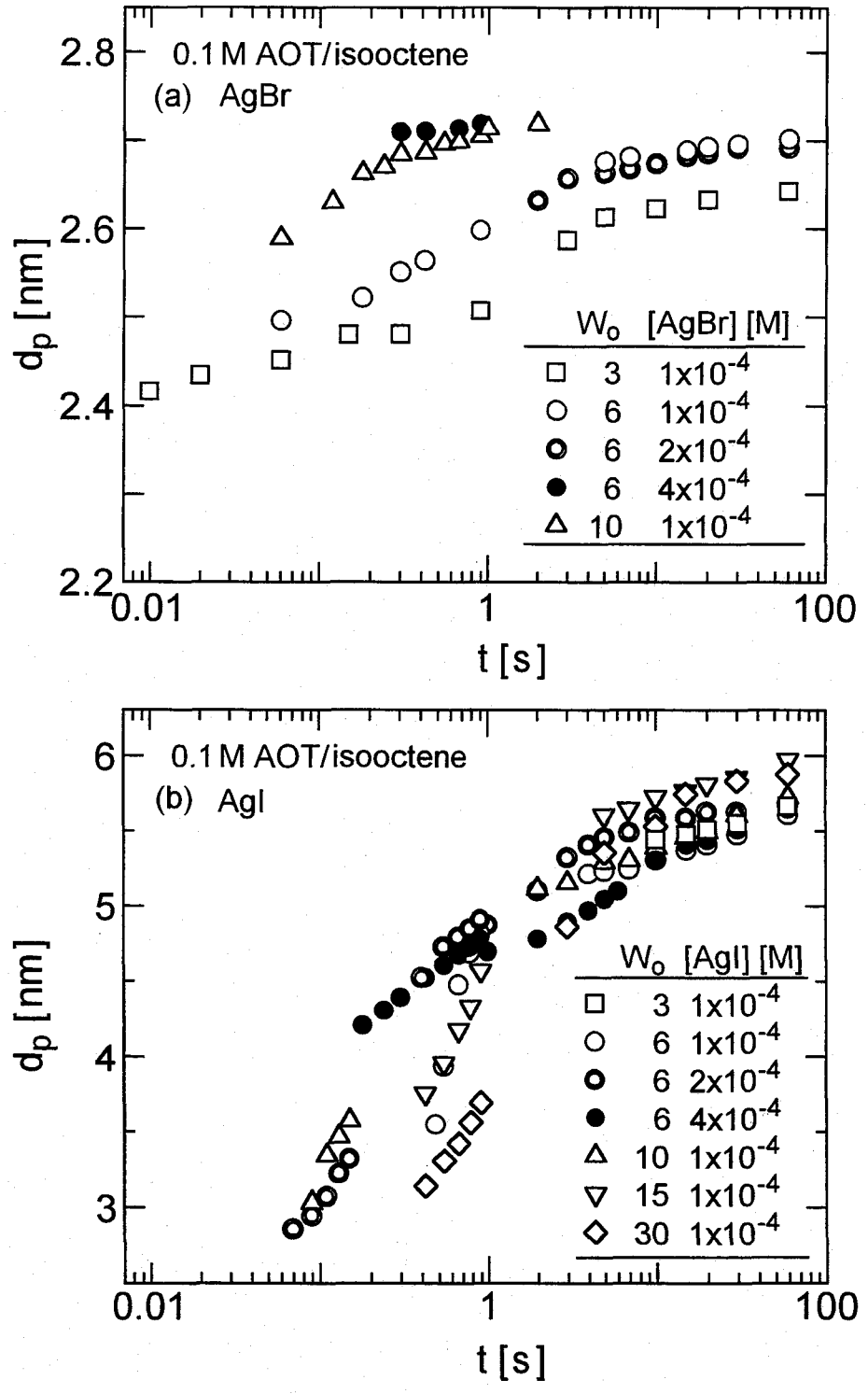

Figure 3–4 Effects of reactant concentration and water content on the size of particles. (a) AgBr; (b) AgI.

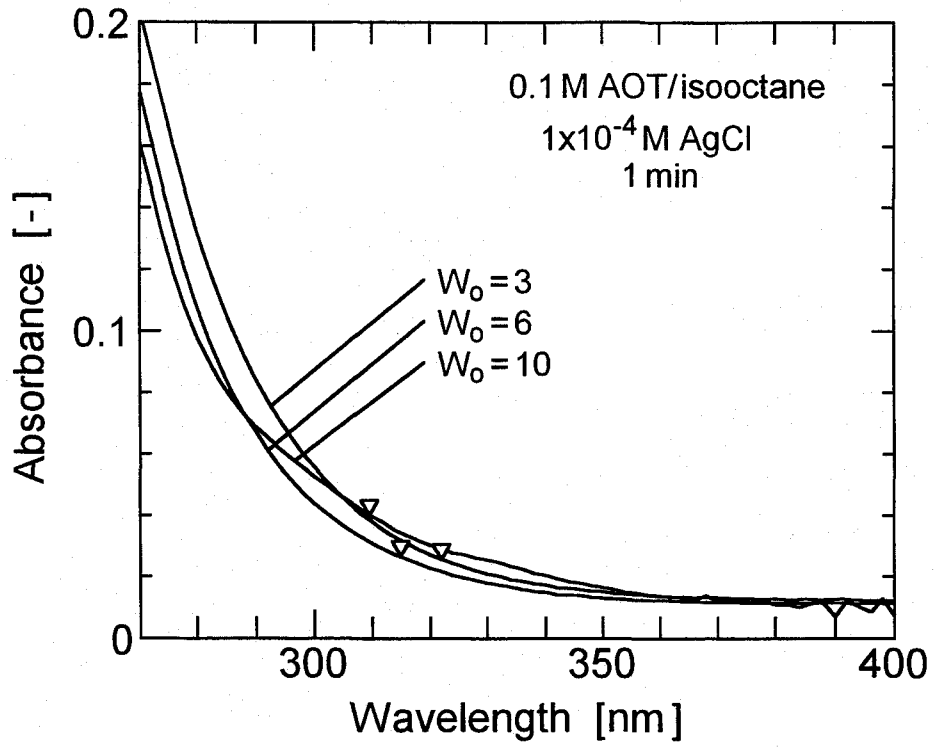

Figure 3–5 Effect of water content on absorption spectra of AgCl particles.

3. Analysis of kinetics for rapid coagulation process

Nucleation and particle growth of AgBr particles are very fast and seen to be complete within 0.02 s. The concentration of formed particles was calculated from the particle size data in the same manner as that used for the metal sulfide particles in Chapter II by assuming that all the precursor ions were converted to particles. The results for AgBr and AgI particles are shown in **Figures 3–6(a) and (b),** respectively. The concentration of particles decreases with time and increases with increasing reactant concentration. The concentration of particles is less than that of the micelles shown in Table 3–1, showing that the coagulation proceeds via an intermicellar process and that it is therefore necessary to consider the exchange process of the reverse micelles. The time-course change in the concentration of particles was thus analyzed based on the coagulation kinetics. At first, the coagulation kinetics was analyzed by a second-order kinetics. The second-order coagulation rate

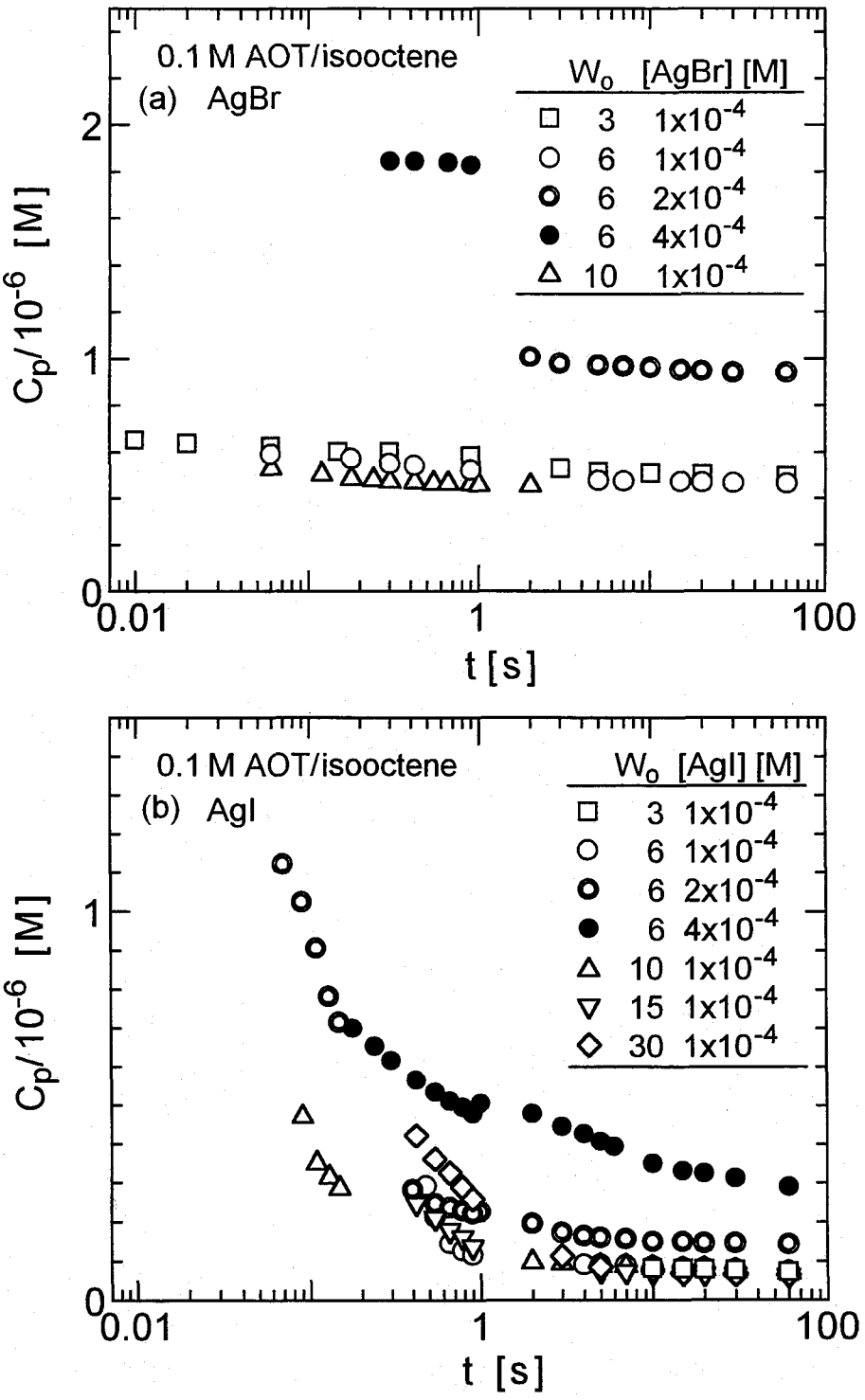

Figure 3-6 Time-course variation of concentration of particles.
(a) AgBr; (b) AgI.

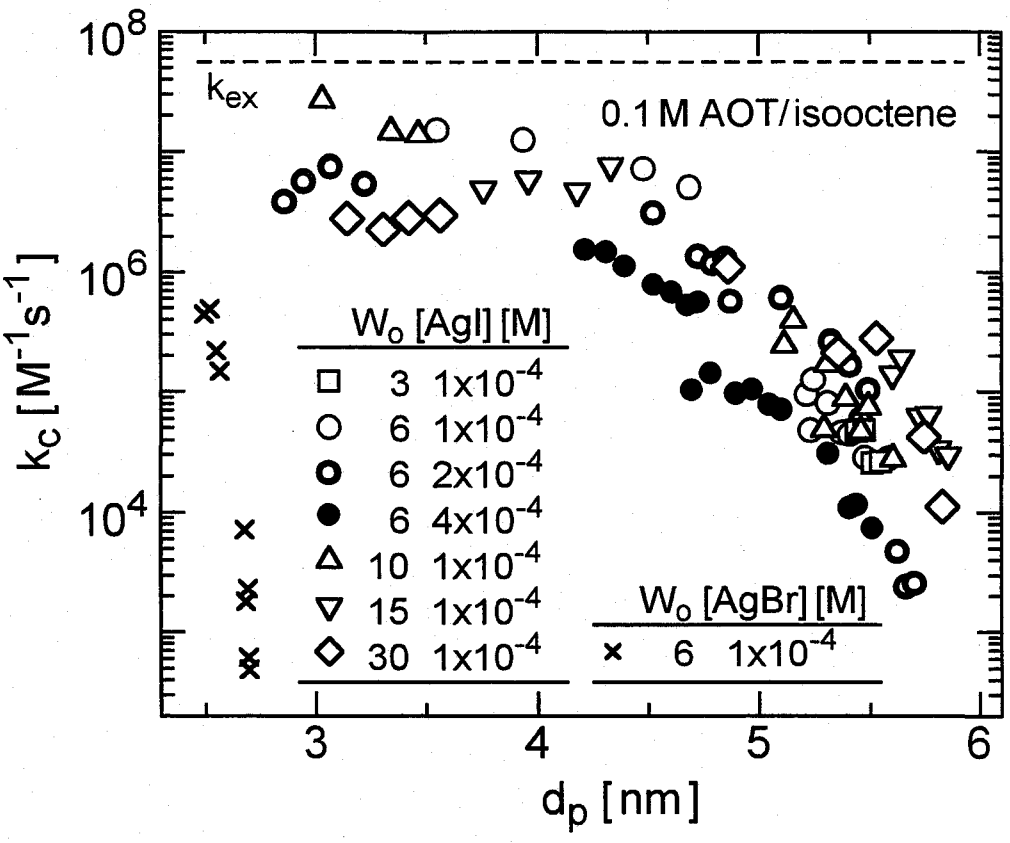

Figure 3–7 Second-order coagulation rate constant of AgBr and AgI particles.

constant, k_c, was calculated from the rate of decrease in the concentration of particles using Eq. 2–10.

Figure 3–7 shows the relationship between the rate constant and particle diameter of AgBr and AgI particles. The values of k_c of AgBr particles decrease with increasing particle diameter more quickly than those of AgI particles. The values for AgI particles are almost independent of particle diameter at the diameters smaller than about 4.5 nm. In this region, the values are close to an estimated value for the rate constant of the exchange process of the $W_o = 6$ reverse micelles obtained by the analysis of coagulation kinetics of CdS particles described in Chapter II, $k_{ex} = 5.6 \times 10^7\ M^{-1}s^{-1}$. This indicates that coagulation in this region can be expressed by the rapid coagulation model proposed by Towey *et al.* (1990). The value of k_c in this d_p region slightly

decreases with increasing water content of the system. This result suggests that the exchange rate constant of reverse micelles depends on water content. The effect of water content on the intermicellar exchange rate constant has been investigated and two contrary results have been reported. Fletcher *et al.* (1987) reported a decrease in the rate constant with increasing water content using three different reactions. Verbeeck and DeSchryver (1987) and Lang *et al.* (1988) reported an increase using the other reactions. The actual effect of water content on k_{ex} has not been clarified. The intermicellar exchange process is, therefore, possibly affected by the solubilized ions as well as water content.

4. Analysis of kinetics for reduced rate coagulation process

The coagulation rate constants, k_c, of AgBr particles in the whole range and of AgI particles greater than 4.5 nm decrease with increasing particle diameter as observed in the case of the metal sulfide particles. The coagulation process is no longer controlled by the intermicellar exchange rate in these cases. A model for the coagulation process slower than the intermicellar exchange process was applied as the case of the later part of the coagulation process of the metal sulfide particles. The first-order rate constant for the coagulation in micelles containing two or more particles, k_{mc}, was calculated using Eqs. 2-11 and 2-12.

Figures 3-8(a) and (b) show the effects of the reactant concentration and water content on the first-order coagulation rate constant (k_{mc}) of AgBr and AgI particles. The values of k_{mc} of AgBr particles shown in Figure 3-8(a) are almost independent of reactant concentration, although some scatters of the data are seen. This indicates that the coagulation kinetics is controlled by the concentration of micellar droplets pregnant with two or more particles. The range of the reactant concentration is hardly extended because of the drift of the base line of the spectrum and difficulty in the solubilization of a large

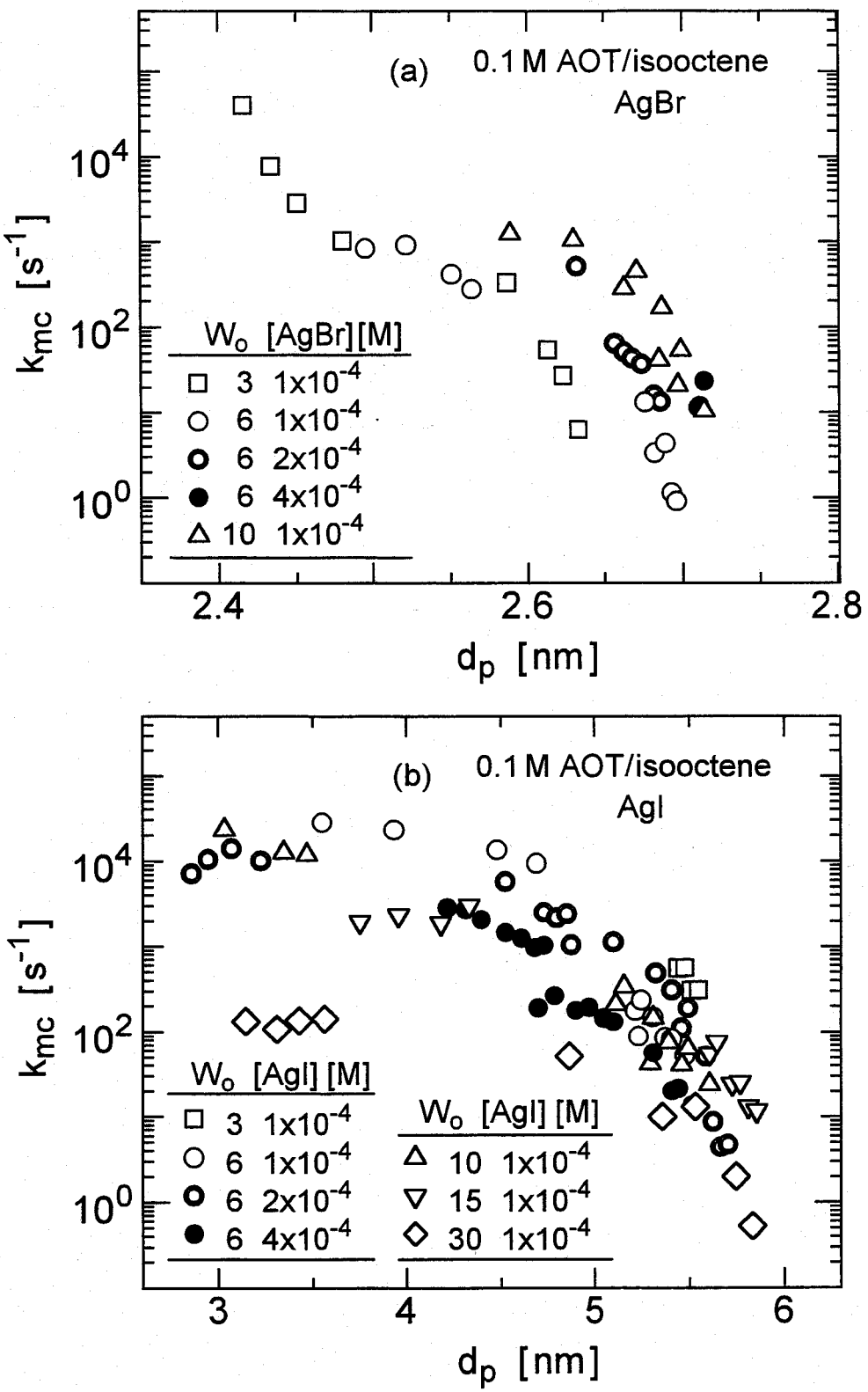

Figure 3–8 Effects of reactant concentration and water content on first-order coagulation rate constant. (a) AgBr; (b) AgI.

concentration of reactants into the reverse micelles. The effect of water content on the size of formed AgBr particles shown in Figure 3-4(a) can be explained from the concentration of the reverse micellar droplets. Since the total concentration of the micellar droplets decreases with increasing water content as shown in Table 3-1, C_{mc} increases and therefore the coagulation rate increases. On the other hand, the values of k_{mc} at a given diameter decreased with decreasing water content. Since the size of the micelles decreases with decreasing water content as shown in Table 3-1, the variation of k_{mc} with water content may be caused by a restraint on the rate of coagulation by the micellar interface owing to an approach in the relative sizes of the micelles and particles and to the deviation in the distribution of particles from Poisson distribution as observed in the case of CdS particles in Chapter II.

Figure 3-8(b) shows the results for AgI particles. When diameter is greater than 4.5 nm, the values of k_{mc} are almost independent of reaction conditions. This indicates that coagulation in this region is controlled by C_{mc} and independent of the intermicellar exchange rate as observed in the case of AgBr particles. The coagulation rate constants of AgI particles for the $W_o = 3$ case are slightly larger than those for the other W_o cases. This is a contrary result of AgBr, CdS, ZnS, and PbS particles. The diameter of AgI particles is greater than that of AgBr particles and reaches a value around 6 nm. The size of particles is likely to exceed that of the micelles shown in Table 3-1 in low water content solution and thus the particles are likely to coagulate at outside of the micelles. Actually, visible particles are observed to be settled after 1 day of reaction in the $W_o = 3$ and 6 solutions. Hence, this model can not be applicable when the particles grow much larger than the size of the micelles. On the other hand, when water content is greater than 6 and the diameter of AgI particles is greater than 4.5 nm, the diameter slightly increases with increasing water content as shown in Figure 3-4(b). This can be explained by

the decrease in total concentration of the micellar droplets as the case of AgBr particles.

Summary

The mechanism of formation of ultrafine silver halide semiconductor particles in AOT/isooctane reverse micellar systems by the reaction between silver ion and halide ion was studied. The particle formation process was followed by UV-visible absorption spectra and the following results were obtained:

1. The formation process of silver halide particles is seen to be very fast and succeeding coagulation of the particles is observed as in the case of the metal sulfide particles. The diameter of formed AgBr and AgI particles increases with increasing reactant concentration and water content as observed for the metal sulfide particles. AgI particles can grow larger than the reverse micelles in low water content solution and tend to form visible particles. The value of the size of AgCl particles could not be estimated since the effective mass of hole in AgCl had not been reported.

2. The dissolution of formed AgBr and AgCl particles into the solution is observed. This is possibly induced by some impurities in AOT. The dissolution of AgCl particles is more significant than that of AgBr particles. The dissolution becomes marked with increasing water content, and thus the size of formed AgCl particles decreases with increasing water content.

3. The kinetics of initial stage of coagulation of AgI particles is controlled by the rate of exchange process until the diameter achieves about 4.5 nm. The rate of coagulation of whole range of AgBr particles and AgI particles greater than 4.5 nm can be expressed in the same way as that for the metal sulfide particles, by the first-order kinetics with respect to the concentration of micellar droplets containing two or more particles. The rate constant decreases with increasing diameter of particles.

Chapter IV
Mechanism of Formation of Ultrafine Particles Using Gas Injection Method

Introduction

In Chapters I, II, and III, the reactants were fed into reverse micelles by means of the solution. Ultrafine particles are also prepared in the reverse micelles by injection of reactant gas into the reverse micellar solution containing another reactant (gas injection method). The preparation of CdS (Meyer *et al.*, 1984), $CaCO_3$ (Kandori *et al.*, 1988), Cu (Lisiecki and Pileni, 1993), and Rh (Kishida *et al.*, 1995) ultrafine particles by this method has been reported. This method is important practically since the amount and rate of injection of the reactant can be controlled over the wide range and further since the volume of the solution does not increase by the addition of reactants. There have been reported no kinetic studies of formation process of ultrafine particles using the gas injection method.

It is now necessary in this work to extend the kinetic studies for the solution mixing method in Chapter II to the gas injection method from the investigation of the mechanism of formation of metal sulfide particles by the injection of H_2S gas into reverse micelles. Here the gas absorption step is possibly the slowest and the time involved for the injection of gas into the system is certainly much greater than that for the conversion of the ions to the particles in the micelles. The whole process from the dissolution of H_2S into the organic phase (gas absorption), the transfer of H_2S from the organic phase to the water cores in the reverse micelles, and the formation of particles in the water cores was followed using the continuous measurement of absorption spectra. A kinetic scheme for the steps in particle formation was proposed, based on the findings for both gas injection and solution mixing methods.

Experimental section

1. Preparation of particles

Sodium bis(2-ethylhexyl) sulfosuccinate (AOT), cadmium nitrate, zinc nitrate, and sodium sulfide were supplied by Wako Pure Chemical Industries, hydrogen sulfide was supplied by Sumitomo Seika, and isooctane (2,2,4-trimethylpentane) was supplied by Ishizu Seiyaku. All reagents were used without further purification. Distilled water was filtered using a 0.45−μm membrane filter and any dissolved oxygen was purged by Ar gas bubbling, prior to use. The reverse micellar solutions containing $Cd(NO_3)_2$ and $Zn(NO_3)_2$ were prepared in the same manner as described in Chapter II. The water content of the solution was varied in the range 3−10.

CdS particles were prepared by the injection of H_2S into a reverse micellar solution containing $Cd(NO_3)_2$, using a gas-tight syringe (Hamilton Co.). The quantity of gas injected was only a few percent greater than the stoichiometric amount. The time duration of the gas injection varied from 2 s (rapid gas injection method) to 13 s (intermittent gas injection method). The instant when the injection was started was defined as $t = 0$ s. The temperature of the reverse micellar solution was maintained at 25 ℃. $Zn(NO_3)_2$ was employed for the preparation of ZnS ultrafine particles instead of $Cd(NO_3)_2$. Otherwise, the operations were the same as those for CdS particles.

2. Measurements

A Hewlett-Packard 8452A diode array spectrophotometer was used to record the spectral change of the micellar solution following the injection of H_2S. H_2S was injected into a quartz cell containing the reverse micellar solution (3 m*l*) dissolving $Cd(NO_3)_2$ with mild stirring generated by a magnetic stirrer, for the measurement of spectra of periods from $t = 1$ s to 3 min. With

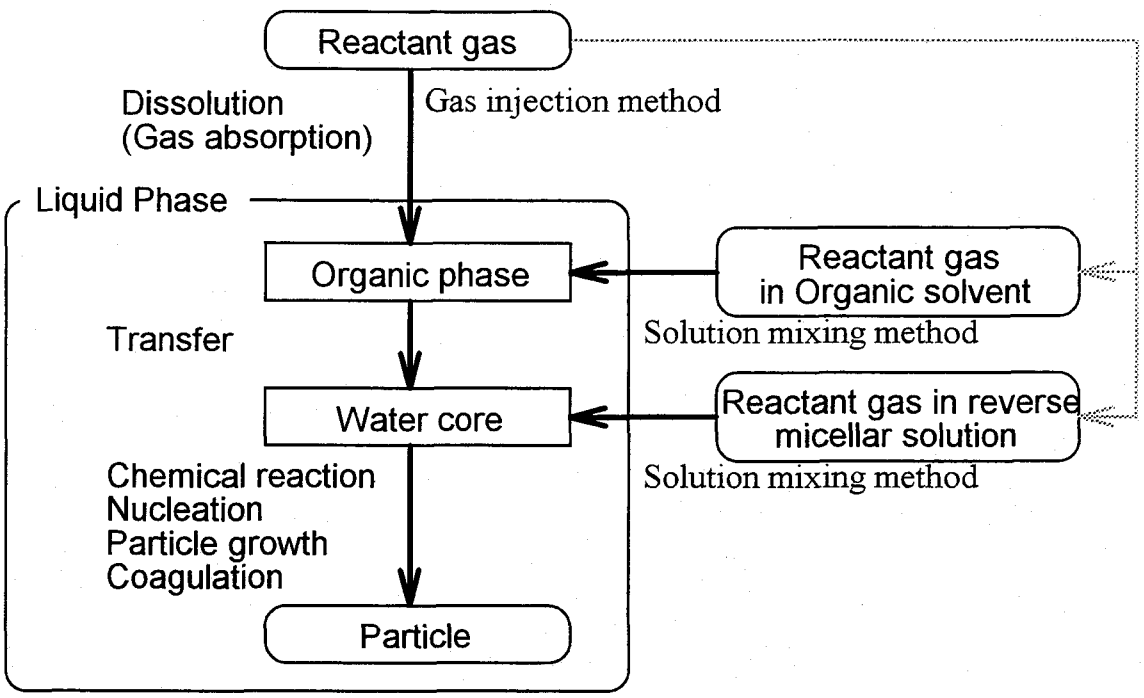

Figure 4-1 Schematic diagram of particle formation processes from reactant gas.

the reaction times (t) greater than 10 min, the reaction was performed in a beaker-type glass reactor (20 ml) with lid. H_2S was injected into 10 ml of the reverse micellar solution in the reactor. When injection was complete, the reactor was sealed and shaken by hand. The solution in the reactor was transferred to a quartz cell in order to measure the absorption spectra as required. The diameter of the formed particles was estimated from the band gap energy as determined by the absorption spectra using the equation proposed by Brus (1984) and as described in Chapter II.

Results and Discussion

1. Spectral change during particle formation

A schematic picture of the particle formation processes from reactant gas is illustrated in **Figure 4-1.** In the case of preparation of CdS particles by the

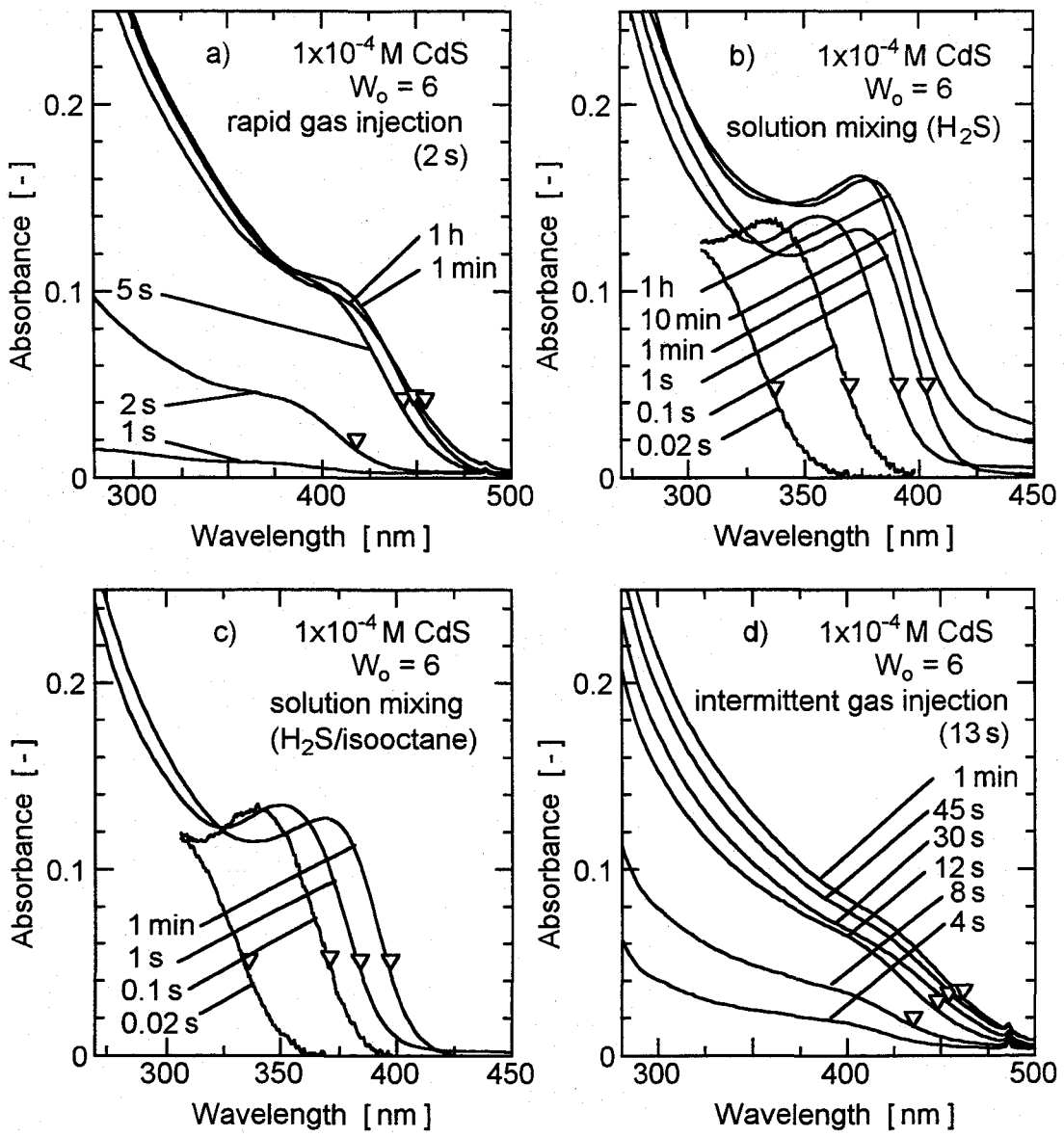

Figure 4–2 Change in absorption spectra during preparation of CdS particles using various feeding conditions of H_2S. (a) rapid gas injection method in 2 s; (b) solution mixing method using H_2S dissolved in reverse micellar solution; (c) solution mixing method using H_2S dissolved in isooctane; (d) intermittent gas injection method in 13 s.

gas injection method using H_2S as reactant, the process includes dissolution of H_2S into the organic continuous phase in the reverse micellar solution, transfer of H_2S from the organic phase to the water cores in the micelles, and chemical reaction between Cd^{2+} ion and S^{2-} ion in the water cores. There are some other feeding methods of H_2S into the water cores in the reverse micelles containing the other reactants using H_2S dissolved in solution by the solution mixing method.

UV–visible absorption spectra of the solution during preparation of CdS particles under different H_2S feeding conditions are shown in **Figures 4–2(a), (b), (c), and (d).** Figure 4–2(a) shows the change in the spectra observed during the formation of CdS particles using the rapid gas injection method, for H_2S gas injection in 2 s. An increase in absorption intensity for times up to $t = 5$ s and a continuous red-shift in absorption threshold shown by the small arrows are observed. The former effect indicates the increase in the quantity of the formed particles and the latter indicates the decrease in band gap energy caused by the increase in particle diameter. The conversion of the precursor ions (Cd^{2+} and S^{2-}) for both nucleation and particle growth is seen to be complete by 5 s. The absorbance at the wavelength of shoulder peak measured after $t = 5$ s is therefore expected to indicate the total quantity of ions converted to the particles. There is an adequate quantity of H_2S to convert all the metallic ions, as the absorbance increases with increasing quantity of H_2S up to the stoichiometric value but is then almost unchanged by further increase. This confirms that the stoichiometric quantity of H_2S is almost sufficient to convert all the metallic ions.

The period required to obtain complete conversion of the ions to the particles (5 s), for the gas injection method, is much greater than that needed using the solution mixing method shown in Figure 2–1 (0.02 s). Several experiments were carried out, the manner in which the H_2S was supplied to the

micellar solution was varied. Firstly, an adequate quantity of H_2S was injected into a reverse micellar solution and this solution was rapidly mixed with the equal volume of another reverse micellar solution containing $Cd(NO_3)_2$. This is the same approach as that used in a previous solution mixing method using Na_2S as a reactant, but here using H_2S as the S^{2-} source. The resulting spectral change is shown in Figure 4-2(b). Here, the absorption of the formed particles is observed at 0.02 s after mixing, and thus indicating that H_2S dissolved in the reverse micelles reacts with the Cd^{2+} ion very rapidly as the case of Na_2S. Secondly, the kinetics of the transfer of H_2S from the organic phase to the water cores was examined. In this case, H_2S was dissolved in pure isooctane rather than reverse micellar solution and this was mixed with the equal volume of reverse micellar solution containing $Cd(NO_3)_2$. The feed reverse micellar solution contained double the quantity of surfactant to make the resultant surfactant concentration the same as that of the other cases. The spectral change obtained is shown in Figure 4-2(c). Here there is no significant difference between the data shown in Figure 4-2(b) and Figure 4-2(c), thus indicating that the transfer from the organic phase to the micellar water core also proceeds very rapidly. With H_2S injection for 13 s, an increase in absorption intensity is observed for times up to 30 s as shown in Figure 4-2(d). The dissolution of H_2S into the organic phase (gas absorption) is, therefore, the dominant rate-determining step in the overall particle growth process.

Data for the gas injection and solution mixing methods obtained at 10 min after the initiation are compared in **Figures 4-3(a) and (b).** The absorption threshold wavelength for the gas injection method is longer than that for the solution mixing method. The size of the particles prepared by the gas injection method is, therefore, greater than that for the solution mixing method.

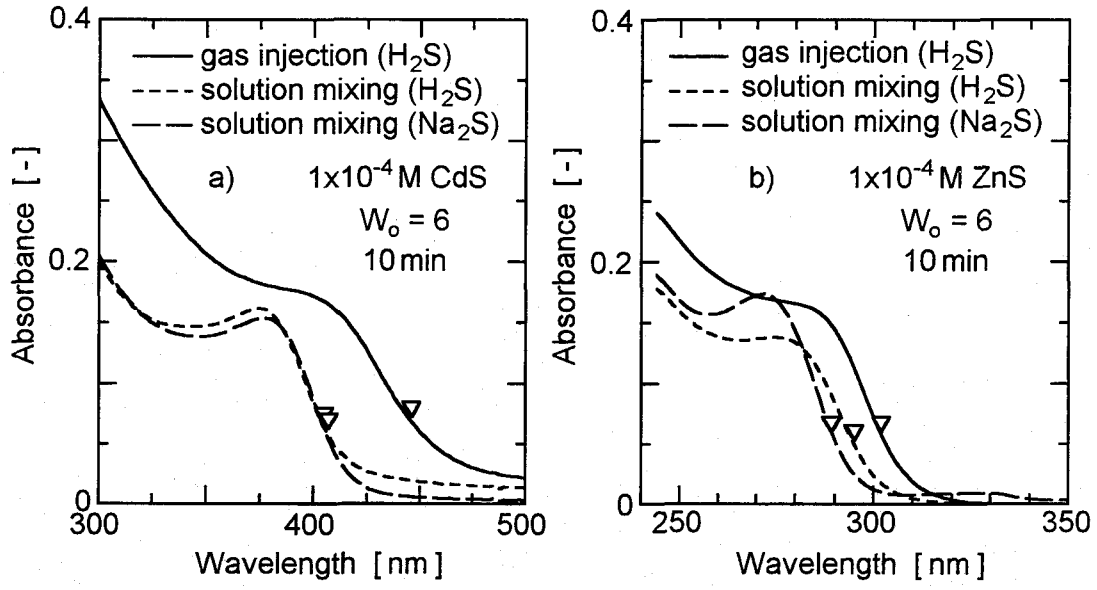

Figure 4–3 Effect of preparation method on absorption spectra of particles. (a) CdS; (b) ZnS.

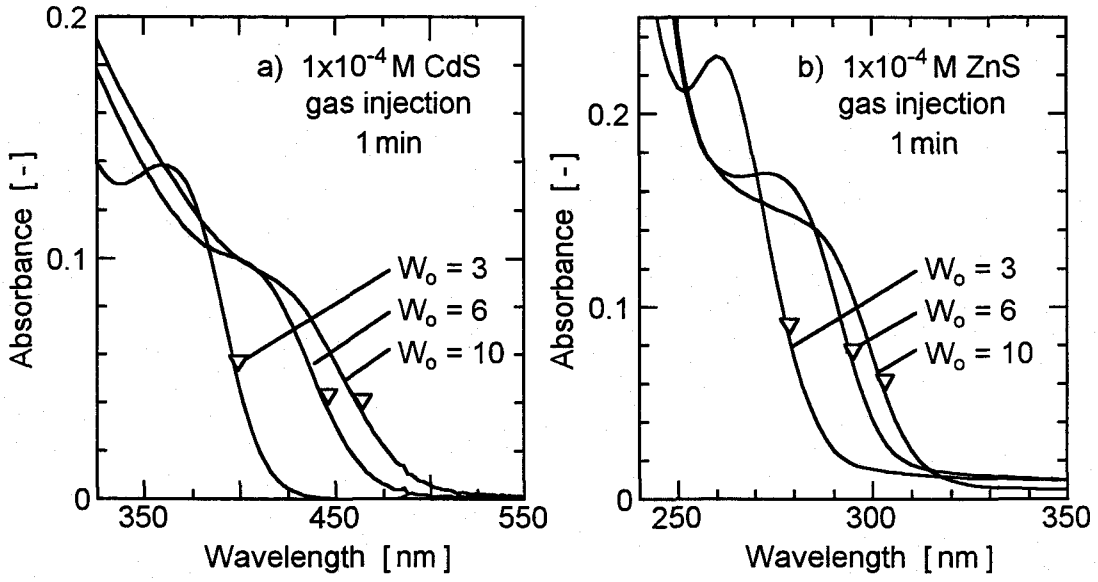

Figure 4–4 Effect of water content on absorption spectra of particles prepared by gas injection method. (a) CdS; (b) ZnS.

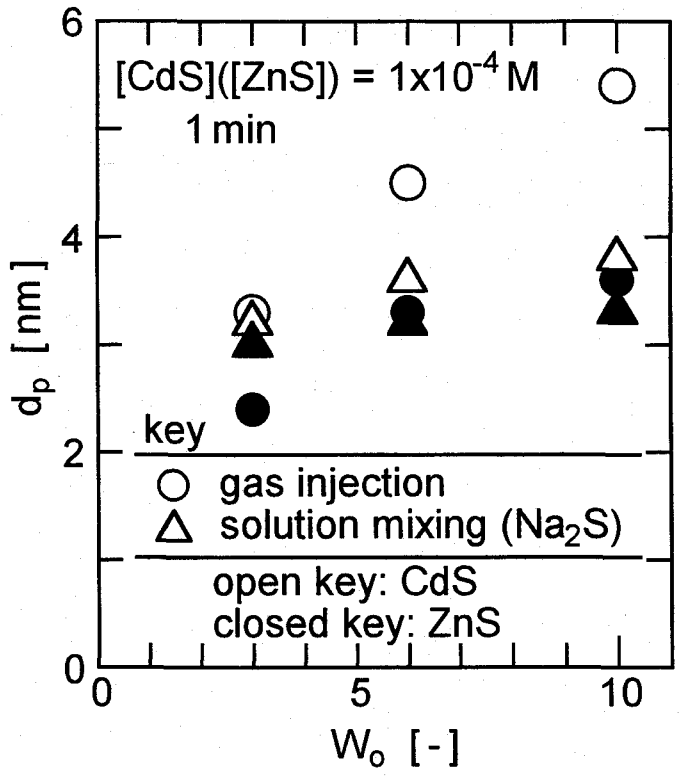

Figure 4–5 Comparison of diameters of formed particles for gas injection method and solution mixing method using Na_2S.

Figures 4–4(a) and (b) show the effect of water content on the spectra obtained at $t = 1$ min for the gas injection method with CdS and ZnS particles, respectively. A red-shift in the absorption threshold with increasing water content is seen, indicating the increase in particle diameter. The diameters estimated from these spectra are shown in **Figure 4–5.** The results for the solution mixing method using Na_2S are also shown in this figure. The effect of W_o on d_p for the gas injection method is more notable than that for the solution mixing method. The diameters for the gas injection method are larger than those for the solution mixing method except for the case of ZnS particle in the $W_o = 3$ solution.

2. Analysis of kinetics for particle formation

The particle formation process for the solution mixing method using H_2S

was investigated and compared with that obtained with Na_2S in Chapter II. The red-shift observed following $t = 0.02$ s and expressing coagulation of the particles was also analyzed in the same manner as performed in Chapter II. There, when particles had achieved diameters greater than about 2.4 nm, the coagulation rate (r_c) was found to follow first-order kinetics with respect to the concentration of the micellar droplets containing two or more particles (C_{mc}), since coagulation was considered to proceed in such micelles. Hence:

$$r_c = - dC_p/dt = k_{mc}C_{mc} \qquad (4\text{-}1)$$

where C_p and k_{mc} are the molar concentration of the particles and the first-order rate constant for coagulation, respectively. The value of C_{mc} is given by Eq. 2-12 with assuming a Poisson distribution of the particles (Atik and Thomas, 1981).

The first-order rate constant, k_{mc}, was thus calculated from the time-course variation of C_p. The value of C_p was calculated by the total number of ions converted to the particles and the number of ions in a particle as in Chapter II. **Figure 4-6** shows k_{mc} as a function of particle size for the solution mixing method using H_2S as reactant. The results obtained using Na_2S are also plotted for comparison. While some deviations are observed, the values of k_{mc} for both mixing methods seem to be almost identical. Since coagulation is the principal step in the solution mixing method as shown in Chapter II, the diameters of the formed particles obtained by the solution mixing methods using either H_2S or Na_2S are almost identical.

The mechanism of dissolution of H_2S is important since this is possibly the slowest step in the overall particle formation process using the gas injection method. However, only a few data for the analysis are obtained using the rapid gas injection method. This is because the rate of increase in the absorption intensity is very fast and is complete in as short a time as 5 s.

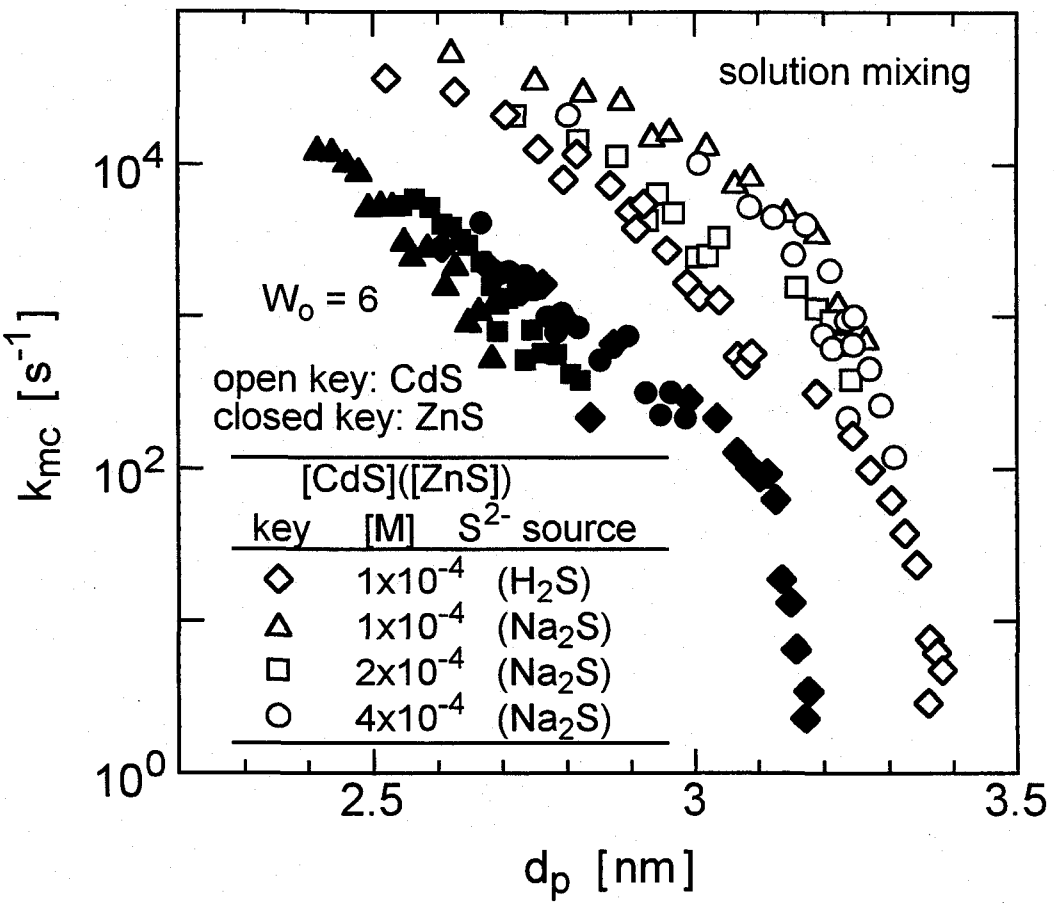

Figure 4-6 Comparison of first-order coagulation rate constants for solution mixing methods using H_2S and Na_2S.

The intermittent gas injection method was then employed. In this, a small aliquot (0.5 μl) of H_2S was injected repeatedly (14 times) into the $W_o = 3$ reverse micellar solution (3 ml) containing 1 x 10^{-4} M $Cd(NO_3)_2$ in a quartz cell using a syringe with a repeating dispenser and time interval of 1 s. Thus, a total of 7 μl of H_2S was injected over a time period of 13 s. Figure 4-2(d) shows the spectral change during this procedure. An increase in the absorption intensity in the initial stage and a continuous red-shift in the absorption threshold are observed as in the case of the rapid gas injection method in 2 s shown in Figure 4-2(a). The conversion of the precursor ions to particles (X_p) was calculated using the absorbance at the peak or shoulder wavelength which

was 400–430 nm for the CdS in this case. The time-course changes in X_p, particle concentration (C_p), and size of particles (d_p) were calculated using the spectra shown in Figure 4–2(d). The results are shown in **Figure 4–7(a)** and the results obtained similarly for ZnS particles are shown in **Figure 4–7(b).** The changes can be separated into two stages. In the initial stage which occurs up to about $t = 30$ s for CdS and $t = 50$ s for ZnS, both X_p and C_p increase rapidly, indicating the progress in particle growth and nucleation, respectively. In the case of CdS following this initial stage, a slow increase in d_p and a decrease in C_p are seen to occur without any increase in X_p as observed in the case of the solution mixing method described in Chapter II; changes are attributable to particle coagulation.

3. Model for particle formation

A kinetic scheme for the simultaneous nucleation, particle growth, and coagulation during the initial stage of the gas injection method was formulated; having particular emphasis on the rate of dissolution of H_2S into the micellar solution. In general, balance equations for the concentrations of the particles (C_p) and the metallic ion (C_M) may be expressed in terms of the rates of nucleation (r_n), particle growth (r_g), and coagulation (r_c). Hence,

$$dC_p / dt = r_n - r_c \qquad (4\text{–}2)$$

$$dC_M / dt = - r_n - r_g \qquad (4\text{–}3)$$

Defining $C_{S,t}$ as the total concentration of the unconverted H_2S in the solution, including S^{2-} ion in the water cores, H_2S in the organic phase, and H_2S in small bubbles in the solution; the balance equation of $C_{s,t}$ is,

$$dC_{S,t} / dt = - r_n - r_g + r_{inj} \qquad (4\text{–}4)$$

where r_{inj} is the rate of injection of H_2S into the reverse micellar solution. The rate of consumption of precursor ions by nucleation and particle growth in the gas injection method is determined by the rate of the rate-determining

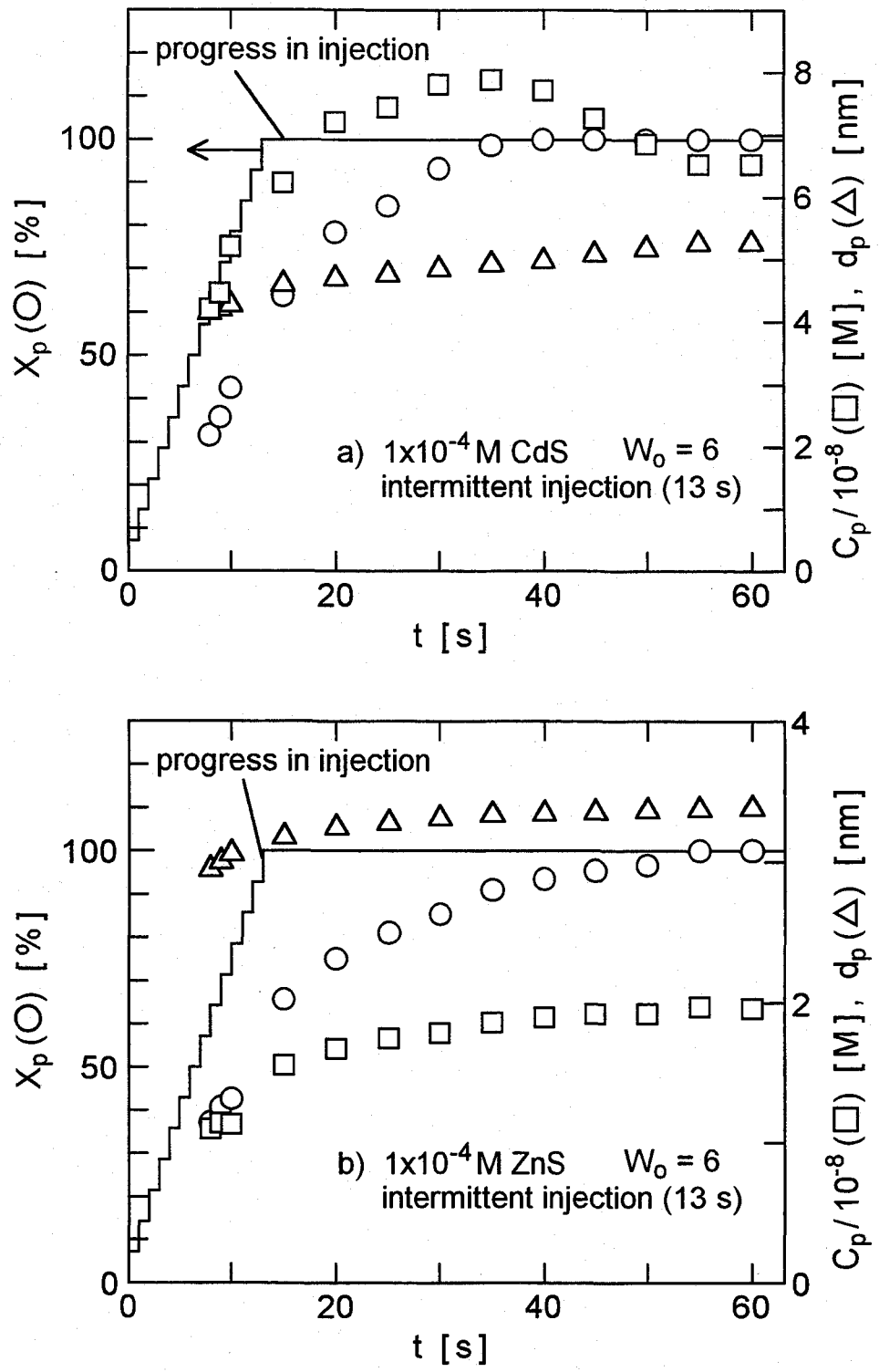

Figure 4–7 Time-course variations of particle diameter (d_p), conversion of precursor ions to particles (X_p), and concentration of particles (C_p) during particle formation using intermittent gas injection method in 13 s. (a) CdS; (b) ZnS.

dissolution of H_2S into the solution (r_{diss}). The concentration of H_2S dissolved in the water cores is negligible and the rate of consumption of H_2S is, thus, expressed as,

$$r_n + r_g = r_{diss} \tag{4-5}$$

The concentration of H_2S, not dissolved in the water cores, is almost identical to $C_{S,t}$. Thus, r_{diss} is expressed by a first-order kinetics with respect to $C_{S,t}$. Hence,

$$r_{diss} = r_n + r_g = k_{diss}\, C_{S,t} \tag{4-6}$$

where k_{diss} is the rate constant for the dissolution of H_2S.

Nucleation and particle growth proceed competitively and the sum of these rates is controlled by the rate of slower dissolution as shown by Eq. 4-6. If the average number of the reactant per micelle is much less than unity, the rate of the process slower than the intermicellar exchange process can be expressed by the first-order kinetics with respect to the concentration of micellar droplets containing all required reactants as shown in Chapters I and II. Both the rates of nucleation (r_n) and particle growth (r_g) are thus assumed to be expressed by first-order kinetics, *i.e.* for nucleation with respect to the concentration of micelles containing both Cd^{2+} ion and H_2S (C_{mn}) and for particle growth with respect to that of micelles containing Cd^{2+} ion, H_2S, and particles (C_{mg}), respectively. Hence,

$$r_n = k_{mn}\, C_{mn} \tag{4-7}$$

$$r_g = k_{mg}\, C_{mg} \tag{4-8}$$

where k_{mn} and k_{mg} are first-order rate constants for nucleation and particle growth, respectively. The values of C_{mn} and C_{mg} can be estimated from the probability of containment of each reactant in a micelle. Since the concentrations of reactants are much smaller than the concentration of the micellar droplets (4.31×10^{-4}–5.89×10^{-3} M), the probability is thus identical

to the average number of the reactant molecules per micellar droplet. The values of C_{mn} and C_{mg} are therefore obtained as follows,

$$C_{mn} = C_m\,(C_M/C_m)\,(C_S/C_m) \qquad (4\text{-}9)$$

$$C_{mg} = C_m\,(C_M/C_m)\,(C_S/C_m)\,(C_p/C_m) \qquad (4\text{-}10)$$

Finally, the ratio of the respective rates is obtained from Eqs. 4-7, 4-8, 4-9, and 4-10.

$$r_n/r_g = k_{mn}C_{mn} \,/\, k_{mg}C_{mg} = (k_{mn}/k_{mg})\,(C_m/C_p) \qquad (4\text{-}11)$$

The rate of coagulation (r_c) for the intermittent gas injection method was investigated. However, the diameter of particles formed in the $W_o = 6$ reverse micelles is too large to analyze the coagulation kinetics precisely. For $W_o = 3$, the coagulation rate constant (k_{mc}) for CdS particles obtained following completion of particle growth (30 s) and the data obtained for the solution mixing method using Na_2S are shown to correlate well together as shown in **Figure 4-8.** This indicates that the coagulation kinetics for the intermittent gas injection method, in this period, follows the same first-order kinetics of the case using Na_2S expressed by Eq. 4-1. Thus, the coagulation rate constant for $W_o = 6$ may be estimated from the data obtained from the previous solution mixing method shown in Figure 2-12(c). Assuming a linear relationship between the logarithm of k_{mc} and d_p,

$$\ln(k_{mc}/s^{-1}) = 58.4 - 15.9\,d_p/nm \qquad (4\text{-}12)$$

However, as proposed by Towey *et al.* (1990), the coagulation rate can not exceed that of the rapid coagulation in reverse micelles. Thus,

$$r_c \le k_{ex}\,C_p^2 \qquad (4\text{-}13)$$

where k_{ex} is the intermicellar exchange rate constant of the reverse micelles and is estimated as $5.6 \times 10^7\ M^{-1}\ s^{-1}$ in Chapter II.

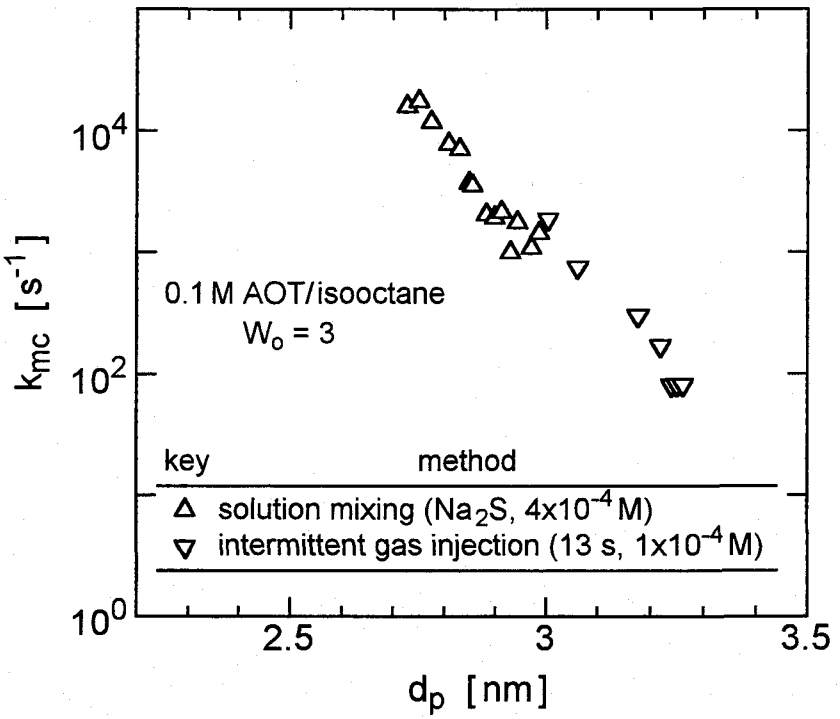

Figure 4–8 Comparison of first-order coagulation rate constants for intermittent gas injection method and for solution mixing method using Na_2S.

4. Application of the model for simulation of particle formation

The proposed model contains four rate constants (k_{diss}, k_{mn}, k_{mg}, and k_{mc}) to be determined. These were estimated from the time-course variations of the observed values of C_p, X_p, and d_p shown in Figure 4–7(a). The values of C_p, d_p, dC_p/dt, and dC_M/dt obtained at t = 8 s (the shortest reaction time at which data are obtained) are 4.2 x 10^{-8} M, 4.2 nm, 3.5 x 10^{-9} M/s, and − 4.1 x 10^{-6} M/s, respectively. The rates of nucleation (r_n), particle growth (r_g), and coagulation (r_c) were then estimated. Values for k_{mc} and C_{mc} are estimated as 6.9 x 10^3 s^{-1} and 1.0 x 10^{-12} M using Eqs. 4–12 and 2–12, respectively. Thus, r_c at time t = 8 s is calculated to be 5.0 x 10^{-16} M/s using Eq. 4–1. The rates, r_n and r_g, are then estimated to be 3.5 x 10^{-9} M/s and 4.1 x 10^{-6} M/s, respectively, from Eqs. 4–2 and 4–3. The value of r_g obtained is found to be greater than both r_n and r_c and it is almost identical to the rate of conversion of Cd^{2+} ion (− dC_M/dt).

This indicates that most of the precursor ions are consumed by particle growth.

The rate constant for dissolution of H_2S, k_{diss}, is estimated from Eqs. 4-3 and 4-6. In this calculation, the value of $C_{S,t}$ at $t = 8$ s is needed. $C_{S,t}$ is estimated as 3.0×10^{-5} M, since 6.2×10^{-5} M of H_2S has been injected in 8 s and 3.2×10^{-5} M of H_2S has been converted to particles as shown by X_p in Figure 4-7(a). The rate constant, k_{diss}, is now obtained as 0.14 s^{-1}. Two rate constants for nucleation and particle growth, k_{mn} and k_{mg}, have not been determined. Since the rates of these steps are controlled by the rate of the slower dissolution step as expressed by Eq. 4-5, the exact values of these rate constants can not be obtained by analysis based on the gas injection method. Thus, the ratio of rate constants (k_{mn}/k_{mg}) is estimated from r_n, r_g, C_p, and C_m using Eq. 4-11. Since the value of C_m for the $W_o = 6$ reverse micelles has been estimated as 9.27×10^{-4} M as shown in Table 2-1, the value of k_{mn}/k_{mg} is finally calculated to be 3.8×10^{-8}.

The complete process in particle formation was simulated using Eqs. 4-2, 4-3, 4-4, 4-6, 4-11, 4-12, and 4-13 using the obtained values of k_{mc}, k_{diss}, and k_{mn}/k_{mg}. The rate of injection of H_2S (r_{inj}) is 7.6×10^{-6} M/s since 1×10^{-4} M H_2S has been injected in 13 s. The calculated values for d_p, X_p, and C_p from the model are indicated by the respective lines shown in **Figure 4-9(a).** These calculated values agree well with the observed data, but the increase in d_p and thus decrease in C_p observed after $t = 40$ s are not shown in the simulation. The observed changes are likely to be caused by particle coagulation. In this simulation, the coagulation rate constant is calculated from Eq. 4-12, which is obtained by the data obtained in the solution mixing method in the d_p range of 3.0-3.3 nm as shown in Figure 2-12(c). Since the particle size has reached at around 5 nm in this case, the actual coagulation rate constant may possible be larger than the calculated value. Furthermore, there may contained inherently be some uncertainty in the estimation of the conversion, since the absorption

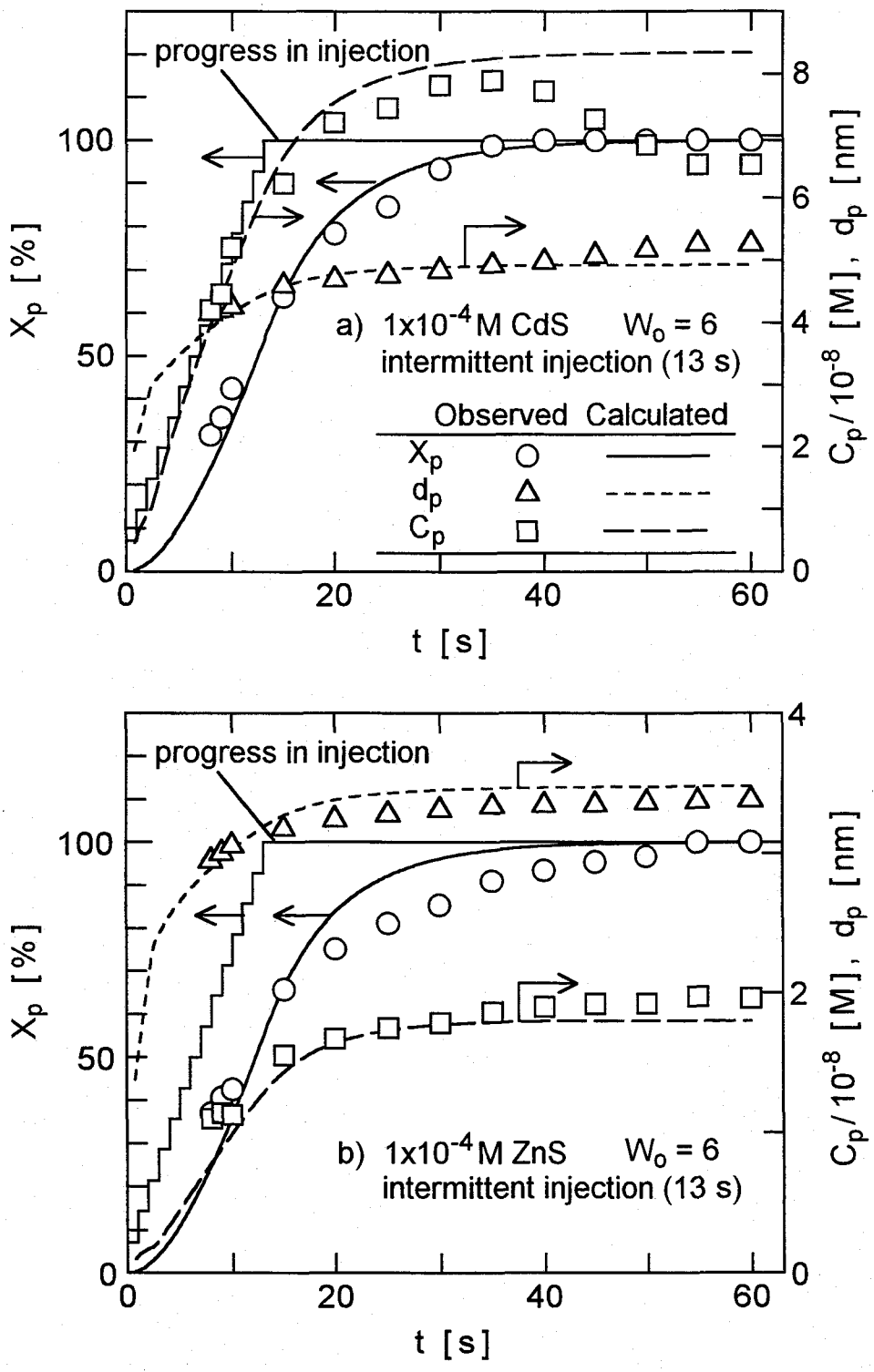

Figure 4–9 Comparison of observed and calculated time-course variations of particle diameter (d_p), conversion of precursor ions to particles (X_p), and concentration of particles (C_p). (a) CdS; (b) ZnS.

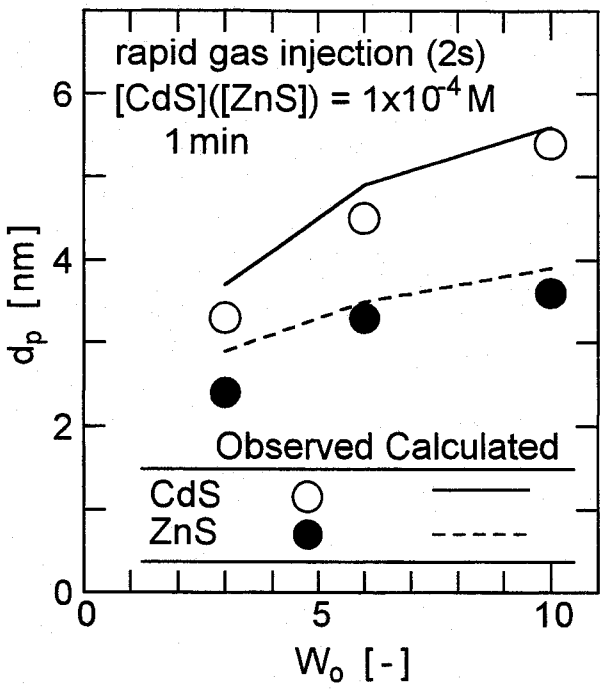

Figure 4–10 Comparison of observed and calculated diameters for the rapid gas injection method at 1 min. The calculated values are obtained using the parameter values in the intermittent gas injection method.

spectrum indicates only a shoulder peak as shown in Figure 4–2(d). If the conversion of precursor ions to the particles has not been complete ever at t = 40–60 s, particle diameter may increase by particle growth.

The simulation for ZnS particles was also carried out in the same manner from the time-course variations shown in Figure 4–7(b) and the following relationship between k_{mc} and d_p obtained based on the solution mixing method data shown in Figure 2–12(c).

$$\ln(k_{mc}/\mathrm{s}^{-1}) = 32.3 - 9.03\, d_p/\mathrm{nm} \qquad (4\text{–}14)$$

The estimated values of k_{diss} and k_{mn}/k_{mg} are 0.15 s^{-1} and 2.0 x 10^{-7}, respectively, and the simulated time-course variations are shown in **Figure 4–9(b).** These show a good agreement with the observed data. The values of the rate constant of dissolution step, k_{diss}, agree well for both CdS

and ZnS particles and are thus almost independent of the material of the particles, as expected.

The present results were applied to the case of the rapid injection method by changing the time duration and the rate of the gas injection, r_{inj}, to 2 s and 5 x 10^{-5} M/s (= 10^{-4} M/2 s), respectively. The simulation was also applied to other W_o cases using the values of C_m shown in Table 2-1 and the relationships between k_{mc} and d_p for each W_o shown in Figure 2-12(b). Other parameters were assumed to be independent of W_o. The calculated and observed diameters for CdS and ZnS particles for t = 1 min are shown in **Figure 4-10.** The calculated values agree well with the observed data. The proposed model is therefore shown to explain the diameter of formed particles both in the rapid gas injection method and in the intermittent gas injection method successfully.

Summary

The mechanism of formation of CdS and ZnS ultrafine particles in reverse micelles by injection of H_2S gas was studied. The particle formation process was followed by the measurement of UV-visible absorption spectra and the following results were obtained:

1. When H_2S gas is injected in 2 s, the conversion of metallic ion and H_2S gas to the particles due to nucleation and particle growth continues for about a further 5 s which is much longer than that for the solution mixing method using H_2S or Na_2S (0.02 s). The rate-determining step is the transfer of H_2S from the gas phase to the liquid phase (gas absorption). The principal step in the particle formation is particle growth and the rate of this step depends on the feeding condition of H_2S.

2. The rates for the steps in the particle formation process were estimated from an analysis of the absorption spectra. Most of dissolved H_2S is consumed for particle growth. This particle growth is controlled by the rate-determining gas absorption step and continues longer time than that in the solution mixing

method. Therefore, the formed particles in the gas injection method are thus larger in size than that in the solution mixing method in most cases. The size of the particles formed in the gas injection method can be controlled by the water content of reverse micellar solution over a more wide range than that in the solution mixing method.

3. A kinetic model is proposed for the complete process in particle formation for the gas injection method, based on the statistical distribution of reactants and particles among the micelles. The particle coagulation rates for both the gas injection method and the solution mixing method using H_2S follow the same kinetics as reported for the solution mixing method using Na_2S. Values of the rate constants for the other steps were also estimated from observed data at a reaction time (8 s). A simulation model based on these results explains observed time-course variations in the diameter and number of particles during particle formation successfully.

Chapter V
Preparation of Composite Ultrafine Particles and Application as Photocatalysts

Introduction

Semiconductor particles have been of great interest in their applications for photocatalysts. Ultrafine semiconductor particles exhibit larger band gap energy than that for the bulk semiconductor due to a quantum-size effect. The increase in band gap energy can extend applications of semiconductor particles as photocatalysts and can improve the photocatalytic activities. Composite particles of different semiconductors have unique optical and electronic properties such as fluorescence activation (Hasselbarth *et al.*, 1993) and quenching (Gopidas *et al.*, 1990) or novel photocatalytic activities (Ueno *et al.*, 1985; Youn *et al.*, 1988). Several attempts for preparation of the composite ultrafine particles in reverse micelles have been reported. CdSe-coated ZnS and the reverse composition composite particles were prepared by Kortan *et al.* (1990). Two types of composite CdS and ZnS ultrafine particles such as mixed crystal structure and core-shell structure were prepared in reverse micelles (Hirai *et al.*, 1994). However, the interests of these studies have been directed to the characteristics of the resulting particles. The quantitative model for the formation of ultrafine single component particles has been presented in the previous chapters for the various reactions and various reactant feeding methods. It is now necessary to extend the study to the formation of composite ultrafine particles.

In this chapter, the mechanism of formation of composite particles having mixed crystal or core-shell structure was studied, followed by the study on photocatalytic application of single component and composite semiconductor particles. At first, the mechanism of formation of mixed crystal CdS and ZnS

particles by simultaneous precipitation of both materials using the solution mixing method was studied. The effect of the solubility of the materials on the composition of the particles was also studied. The kinetic model applicable to the single component particles was also examined for its applicability to the present case of composite particles. Then, preparation of ZnS-coated CdS and CdS-coated ZnS particles was also attempted by two-step injection of the metallic ions and H_2S gas. The features in the absorption spectra of these particles were compared with those in the previous study (Hirai *et al.*, 1994).

The application of ultrafine semiconductor particles for the photocatalysts was also studied. PbS is a semiconductor with a narrow band gap (0.41 eV) (Ravich *et al.*, 1970), and the reaction photocatalyzed by bulk PbS is much confined. However, PbS shows very large quantum-size effects due to the very small effective masses of electron and hole. In chapter II, it was found that ultrafine PbS particles having a band gap energy of around 1.8 eV which was larger than the energy required to cleavage of water could be stabilized by the addition of excess amount of Pb^{2+} or S^{2-} ions in the $W_o = 3$ reverse micelles. Photocatalytic water reduction to generate H_2 by PbS ultrafine particles was thus studied as an application of the quantum-size effect. Youn *et al.* (1988) and Hirai *et al.* (1994) have showed that composite particles of CdS and ZnS have a larger photocatalytic activity than that of the mixture of separately prepared single component CdS and ZnS particles and that the activity is controlled by the composite structure and composition of the particles. The photocatalytic activity of the composite ultrafine particles prepared by the present gas injection method was thus studied and compared with the previous results obtained by the solution mixing method (Hirai *et al.*, 1994).

Experimental Section

1. Preparation of particles

Sodium bis(2-ethylhexyl) sulfosuccinate (AOT), sodium sulfide, cadmium nitrate, zinc nitrate, lead nitrate, and potassium tetrachloroplatinate (II) were supplied by Wako Pure Chemical Industries. Isooctane (2,2,4-trimethylpentane) was supplied by Ishizu Seiyaku. Hydrogen sulfide was supplied by Sumitomo Seika. All reagents were used without further purification. Distilled water was filtered with a 0.45−μm membrane filter and any dissolved oxygen was purged by Ar gas bubbling, prior to use.

For the preparation of coprecipitated particles of CdS and ZnS using the solution mixing method, the reaction was initiated by rapid mixing of a reverse micellar solution (1.2 m*l*) containing both $Cd(NO_3)_2$ and $Zn(NO_3)_2$ and an equal volume of a reverse micellar solution containing Na_2S at 25 ℃ using the mixing unit of the stopped-flow spectrophotometer. For the preparation of the coprecipitated particles using the gas injection method, the reaction was initiated by the injection of H_2S gas into a reverse micellar solution containing both $Cd(NO_3)_2$ and $Zn(NO_3)_2$ using a syringe. Two parameters, C_f and x_f, were defined in order to represent the feed composition of each reactant in the reverse micellar solution, where:

$$C_f = [Cd^{2+}] + [Zn^{2+}] \qquad (5\text{-}1)$$

$$x_f = [Zn^{2+}] / ([Cd^{2+}] + [Zn^{2+}]) \qquad (5\text{-}2)$$

The concentrations of all materials are defined in terms of moles per liter of mixed micellar solution. The instant when the solutions were mixed or when the injection of H_2S gas was started was defined as $t = 0$ s.

For the preparation of the composite ultrafine particles expected to have a core-shell structure, ZnS-coated CdS particles ($(ZnS)_{0.5}(CdS)_{0.5}$) by solution mixing method, alternate and repeated addition of small aliquots of two reverse

micellar solutions containing Zn^{2+} ion or S^{2-} ion was done into a reverse micellar solution containing CdS core particles (Hirai *et al.*, 1994). This was done to grow ZnS on the core particles by preventing both nucleation of new particles of ZnS and particle coagulation. In the case of the gas injection method, the core CdS particles were at first prepared by injecting a stoichiometric amount of H_2S into a $W_o = 2$ reverse micellar solution containing 5×10^{-5} M $Cd(NO_3)_2$. An aqueous solution containing $Zn(NO_3)_2$ was, then, added to this solution 10 minutes after initiation. The resulting solution contained 5×10^{-5} M Zn^{2+} with a W_o value of 3. The required amount of H_2S was then injected to form the ZnS shell. The preparation of CdS-coated ZnS particles ($(CdS)_{0.5}(ZnS)_{0.5}$) was also carried out but reversing the reactants.

The preparation of PbS ultrafine particles was described in Chapter II. The UV–visible absorption spectra during the formation of particles were measured in the same manner as described in Chapter II for the solution mixing method and in Chapter IV for the gas injection method.

2. Photocatalytic reduction of water

The method of irradiation of light for the photocatalytic generation of H_2 has been described in detail in a previous paper (Hirai *et al.*, 1994) and only a brief description is made here. A reverse micellar solution (20 m*l*) containing the ultrafine particles was irradiated with a 500 W Xenon lamp (Ushio UXL-500D) after the solution had been treated with Ar gas bubbling for 1 h. The amount of H_2 generated was determined by gas chromatograph with TCD (Shimadzu GC-14B). The column was packed with Activated Charcoal (2 m) and Molecular Sieves 5A (1 m). To load Pt on PbS ultrafine particles, the reverse micellar solution containing PbS particles was treated with Ar gas bubbling for 1 h and 8×10^{-7} M K_2PtCl_4 was then added to the solution and finally Pt was precipitated onto the particles by 1 h irradiation using the Xe lamp.

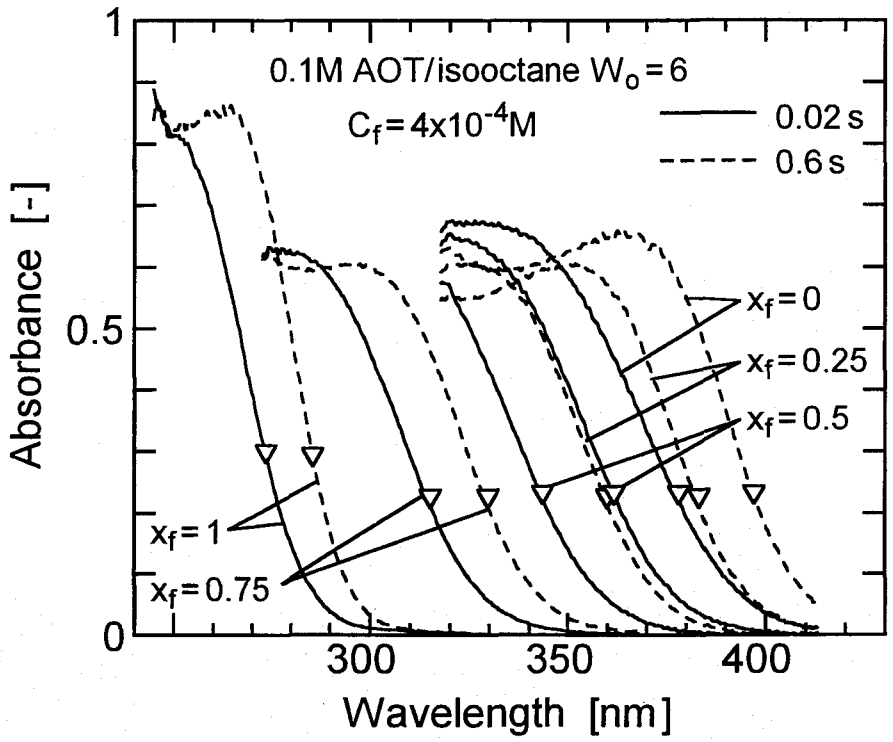

Figure 5-1 Effect of feed molar fraction of Zn (x_f) on absorption spectra of coprecipitated particles of CdS and ZnS prepared by solution mixing method.

Results and Discussion

1. Absorption spectra of coprecipitated particles

The values of bulk band gap energy ($E_{g,bulk}$) for CdS and ZnS are 2.5 eV and 3.7 eV, respectively, as shown in Table 2-2. The value of $E_{g,bulk}$ for the mixed crystal CdS and ZnS ($Cd_{1-x}Zn_xS$) is known to change parabolically from 2.5 eV to 3.7 eV with increasing molar fraction of ZnS (x) as expressed by Eq. 5-3 (Suslina *et al.*, 1976).

$$E_{g,bulk} / \text{eV} = 2.5 + (3.7 - 2.5 - 0.61)\,x + 0.61\,x^2 \qquad (5\text{-}3)$$

This causes the change in the wavelength of the absorption threshold from that of CdS to that of ZnS with increasing x.

Figure 5-1 shows the UV-visible absorption spectra of coprecipitated

$Cd_{1-x}Zn_xS$ particles prepared by the solution mixing method for various x_f values (*i.e.* molar faction of Zn for the total of Zn and Cd in the feed solution) measured at $t = 0.02$ and 0.6 s. Only one threshold in the absorption spectrum between that of CdS ($x_f = 0$) and that of ZnS ($x_f = 1$) is shown by the coprecipitated particles. The wavelength of the threshold decreases with increasing x_f. Since core-shell structure composite semiconductor particles exhibit two thresholds in the absorption spectrum (Youn *et al.*, 1988; Hirai *et al.*, 1994), the observed spectra indicate the formation of mixed crystal particles of CdS and ZnS. A red-shift in the absorption threshold with increasing time from $t = 0.02$ to 0.6 s is observed and any increase in absorption magnitude is not seen during this period. These results indicate that the conversion of ions to particles is complete within 0.02 s after mixing. The Zn fraction of the particles (x) can thus be assumed to remain constant with time following $t = 0.02$ s and the red-shift can thus be attributed to particle coagulation, as observed in the cases for CdS and ZnS single component particles shown in Chapter II.

The coprecipitated particles were also prepared by injecting H_2S gas. The solid lines in **Figure 5-2** show the UV-visible absorption spectra for $Cd_{1-x}Zn_xS$ particles prepared by the gas injection method for various x_f values measured at $t = 1$ h. Each spectrum shows only one threshold and the wavelength of the threshold also decreases with increasing x_f which agree with the results of the solution mixing method shown by the dotted lines. These findings indicate the formation of mixed crystal particles of CdS and ZnS. The wavelengths of the absorption threshold for the gas injection method are longer than those for the solution mixing method, indicating that the particles prepared by the gas injection method are larger in size than those obtained by the solution mixing method as observed also in the case of single component

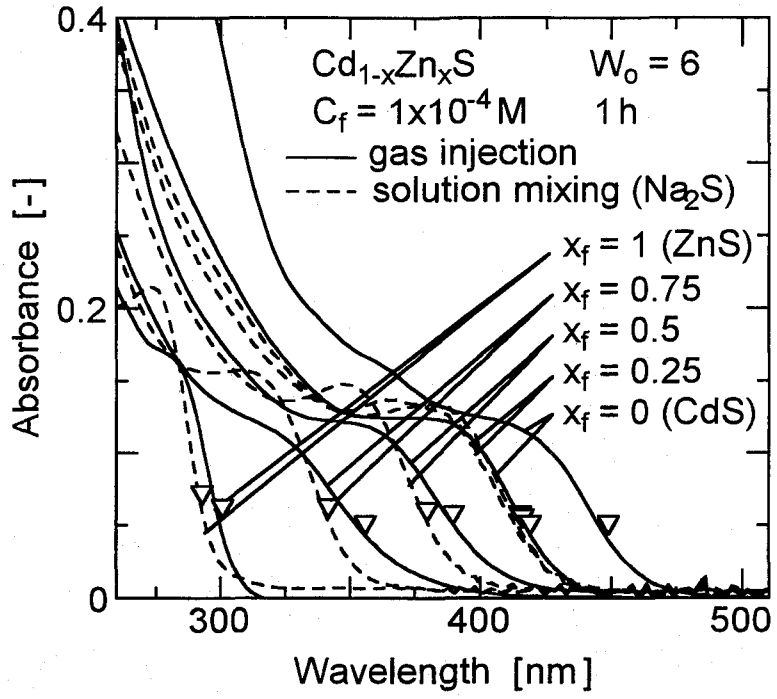

Figure 5–2 Effect of feed molar fraction of Zn on absorption spectra of coprecipitated particles of CdS and ZnS. Comparison of the gas injection method and solution mixing method.

particles in Chapter IV.

The band gap energy (E_g) was determined by the absorbance data using Eq. 2–6. The dots on the solid lines in **Figures 5–3(a) and (b)** show E_g of $Cd_{1-x}Zn_xS$ particles for various feed compositions (x_f) for both feeding methods. The band gap energy for the bulk materials ($E_{g,bulk}$) is also shown by means of the dotted line. The quantum-size effect is clearly seen. The band gap energy of the composite ultrafine particles is greater than that of bulk material having the same composition in most cases. The band gap energy increases parabolically with increasing x_f as for bulk materials. In the case of solution mixing method, however, the relationship became a little more linear with increasing feed ion concentration (C_f) as shown in Figure 5–3(a). The $E_g - x_f$ relationship for the gas injection method shown in Figure 5–3(b) is a little more linear than that for the solution mixing method. These results can be explained

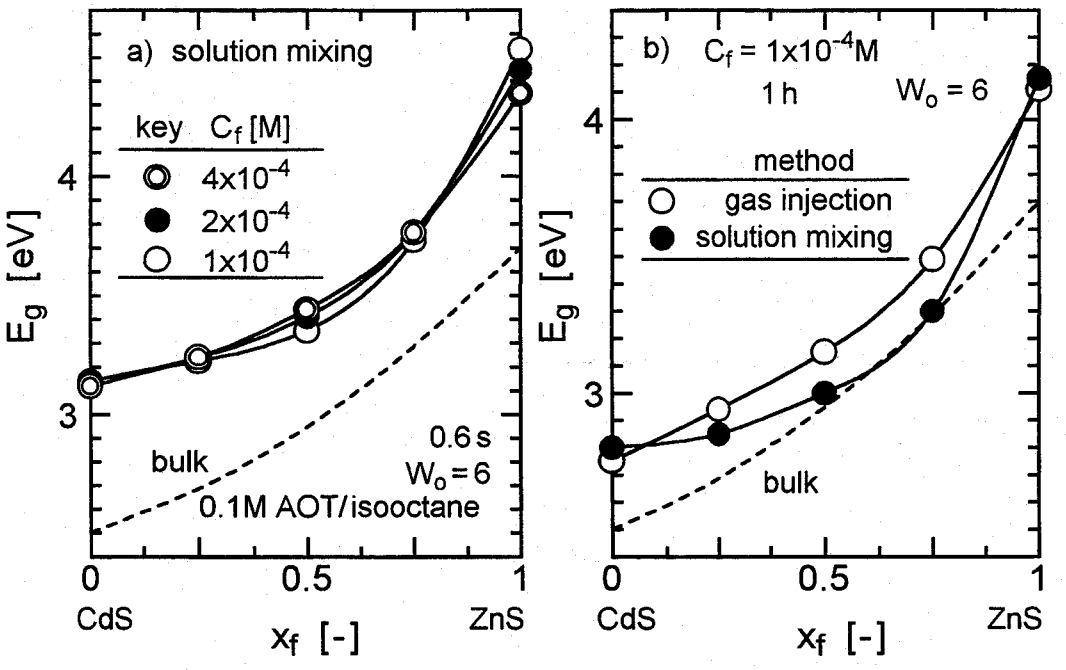

Figure 5-3 Effect of feed molar fraction of Zn of coprecipitated particles on band gap energy. (a) Various feed ion concentration; (b) Comparison of the gas injection method and solution mixing method.

by the effect of the feed ion concentration on the composition of the formed particles.

2. Composition of coprecipitated particles

The coprecipitated particles prepared by the simultaneous precipitation of CdS and ZnS were reported to be richer in CdS as compared to the feed ratio of the Cd^{2+} and Zn^{2+} ions (Youn *et al.*, 1988; Hirai *et al.*, 1994). This is possibly due to a difference in the concentration of the residual ions in solution caused by the difference in the solubility values of CdS and ZnS. The concentration of the residual ions in solution is controlled by the solubility product of the particle material as expressed by Eq. 2-9. Hence,

$$[Cd^{2+}][S^{2-}] / M^2 = K_{sp,CdS} \qquad (5-4)$$

$$[Zn^{2+}][S^{2-}] / M^2 = K_{sp,ZnS} \qquad (5-5)$$

where $K_{sp,CdS}$ and $K_{sp,ZnS}$ are solubility product of CdS and ZnS, respectively. From these relationships, the ratio of the residual Cd^{2+} and Zn^{2+} ions in solution can be expressed by the following equation,

$$[Zn^{2+}] / [Cd^{2+}] = K_{sp,ZnS} / K_{sp,CdS} \qquad (5\text{-}6)$$

The solubility product values of CdS and ZnS in the form of ultrafine particles are estimated as 1×10^{-10} and 4×10^{-10}, respectively, in Chapter II. The concentration of the residual Zn^{2+} ion in the solution is thus greater than that of the Cd^{2+} ion, and hence, the formed particles become richer in CdS than the feed composition. With increasing conversion of the metallic ions to the particles, namely, with decreasing quantities of the residual metallic ions in the solution, the composition of the formed particles approaches more closely to that of the feed composition. As expected from Eqs. 5-4 and 5-5, an excess amount of S^{2-} ion (Hirai *et al.*, 1994) or an increase in the concentrations of both metallic and S^{2-} ions can increase the conversion of the metallic ions to the particles.

The composition of the formed particles was estimated from the solubility product values. In the case of solution mixing method, when the concentration of all the supplied metallic ions is identical to that of S^{2-} ion, the concentration of the residual ions in the solution is expressed by the condition that:

$$[Cd^{2+}] + [Zn^{2+}] = [S^{2-}] \qquad (5\text{-}7)$$

The concentrations of residual Cd^{2+}, Zn^{2+}, and S^{2-} ions were calculated as 4.5×10^{-6}, 1.8×10^{-5}, and 2.2×10^{-5} M, respectively, for all x_f and C_f values except for the cases of single component particles, based on Eqs. 5-4, 5-5, and 5-7 and the solubility product values.

Table 5-1 shows the calculated Zn fraction of the formed coprecipitated particles (x_{cal}) for the solution mixing method based on the feed and residual quantities of the ions. The calculated value (x_{cal}) approaches that of the

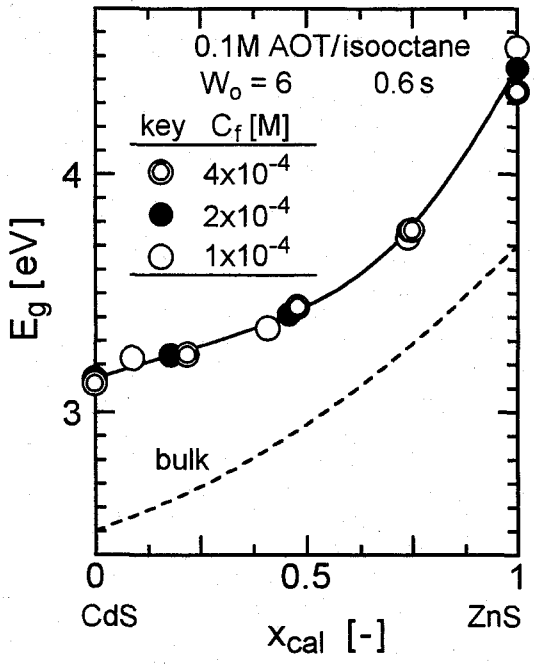

Figure 5–4 Relationship between band gap energy and calculated molar fraction of Zn in particles.

Table 5–1 Particle composition estimated from solubility (x_{cal}).

C_f [M]	x_f				
	0	0.25	0.5	0.75	1
1 x 10^{-4}	0	0.09	0.41	0.74	1
2 x 10^{-4}	0	0.18	0.46	0.74	1
4 x 10^{-4}	0	0.22	0.48	0.75	1

feed (x_f) with increasing feed concentration (C_f). The band gap energy (E_g) for the solution mixing method is now plotted as a function of x_{cal} as compared to x_f. The results shown in **Figure 5–4** indicate that the $E_g - x_{cal}$ relationship is almost independent of C_f. This shows that the x_{cal} value gives a good estimate of the particle composition. In the case of gas injection method, the $E_g - x_f$ relationship is more linear than that for the solution mixing method as shown in Figure 5–3(b). However, since the precise amount of dissolved H_2S gas can not be obtained, the value of x_{cal} for the gas injection method can not be

Table 5–2 Parameters for CdS, ZnS, and their solid solution particles.

	CdS	ZnS	$Cd_{1-x}Zn_xS$
$E_{g,bulk}$ [eV]	2.5	3.7	$2.5 + (3.7-2.5-0.61)\,x + 0.61x^2$
$\varepsilon/\varepsilon_0$	5.7	5.2	$5.7 + (5.2-5.7)\,x$
m_e/m_0	0.19	0.25	$0.19 + (0.25-0.19)\,x$
m_h/m_0	0.8	0.59	$0.8 + (0.59-0.8)\,x$
a [nm]	0.4136	0.3820	$0.4136 + (0.3820-0.4136)\,x$
c [nm]	0.6714	0.6260	$0.6714 + (0.6260-0.6714)\,x$

calculated. Since a little excess amount of H_2S has been injected, almost all metallic ions are expected to have converted to the particles, thus, the composition of formed particles becomes almost identical to the feed composition.

3. Analysis of coagulation kinetics of coprecipitated particles

The size of the $Cd_{1-x}Zn_xS$ particles was estimated from E_g using Eq. 2–4 in the same manner as that used for the CdS and ZnS single component particles described in Chapter II. In order to calculate this, the electric parameters for $Cd_{1-x}Zn_xS$ particles at various compositions are needed. The bulk band gap energy was calculated by means of Eq. 5–3. The other parameters, the dielectric constant of semiconductor (ε), the effective mass of electron (m_e), and the effective mass of hole (m_h) were assumed to have a linear dependence on particle composition. The relationships used for the parameters in terms of x are summarized in **Table 5–2.**

Figure 5–5 shows the time-course variation of the size of 4×10^{-4} M $Cd_{1-x}Zn_xS$ particles prepared by the solution mixing method for various values of x_{cal}. The particle size is seen to increase continuously with time and ZnS particles are shown to be smaller than both CdS and $Cd_{1-x}Zn_xS$ particles at the same reaction time. This indicates that the kinetics of coagulation is dependent

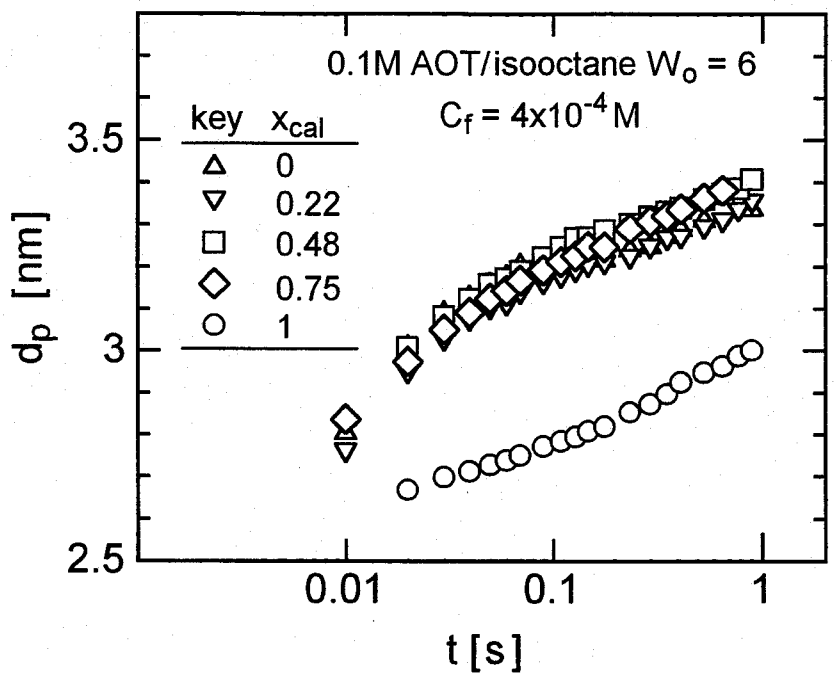

Figure 5–5 Effect of feed molar fraction of Zn on time-course variation of size of particles.

on the particle composition. For the cases of CdS and ZnS single component particles with particle diameters greater than about 2.4 nm, the rate of coagulation decreases with increasing particle diameter and is dominated by the particle material and the concentration of micellar droplets containing two or more particles as described in Chapter II. Consequently, the effect of particle composition on the coagulation of $Cd_{1-x}Zn_xS$ particles larger than 2.4 nm was investigated in the same manner as the single component particles. The first-order rate constant, k_{mc}, was calculated based on Eqs. 2–11 and 2–12 from the concentration of particles. The concentration of particles was calculated by the total number of ions converted to particles estimated from the solubility product (Eqs. 5–4 and 5–5) and the number of ions in a particle using lattice constants shown in Table 5–2 by assuming the wurtzite structure of particles.

Figures 5–6(a) and (b) show the relationships between the values of k_{mc}

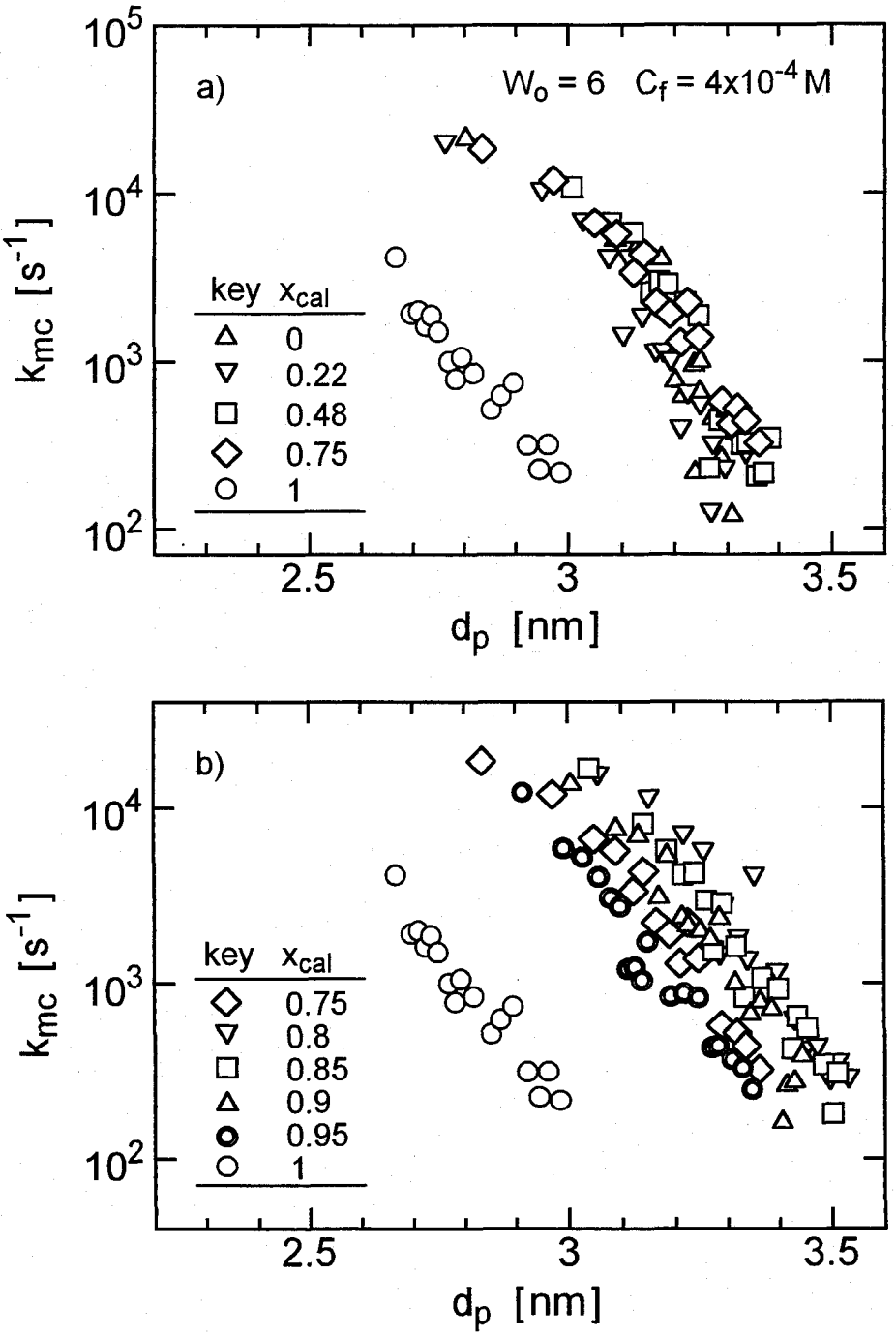

Figure 5–6 Effect of feed molar fraction of Zn on relationship between first-order coagulation rate constant and particle diameter.

and d_p for single component and coprecipitated particles with different x_{cal} values. The rate constants for the coprecipitated particles decrease with increasing particle diameter as observed in the cases of CdS and ZnS single component particles ($x_{cal} = 0$ and 1). The rate constants are almost independent of the composition in the x_{cal} range of 0–0.95. When the Cd content is reduced to 5 % or lower, the behavior of the composite particles sharply approaches that of single component ZnS particles.

A possible explanation of this result lies in the change in the crystal structure of $Cd_{1-x}Zn_xS$ particles. Both CdS and ZnS exist in two structural types, namely, wurtzite and zinc blende. Wurtzite is the low-temperature form for CdS, whereas zinc blende is that for ZnS (Sakaguchi *et al.*, 1977). The structure of ultrafine particles prepared in reverse micelles is reported to be wurtzite for CdS (Jain *et al.*, 1992) and zinc blende for ZnS (Motte *et al.*, 1992). The structure of the $Cd_{1-x}Zn_xS$ will therefore change from wurtzite to that of zinc blende as the value of x increases (Sakaguchi *et al.*, 1977). The region for x in which the transformation occurs depends on the environment, but should be somewhere between the values of 0.95 and 1 for the present case.

The assumption of wurtzite structure at all values of x was used in the calculation of the number of the formed particles. This assumption however no longer applies to the case of ZnS particles. When the value of 0.5409 nm is used for the lattice constant of zinc blende ZnS, however, the number of Zn^{2+} or S^{2-} ions in a zinc blende ZnS corresponds to 357.3 for a value of $d_p = 3$ nm and this is nearly equal to the value for that in wurtzite (357.4 for $d_p = 3$ nm). Hence, the number of particles can be regarded to be independent of the form of the crystal structure of ZnS.

The effects of the feed ion concentration and the water content of the micellar solution on the coagulation kinetics of $Cd_{1-x}Zn_xS$ particles were also studied as in the case of single component particles. **Figure 5–7** shows the

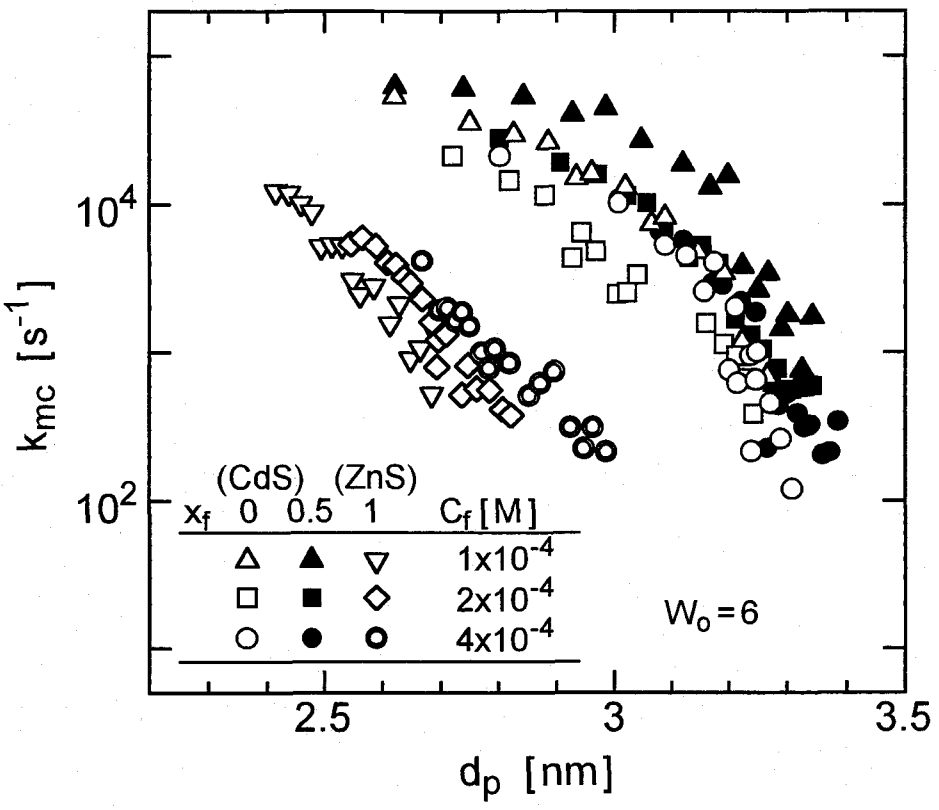

Figure 5–7 Effect of feed ion concentration on first-order coagulation rate constant.

effect of the feed ion concentration (C_f) on the coagulation rate constant (k_{mc}). In the cases of CdS and ZnS single component particles, the value of k_{mc} is almost independent of C_f, as described in Chapter II. For $x_f = 0.5$ coprecipitated particles, k_{mc} is also independent of the feed concentration, C_f. The value of x_{cal} however decreases with decreasing C_f as shown in Table 5–1. Since k_{mc} is independent of x_{cal} in the range 0–0.95 as shown in Figure 5–6, the value of k_{mc} of the coprecipitated particles is thus independent of C_f for this range of x_{cal} values.

The effect of the water content of the reverse micellar solution on the coagulation kinetics was then investigated. The results are shown in **Figure 5–8.** The value of k_{mc} decreases with decreasing water content, namely, decreasing size of micelles as shown in Table 2–1. The decrease in k_{mc} may be

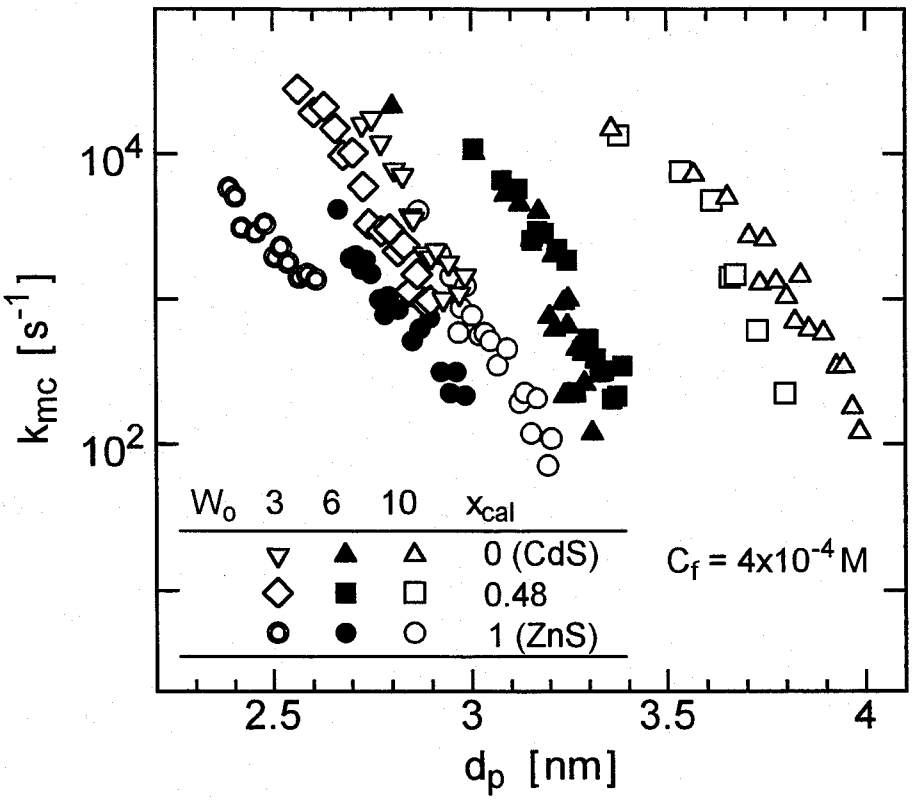

Figure 5-8 Effect of water content on first-order coagulation rate constant.

caused by a restraint on the rate of coagulation by the micellar interface owing to an approach in the relative sizes of the micelles and particles, as discussed in Chapter II. The effect of water content on k_{mc} for ZnS particles is much smaller than that for CdS particles, confirming the results described in Chapter II, and smaller than $Cd_{1-x}Zn_xS$ particles.

4. Preparation of core-shell structure particles using gas injection method

Figure 5-9(a) shows the absorption spectra of ZnS-coated CdS particles ($(ZnS)_{0.5}(CdS)_{0.5}$) and CdS-coated ZnS particles ($(CdS)_{0.5}(ZnS)_{0.5}$), as prepared by the two-step injection of both metallic ions and H_2S gas and measured at 1 h after the second H_2S addition. The absorption spectra of the single component CdS and ZnS particles and coprecipitated particles of CdS and ZnS

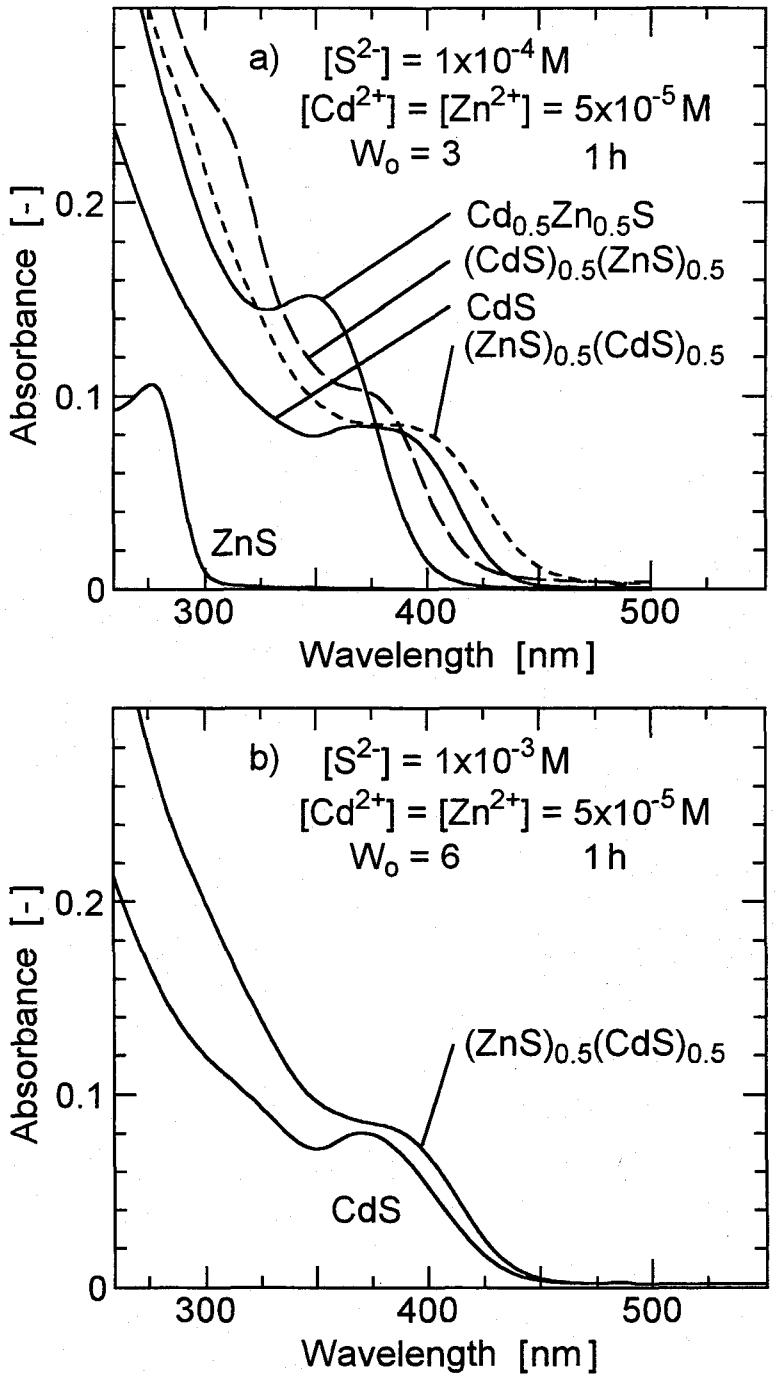

Figure 5–9 Absorption spectra of composite particles of CdS and ZnS.
(a) Prepared with stoichiometric amount of H_2S;
(b) prepared with a 10-fold excess amount of H_2S.
$Cd_{0.5}Zn_{0.5}S$: solid solution CdS and ZnS particles,
$(CdS)_{0.5}(ZnS)_{0.5}$: CdS-coated ZnS particles,
$(ZnS)_{0.5}(CdS)_{0.5}$: ZnS-coated CdS particles.

($Cd_{0.5}Zn_{0.5}S$) are also shown for comparison. The absorption spectrum for the $(ZnS)_{0.5}(CdS)_{0.5}$ particles is significantly different from those of $(CdS)_{0.5}(ZnS)_{0.5}$ and coprecipitated $Cd_{0.5}Zn_{0.5}S$ particles. An increase in absorbance is observed at wavelengths less than 360 nm compared with the spectrum of CdS particles, and can be attributed to the formation of a ZnS shell (Hirai *et al.* 1994). On the other hand, $(CdS)_{0.5}(ZnS)_{0.5}$ particles exhibit two obvious absorption thresholds close to those of CdS and ZnS particles. These spectral features suggest the formation of core-shell structure composite particles in both cases.

In the case of an alternate solution injection method, the addition of an excess amount of Na_2S was reported to be necessary to prepare core-shell structure particles (Hirai *et al.*, 1994). Thus the injection of a 10-fold excess amount of H_2S was also employed. The resulting spectrum is shown in **Figure 5-9(b)** and almost same features are seen in the difference in absorption spectra between $(ZnS)_{0.5}(CdS)_{0.5}$ particles and CdS particles. Thus core-shell structure particles can be prepared by the gas injection method in a much more convenient procedure than by the alternate solution injection method. This is because particle growth is the principal mechanism of the gas injection method as discussed in Chapter IV while coagulation is that of the solution mixing method as in Chapter II.

5. Photocatalytic activity of ultrafine particles

(1) PbS particles

The photocatalytic activity of ultrafine PbS particles was investigated. To avoid photocorrosion of the particles, it is necessary to add a hole scavenger to the solution before light irradiation. Since a large excess amount of Na_2S was used as scavenger (Kakuta *et al.*, 1985; Hirai *et al.*, 1994), a 10-fold excess amount of Na_2S was therefore used at the preparation stage of particles using

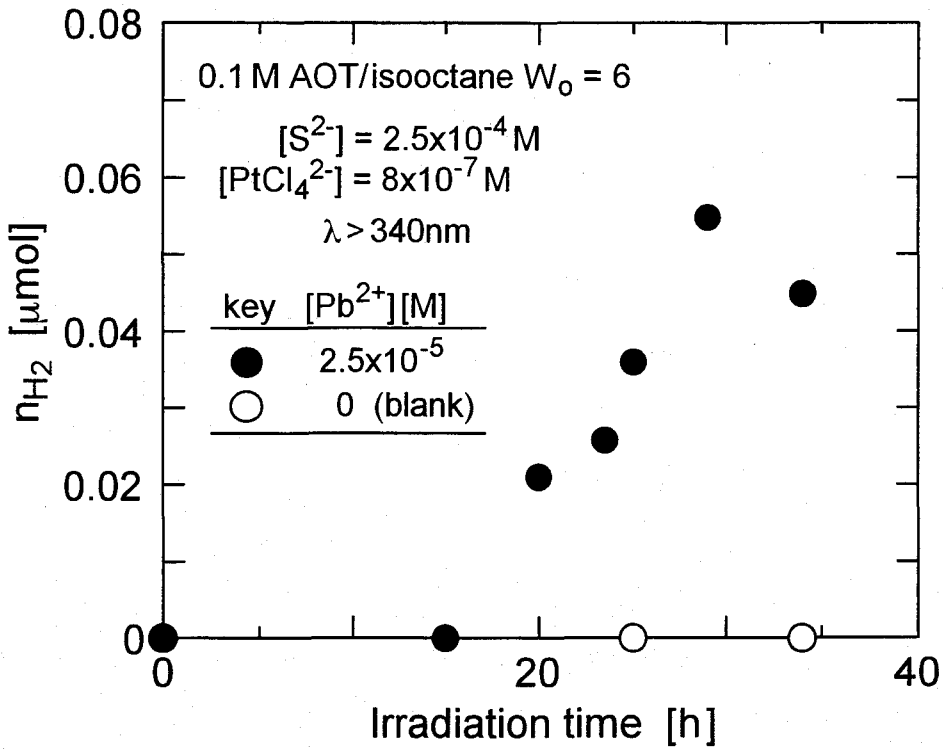

Figure 5–10 Photocatalytic activity of PbS ultrafine particles for water cleavage to generate H_2.

the solution mixing method. The amount of photogenerated H_2 by PbS itself is very small and thus the determination of amount of H_2 using gas chromatograph is not reproducible. Since the activity of semiconductor particles for photocatalytic reduction of water was known to be enhanced by Pt-loading on the semiconductor particles (Meyer *et al.*, 1984), Pt was loaded on the PbS semiconductor particles. **Figure 5–10** shows the amount of H_2 generated (n_{H_2}) by the irradiation of the reverse micellar solution containing the Pt-loaded PbS particles together with the results for the solution containing no PbS particles but containing $PtCl_4^{2-}$ and S^{2-} ions as a blank test. It has been shown that the photocatalytic function of PbS particles is originated by the increase in band gap energy caused by the decrease in particle size.

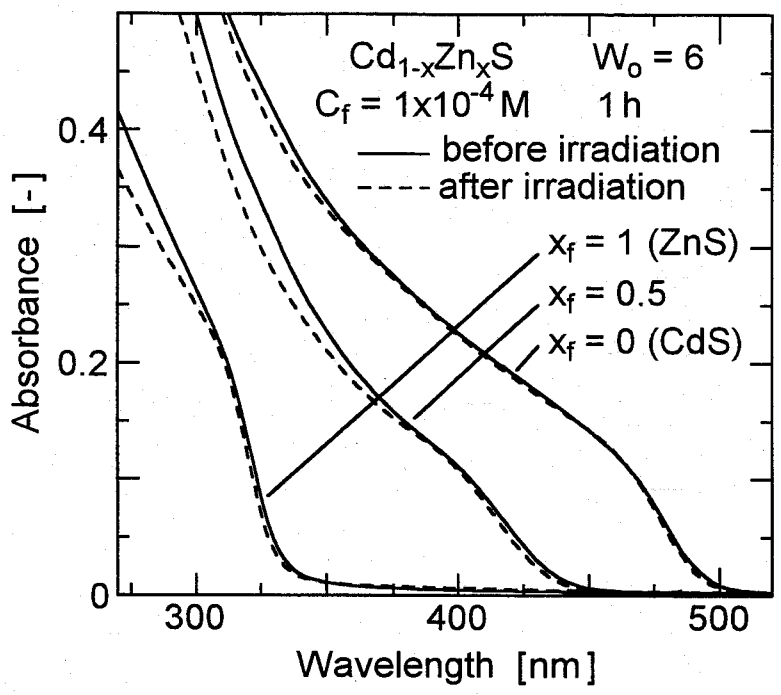

Figure 5–11 Absorption spectra of coprecipitated particles of CdS and ZnS before and after 24 h irradiation by Xe lamp.

(2) Composite CdS and ZnS particles

The photocatalytic activity of composite CdS and ZnS particles prepared by the gas injection method was investigated. Since a large excess amount of Na_2S was used for the scavenger in the previous case of PbS particles prepared by the solution mixing method, a 10-fold excess amount of H_2S gas was injected at the preparation stage of particles in the present case. **Figure 5–11** shows the absorption spectra of CdS, ZnS, and $Cd_{0.5}Zn_{0.5}S$ particles prepared with the excess H_2S measured before and after 24 h irradiation by Xenon lamp. The spectra are almost unchanged by the irradiation, indicating that the excess amount of H_2S can be used for the hole scavenger.

The amount of H_2 formed by the 20 h irradiation to coprecipitated particles (n_{H_2}) is shown in **Figure 5–12**. For wavelengths longer than 320 nm, H_2 production increases linearly with increasing x_f as shown by the open circles. This is the similar to the result reported previously for the solution mixing

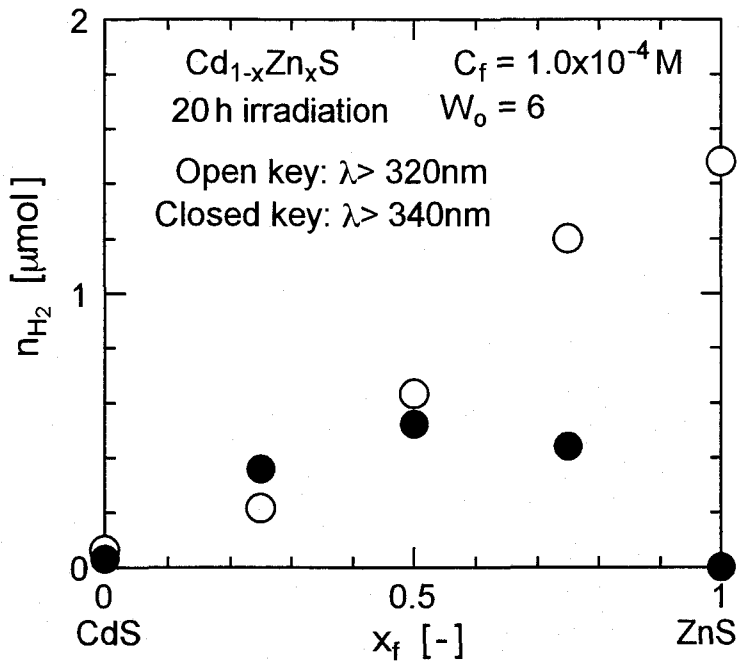

Figure 5–12 Effects of molar fraction of Zn in the particles and irradiation wavelength on photocatalytic activity of coprecipitated particles of CdS and ZnS.

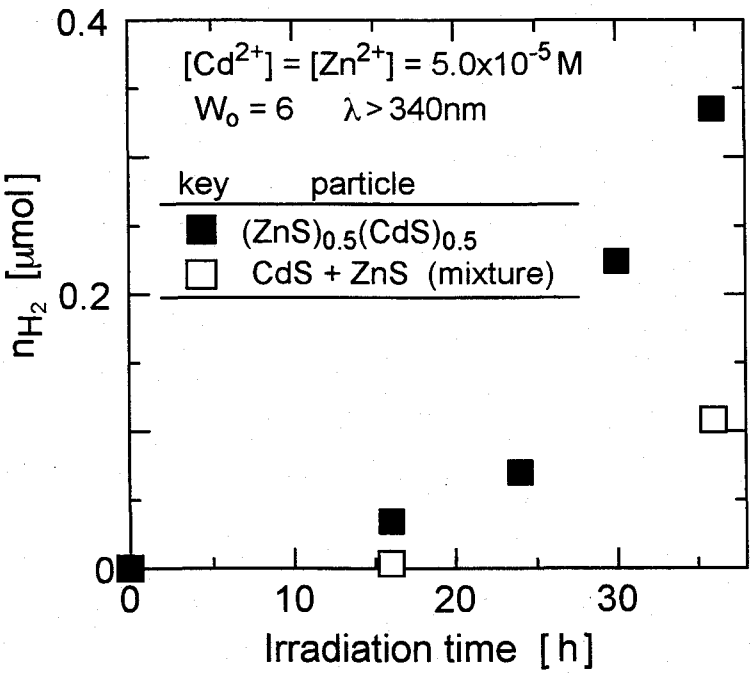

Figure 5–13 Photocatalytic activities of ZnS-coated CdS particles and mixture of separately prepared single component CdS and ZnS particles.

method and has been explained by the increase in the reducing ability of the photoexcited electron as a function of increasing Zn content (Hirai *et al.*, 1994). Changing the cut-off wavelength to 340 nm, H_2 production decreases greatly in the range of x_f from 0.75 to 1 as shown by the closed circles. Since the wavelength of the absorption threshold decreases with increasing x_f as shown in Figure 5-11, the photoexcitation of electron by wavelengths longer than 340 nm becomes more difficult with increasing x_f. ZnS ($x_f = 1$) particles especially can not absorb 340 nm light. This difficulty of photoexcitation in this x_f range causes the decrease in the activity.

The photocatalytic activity of ZnS-coated CdS particles was also investigated. **Figure 5-13** shows the amount of H_2 generated by $(ZnS)_{0.5}(CdS)_{0.5}$ particles with cut-off wavelength of 340 nm for various irradiation times (closed key) and that for a mixture of separately prepared single component CdS and ZnS particles (open key). The coated particles show a higher H_2 photogeneration activity compared to the mixture of single component particles, but this activity is smaller than that for the coprecipitated particles shown in Figure 5-12. This result again corroborates the earlier findings obtained with coated particles prepared by the solution mixing method (Hirai *et al.*, 1994).

Summary

The preparation of composite ultrafine particles of CdS and ZnS having coprecipitated or core-shell structure was studied using the solution mixing method and the gas injection method. Photocatalytic activity of ultrafine particles for reduction of water to generate H_2 was also investigated as an application of semiconductor particles. Single component PbS ultrafine particles and composite ultrafine particles of CdS and ZnS were examined and the following results were obtained:

1. Coprecipitated ultrafine particles of CdS and ZnS were prepared by simultaneous precipitation of CdS and ZnS using the solution mixing method. The composition of formed particles is found to be controlled by the feed ion ratio and the solubility product of the materials. The kinetics of coagulation of the composite particles is also expressed by the kinetic model proposed in Chapter II for the single component particles.

2. Coprecipitated and core-shell structures composite ultrafine particles of CdS and ZnS were prepared, respectively, by the one-step and two-step injection of metallic ions and H_2S gas. The composition of coprecipitated particles prepared by the gas injection method is more close to the feed composition than that by the solution mixing method. The core-shell structure particles can be prepared in a more convenient process using the gas injection method than that using the solution mixing method, since the particle growth is the predominant step of the gas injection method.

3. The generation of H_2 by the reduction of water due to the photo-irradiation of the particles was also investigated. Ultrafine PbS particles stabilized at a large band gap energy by excess amount of S^{2-} ion are found to be applicable to this reaction. The activity of composite ultrafine CdS and ZnS particles is found to be greater than that for the mixture of the single component particles and depends on the composite structure of the particles as observed previously in studies using the solution mixing method.

General Conclusions

The mechanism of formation of ultrafine particles in the reverse micelles was investigated with the aim of establishment of "Unit Operation for the Preparation of Ultrafine Particles". Preparation of the particles using several kinds of reactions having different reaction rates and various reactant feeding methods was studied for understanding the kinetics of the particle formation process and for illuminating the principal factors controlling both the kinetics of the steps in the process and the characteristics of the resulting particles such as the diameter and the number of the particles. The micellar solution was detected continuously during the whole process of particle formation by UV-visible absorption spectra.

A quantitative and reasonably complete model for the successive steps in the formation process was then proposed from dissolution step of reactants into the reverse micellar solution to particle coagulation step. Possible rate expressions are summarized as follows,

Dissolution of reactants into water cores

$$r_{diss} = k_{diss}\, C_{undiss} \qquad (1)$$

Chemical reaction

$$r_r = k_r\, C_r \qquad (2)$$

Nucleation

$$r_n = n\, k_{mn}\, C_{mn} \qquad (3)$$

Particle growth

$$r_g = k_{mg}\, C_{mg} \qquad (4)$$

Coagulation

(Rapid coagulation)

$$r_c = k_{ex}\, C_p^{\,2} \qquad (5)$$

(Reduced rate coagulation process)

$$r_c = k_{mc}\, C_{mc} \qquad (6)$$

One of these is considered to be the rate-determining step in the process, depending on the reactions and feeding methods employed. The parameters of the model, rate constants of the steps, can be determined from the time-course variations of the diameter and number of the particles, which are estimated from absorption spectra of the particles.

In the case of the formation of TiO_2 ultrafine particles by slow hydrolysis of titanium tetrabutoxide (TTB), nucleation is the rate-determining step as shown in Chapter I. The rate of this step can be expressed by a first-order kinetics with respect to the concentration of the micelles containing a sufficient number (5 in this case) of hydrolyzed TTB molecules. The particle formation process was analyzed using a kinetic scheme including the hydrolysis of TTB, nucleation, and particle growth in the micelles, based on the statistical distribution of species and particles among the micelles. This scheme successfully explains the spectral change during the reaction and the diameter of the resulting particles.

When the steps from dissolution to nucleation are very rapid, the final step, coagulation becomes the most important step, since reactants are converted to a large number of particles very rapidly. This situation is seen in the preparation of metal sulfide and silver halide particles using the solution mixing method, as shown in Chapters II and III. The kinetics of coagulation is controlled by the rate of the intermicellar exchange process at the initial stage (up to about 0.02 s). When the particle diameter achieves a value (around 2.0–4.5 nm), the rate constant starts to decrease with increasing particle diameter. The kinetics of the reduced rate coagulation process becomes first-order with respect to the concentration of micellar droplets containing two or more particles.

In the case of AgBr and AgCl particles, the dissolution of the formed particles into the solution is observed as shown in Chapter III. This is possibly

caused by the formation of water-soluble complex of silver halide and some impurities in AOT. Ostwald ripening is seen in the case of the particles having a relative large solubility (PbS) as shown in Chapter II. This can be restrained by the addition of the excess amount of precursor ions, since excess ions restrict the dissolution of particles.

When H_2S gas has been injected as a reactant to the micellar solution, the dissolution of H_2S into the reverse micellar solution is the rate-determining step for the formation of metal sulfide particles as shown in Chapter IV. In this case, the sum of the rates of subsequent nucleation and particle growth steps becomes identical to the rate of gas absorption and most of the dissolved ion is consumed for particle growth. The particle formed is larger in size than that in the solution mixing method in most cases and the size is controlled by water content over a wider range than that in the solution mixing method. The particle formation process was analyzed using a kinetic scheme based on the first-order kinetics for dissolution of H_2S and on the statistical distribution of species and particles among the micelles. This scheme successfully explains the diameter of particles prepared in the reverse micellar solutions having various water content values and also the diameter of particles prepared with different gas injection rate

The extension of the model to the composite particles was also attempted. The scheme for the single component metal sulfide particles is found to be applicable to the kinetics of the formation process of the coprecipitated particles of CdS and ZnS using the solution mixing method as shown in Chapter V. The composition of the particles is controlled by the ratio of the metallic ions in the feed solution and that of the residual ions in the solution. The concentration of the residual ions in the solution is controlled by the solubility product values of the materials in the form of the ultrafine particles and can be estimated from the absorption intensity of formed particles. On the

other hand, the composition of the particles prepared by the gas injection method is closer to the feed ion ratio in comparison with that by the solution mixing method, since a sufficient amount of H_2S to convert almost all supplied metallic ions has been injected.

Core-shell structure composite particles such as ZnS-coated CdS and CdS-coated ZnS particles were prepared by the growth of shell materials on the core particles by preventing nucleation of new particles and coagulation of the particles as shown in Chapter V. The core-shell structure particles can be prepared in a more convenient way using the gas injection method in comparison with the solution mixing method, since particle growth is the dominating step in the gas injection method whereas particle coagulation is that in the solution mixing method.

Finally, the photocatalytic reduction of water to generate H_2 was investigated as an application of ultrafine particles in Chapter V. The composite particles of CdS and ZnS prepared by the gas injection method have a larger photocatalytic activity than the mixture of single component particles of CdS and ZnS. The activity can be maximized by controlling the composition of the particles via changing band gap energy of the particles. These results agree with the previous reported results obtained with particles prepared by the solution mixing method. H_2 is also produced by the photo-irradiation to the ultrafine PbS particles prepared and stabilized in the reverse micelles by an excess amount of Na_2S. This indicates that the band gap energy of the particles is increased from bulk PbS value (0.41 eV) to a required energy level for the reduction of water by a quantum-size effect.

Suggestions for Future Work

The author has devoted himself and has done his best for five years to complete this thesis work, using all the research facilities available at his department. There have been left incomplete points or disadvantage that must be complemented or reconciled in very near future, as follows:

(1) Study of size distribution of particles

The size of formed particles was assumed to be monodispersed throughout the present work. However, there must exist, more or less, some inevitable distribution in the particle size. The size distribution for the rapid coagulation case has been considered theoretically (Smoluchowski, 1916; Towey *et al.*, 1990). In this case, the distribution is shown to become wider with time. The rate of coagulation is found to start to decrease with increasing diameter at a critical diameter in the present work. This will restrict the extension of the size distribution. When the rate of coagulation between two particles having different size can be estimated, the size distribution will be calculated. If information on the actual size distribution of the particles in the reverse micelles may be obtained, the revised model of particle formation process based on the distributed particle size may be obtained.

(2) Analysis of Ostwald ripening

Ostwald ripening was neglected in the present particle formation model since this was the secondary step in the formation process. However, this occurred in the case of PbS particles. Since this is growth of larger particles accompanied by the dissolution of smaller particles caused by the difference in the solubility, the size distribution and the dependency of the rates of particle growth and dissolution on the particle diameter must be investigated.

In the present work, the rate of the particle growth reaction was assumed to be independent of the particle diameter. A simulation of Ostwald ripening has been reported only for the special case of ideal particle system by Parbhakar *et al.*, (1995).

(3) Isolation and collection of formed particles from reverse micelles

Isolation and collection of the formed particles from reverse micelles are important for the practical use of the particles. One of the approach is surface modification of the particles. Some attempts have been reported using the injection of organic solution of the modifier. (Kortan *et al.*, 1990; Hoener *et al.*, 1992). From the results in Chapter V, the suitable method of the injection for the modifier will be a gas injection. Another approach is the fixation of the ultrafine particles on the surface of other materials. In the case of semiconductor ultrafine particles, insulators and organic materials may be used as a carrier without the diminish in the characteristics of the ultrafine particles. When other semiconductors or metals are used for a carrier, these will affect the characteristics of the semiconductor particles and, as a result, a novel function of such composite material will appear in some cases. For this fixation approach, the developments in the preparation and stabilization of larger particles are also needed.

(4) Change in the reverse micellar system

AOT has been a most commonly used surfactant for the preparation of reverse micellar solutions. However, AOT is an anionic surfactant having Na^+ ion as a countercation. This countercation will often move into the prepared particles. To decrease the amount of impurity in the formed particles, the other surfactants should be used. An approach is the substitution of countercation of AOT. Pileni *et al.* (1993) synthesized the Ag^+, Cd^{2+}, and Cu^{2+} salts of AOT

anion and used for the preparation of ultrafine particles. In the case of metal sulfide particles, H_2S gas is recommended for the S^{2-} source, since Na_2S contains the Na^{2+} ion as a countercation. The other approach is use of nonionic surfactants (Ravet *et al.*, 1987; Boakye *et al.*, 1994). The kinetics of exchange process of reverse micelles depends on both surfactant molecules and the solvent of organic phase. The control of the rate of exchange process leads to the control of size of particles formed by fast formation reactions as shown in Chapter II.

Nomenclature

a	= lattice constant of wurtzite crystal for the a-axis	[m]
c	= lattice constant of wurtzite crystal for the c-axis	[m]
C_f	= molar concentration of total feed amount of metallic ion, $[Cd^{2+}] + [Zn^{2+}]$	[M]
C_h	= molar concentration of hydrolyzed TTB molecules	[M]
C_m	= molar concentration of reverse micellar droplets (number of micellar droplets in the solution expressed in the concentration unit)	[M]
C_M	= molar concentration of metallic ion in the solution	[M]
C_{mc}	= molar concentration of reverse micellar droplets containing two or more particles	[M]
C_{mg}	= molar concentration of reverse micellar droplets containing metallic ion, sulfide ion, and particles	[M]
C_{mn}	= molar concentration of reverse micellar droplets containing metallic ion and sulfide ion	[M]
$C_{m,n}$	= molar concentration of reverse micellar droplets containing n or more hydrolyzed TTB molecules	[M]
C_p	= molar concentration of formed particles	[M]
C_r	= molar concentration of reactants	[M]
C_S	= molar concentration of sulfide ion in the solution	[M]
$C_{S,t}$	= molar concentration of total sulfide ion in the system	[M]
C_{TTB}	= molar concentration of TTB in the solution	[M]
C_{undiss}	= molar concentration of undissolved gas in the system	[M]
d	= density of particles	[g/cm^3]
d_m	= average outer diameter of reverse micelles	[nm]
d_p	= average diameter of particles	[nm]
e	= charge of electron, 1.602×10^{-19} C	
E_g	= direct band gap energy of semiconductor particles	[eV]
E_g'	= indirect absorption threshold energy of semiconductor particles	[eV]

$E_{g,bulk}$	= direct band gap energy of bulk semiconductor	[eV]
$E_{g,'bulk}$	= indirect band gap energy of bulk semiconductor	[eV]
h	= Planck constant, 6.626×10^{-34} J·s	
k_c	= second-order rate constant of coagulation process	$[M^{-1}\cdot s^{-1}]$
k_{diss}	= first-order rate constant of dissolution	$[s^{-1}]$
k_{ex}	= second-order rate constant of intermicellar exchange process of reverse micelles	$[M^{-1}\cdot s^{-1}]$
k_G	= first-order rate constant of particle growth in micelles containing a hydrolyzed TTB molecule and a particle	$[s^{-1}]$
k_H	= first-order rate constant of hydrolysis of TTB	$[s^{-1}]$
k_{mc}	= first-order rate constant of coagulation process in micelles containing two or more particles	$[s^{-1}]$
k_{mg}	= first-order rate constant of particle growth in micelles containing metallic ion, sulfide ion, and particles	$[s^{-1}]$
k_{mn}	= first-order rate constant of nucleation in micelles containing metallic ion and sulfide ion	$[s^{-1}]$
k_N	= first-order rate constant of nucleation in micelles containing a sufficient number of hydrolyzed TTB molecules	$[s^{-1}]$
k_r	= first-order rate constant of reaction	$[s^{-1}]$
K_{sp}	= solubility product	[−]
m^*	= reduced effective mass of electron and hole in semiconductor, $(1/m_e + 1/m_h)^{-1}$	[kg]
m_0	= free electron mass, 9.11×10^{-31} kg	
m_e	= effective mass of electron in semiconductor	[kg]
m_h	= effective mass of hole in semiconductor	[kg]
n	= number of precursor molecules to form a stable nuclei	[−]
N_m	= number of micelles in solution	[−]
N_p	= number of particles in solution	[−]
p_i	= probability to have i molecules in a reverse micelle	[−]
r_c	= rate of coagulation	[M/s]
r_{diss}	= rate of dissolution of hydrogen sulfide	[M/s]

r_g	= rate of particle growth	[M/s]
r_{inj}	= rate of injection of hydrogen sulfide	[M/s]
r_n	= rate of nucleation	[M/s]
r_r	= rates of reaction	[M/s]
s	= solubility of material	[g/l]
t	= time after the initiation of reaction	[s]
$t_{1/2}$	= half period of the first-order reaction	[s]
W_o	= $[H_2O]/[AOT]$	[–]
x	= molar fraction of zinc in all the metallic ions in the particles	[–]
x_{cal}	= calculated molar fraction of zinc in all the metallic ions in the particles	[–]
x_f	= molar fraction of zinc in all the metallic ions in the feed solution, $[Zn^{2+}] / ([Cd^{2+}] + [Zn^{2+}])$	[–]
X_p	= conversion of precursor species to particles	[–]
y	= molar ratio of sulfide ion to all the metallic ions in the feed solution, $[S^{2-}] / ([Cd^{2+}] + [Zn^{2+}])$	[–]
ε	= dielectric constant of semiconductor	$[C^2 \cdot J^{-1} \cdot m^{-1}]$
ε_0	= dielectric constant of vacuum	$[C^2 \cdot J^{-1} \cdot m^{-1}]$
λ	= average number of molecules per reverse micelle	[–]
ν	= frequency of absorbed light	[Hz]
σ	= absorption coefficient	$[M^{-1} \cdot cm^{-1}]$
σ_m	= standard deviation of size distribution of reverse micelles	[–]
[ ]	= molar concentration of species in the brackets	[M]

<subscript>

bulk	= bulk materials
CdS	= CdS
ZnS	= ZnS

References

Arriagada, F. J. and Osseo-Asare, K.; "Phase and Dispersion Stability Effects in the Synthesis of Silica Nanoparticles in a Non-ionic Reverse Microemulsion," *Colloid. Surf.*, **69**, 105-115 (1992)

Atik, S. S. and Thomas, J. K.; "Transport of Photoproduced Ions in Water in Oil Microemulsions: Movement of Ions from One Water Pool to Another," *J. Am. Chem. Soc.*, **103**(12), 3543-3550 (1981)

Aveyard, R., Binks, B. P., Clark, S., and Mead, J.; "Interfacial Tension Minima in Oil-Water-Surfactant Systems," *J. Chem. Soc., Faraday Trans. 1*, **82**(1), 125-142 (1986)

Barnickel, P., Wokaun, A., Sager, W., and Eicke, H.-F.; "Size Tailoring of Silver Colloids by Reduction in W/O Microemulsions," *J. Colloid Interface Sci.*, **148**(1), 80-90 (1992)

Berry, C. R.; "Structure and Optical Absorption of AgI Microcrystals," *Phys. Rev.*, **161**, 848-851 (1967)

Bhargava, R. N., Gallagher, D., Hong, X., and Nurmikko, A.; "Optical Properties of Manganese-Doped Nanocrystals of ZnS," *Phys. Rev. Lett.*, **72**(3), 416-419 (1994)

Boakye, E., Radovic, L. R., and Osseo-Asare, K.; "Microemulsion-Mediated Synthesis of Nanosize Molybdenum Sulfide Particles," *J. Colloid Interface Sci.*, **163**(1), 120-129 (1994)

Brus, L. E.; "Electron-electron and Electron-hole Interactions in Small Semiconductor Crystallite: The Size Dependence of the Lowest Excited Electronic State," *J. Chem. Phys.*, **80**(9), 4403-4409 (1984)

Chew, C. H., Gan, L. M., and Shah, D. O.; "The Effect of Alkanes on the Formation of Ultrafine Silver Bromide Particles in Ionic W/O Microemulsions," *J. Dispersion Sci. Technol.*, **11**, 593-609 (1990)

Cizeron, J. and Pileni M. P.; "Solid Solution of $Cd_yZn_{1-y}S$ Nanosize Particles Made in Reverse Micelles," *J. Phys. Chem.*, **99**(48), 17410-17416 (1995)

Dunn, C. M. and Robinson, B. H.; "Photon-correlation Spectroscopy Applied to the Size Characterization of Water-in-oil Microemulsion Systems Stabilized by Aerosol-OT; Effect of Change in Counterion," *Spectrochim. Acta*, **46A**(6), 1017–1025 (1990)

Everett, D. H.; *Basic Principles of Colloid Science*, The Royal Society of Chemistry, London (1988)

Fletcher, P. D. I., Howe, A. M., and Robinson, B. H.; "The Kinetics of Solubilisate Exchange between Water Droplets of a Water-in-oil Microemulsion," *J. Chem. Soc., Faraday Trans. 1*, **83**, 985–1006 (1987)

Gopidas, K. R., Bohorquez, M., and Kamat, P. V.; "Photophysical and Photochemical Aspects of Coupled Semiconductors. Charge-Transfer Processes in Colloidal CdS–TiO_2 and CdS–AgI Systems," *J. Phys. Chem.*, **94**(16), 6435–6440 (1990)

Harris, M. T. and Byers, C. H.; "Effect of Solvent on the Homogeneous Precipitation of Titania by Titanium Ethoxide Hydrolysis," *J. Non-Crystal. Solid.*, **103**, 49–64 (1988)

Hasselbarth, A., Eychmuller, A., Eichberger, R., Giersig, M., Mews, A., and Weller, H.; "Chemistry and Photophysics of Mixed CdS/HgS Colloids," *J. Phys. Chem.*, **97**(20), 5333–5340 (1993)

Henglein, A., Gutiérrez, M., Weller, H., Fojtik, A., and Jirkovský J.; "Photochemistry of Colloidal Semiconductors 30. Reactions and Fluorescence of AgI and AgI–Ag_2S Colloids," *Ber. Bunsenges. Phys. Chem.*, **93**, 593–599 (1989)

Hirai, T., Imamura, E., Matsumoto, T., Kuboi, R., and Komasawa, I.; "Preparation of Metal Oxide Ultrafine Particles by Hydrolysis of Metal Alkoxide in Reverse Micelles (in Japanese)," *Kagaku Kogaku Ronbunshu*, **18**(3), 296–302 (1992)

Hirai, T., Shiojiri, S., and Komasawa, I.; "Preparation of Metal Sulfide Composite Ultrafine Particles in Reverse Micellar Systems and Their Photocatalytic Property," *J. Chem. Eng. Japan*, **27**(5), 589–596 (1994)

Hoener, C. F., Allan, K. A., Bard, A. J., Campion, A., Fox, M. A., Mallouk, T. E., Webber, S. E., and White, J. M.; "Demonstration of a Shell-Core Structure in Layered CdSe-ZnSe Small Particles by X-ray Photoelectron and Auger Spectroscopies," *J. Phys. Chem.*, **96**(9), 3812-3817 (1992)

Ikemoto, T., Uematsu, K., Mizutani, N., and Kato, M.; "Synthesis of Monodispersed Titania Fine Particles by Hydrolysis of Titanium Tetraethoxide (in Japanese)," *Yogyo-kyoukai-shi*, **93**, 261-266 (1985)

Jain, T. K., Billoudet, F., Motte, L., Lisiecki, I., and Pileni, M. P.; "Photochemical Studies of Nanosized CdS Particles Synthesized in Micellar Media," *Prog. Colloid Polym. Sci.*, **89**, 106-109 (1992)

Johansson, K. P., Marchetti, A. P., and McLendon, G. L.; "Effect of Size Restriction on the Static and Dynamic Emission Behavior of Silver Bromide," *J. Phys. Chem.*, **96**, 2873-2879 (1992)

Kakuta, N., Park, K. H., Finlayson, M. F., Ueno, A., Bard, A. J., Campion, A., Fox, M. A., Webber, S. E., and White, J. M.; "Photoassisted Hydrogen Production Using Visible Light and Coprecipitated ZnS-CdS without a Noble Metal," *J. Phys. Chem.*, **89**, 732-734 (1985)

Kandori, K., Kon-no, K. and Kitahara, A.; "Formation of Ionic Water/oil Microemulsions and Their Application in the Preparation of Calcium Carbonate Particles," *J. Colloid Interface Sci.*, **122**, 78-82 (1988)

Kishida, M., Fujita, T., Umakoshi, K., Ishiyama, J., Nagata, H., and Wakabayashi, K.; "Novel Preparation of Metal-supported Catalysts by Colloidal Microparticles in a Water-in-oil Microemulsion; Catalytic Hydrogenation of Carbon Dioxide," *J. Chem. Soc., Chem. Commun.*, 763-764 (1995)

Kortan, A. R., Hull, R., Opila, R. L., Bawendi, M. G., Steigerwald, M. L., Carroll, P. J., and Brus, L. E.; "Nucleation and Growth of CdSe on ZnS Quantum Crystallite Seeds, and Vice Versa, in Inverse Micelle Media," *J. Am. Chem. Soc.*, **112**(4), 1327-1332 (1990)

Kuboi, R., Mori, Y., and Komasawa, I.; "Reverse Micelle Size Distribution and Mechanism of Protein Solubilization into Reverse Micelles (in Japanese)," *Kagaku Kogaku Ronbunshu*, **16**(4), 763-771 (1990)

Kurihara, K., Kizling, J., Stenius, P., and Fendler, J. H.; "Laser and Pulse Radiolytically Induced Colloidal Gold Formation in Water and in Water-in-Oil Microemulsions," *J. Am. Chem. Soc.*, **105**(9), 2574-2579 (1983)

LaMer, V. K.; "Nucleation in Phase Transitions," *Ind. Eng. Chem.*, **44**(6), 1270-1277 (1952)

Lang, J., Jada, A., and Malliaris, A.; "Structure and Dynamics of Water-in-Oil Droplets Stabilized by Sodium Bis(2-ethylhexyl) Sulfosuccinate," *J. Phys. Chem.*, **92**(7), 1946-1953 (1988)

Lianos, P. and Thomas, J. K.; "Small CdS Particles in Inverted Micelles," *J. Colloid Interface Sci.*, **117**(2), 505-512 (1987)

Lisiecki, I., and Pileni, M. P.; "Synthesis of Copper Metallic Clusters Using Reverse Micelles as Microreactors," *J. Am. Chem. Soc.*, **115**(10), 3887-3896 (1993)

Meyer, M., Wallsberg, C., Kurihara, K., and Fendler, J. H.; "Photosensitized Charge Separation and Hydrogen Production in Reversed Micelle Entrapped Platinized Cadmium Sulphide," *J. Chem. Soc., Chem. Commun.*, 90-91 (1984)

McCartney, L. N. and Levine, S.; "An Improvement Derjaguin's Expression at Small Potentials for the Double Layer Interaction Energy of Two Spherical Colloidal Particles," *J. Colloid Interface Sci.*, **30**, 345-354 (1969)

Mizutani, N.; "Preparation of Monodispersed Fine Particles by Hydrolysis of Metal Alkoxides," *Funtai-Kogaku-Kaishi*, **26**, 183-188 (1989)

Motte, L., Petit, C., Boulanger, L., Lixon, P., and Pileni, M. P.; "Synthesis of Cadmium Sulfide in Situ in Cadmium Bis(ethyl-2-hexyl) Sulfosuccinate Reverse Micelle: Polydispersity and Photochemical Reaction," *Langmuir*, **8**(4), 1049-1053 (1992)

Nedeljković, J., Patel, R. C., and Hill, S.; "Formation of Silver Bromide in the Presence of Excess Bromide Studied by Wavelength-Dependent Light Scattering," *J. Imaging Sci.*, **35**, 75-79 (1991)

Nielsen, A. E.; *Kinetics of Precipitation*, Pergamon Press, London, 1964.

Nojik, A. J., Williams, F., Nenadović, M. T., Rajh, T., and Mićić, O. I.; "Size Quantization in Small Semiconductor Particles," *J. Phys. Chem.*, 397-399 (1985)

Ogihara, T., Ikeda, M., Kato, M., and Mizutani, N.; "Continuous Processing of Monodispersed Titania Powders," *J. Am. Ceram. Soc.*, **72**(9), 1598-1601 (1989)

Osseo-Asare, K. and Arriagada, F. J.; "Synthesis of Nanosize Particles in Reverse Microemulsions," *Ceram. Trans.*, **12**, 3-16 (1990)

Parbhakar, K., Lewandowski, J., and Dao, L. H.; "Simulation Model for Ostwald Ripening in Liquids," *J. Colloid Interface Sci.*, **174**(1), 142-147 (1995)

Petit, C., Lixon, P., and Pileni, M. P.; "In Situ Synthesis of Silver Nanocluster in AOT Reverse Micelles," *J. Phys. Chem.*, **97**(49), 12974-12983 (1993)

Pileni, M. P.; "Reverse Micelles as Microreactors," *J. Phys. Chem.*, **97**(27), 6961-6973 (1993)

Ravet, I., Nagy, J. B., and Derouane, E. G.; "On the Mechanism of Formation of Colloidal Monodisperse Metal Boride Particles from Reversed Micelles Composed of CTAB-1-Hexanol-Water," *Stud. Surf. Sci. Catal.*, **31**, 505-516 (1987)

Ravich, Yu. I., Efimova, B. A., and Smirnov I. A.; Semiconducting Lead Chalcogenides, p.52-53, Plenum Press, New York (1970)

Rosseti, R., Hull, R., Gibson, J. M., and Brus, L. E.; "Hybrid Electronic Properties between the Molecular and Solid State Limits: Lead Sulfide and Silver Halide Crystallites," *J. Chem. Phys.*, **83**, 1406-1410 (1985)

Saijo, H., Iwasaki, M., Tanaka, T., and Matsubara, T.; "Electron Microscopic Study of the Growth of Sub-Microcrystals in Nascent Silver Iodide and Silver Bromoiodide Hydrosols," *Photogr. Sci. Eng.*, **26**, 92-97 (1982)

Sakaguchi, M., Ohta, M., Satoh, M., and Hirabayashi, T.; "The Phase Transformation during Crystallization of ZnS," *J. Electrochem. Soc.*, **124**(4), 550-553 (1977)

Smoluchowski, M.; "Three Lectures on Diffusion, Brownian Movement and Coagulation of Colloidal Particles (in German)," *Phys. Z.*, **17**(23), 585–599 (1916)

Sofen, S. R. and Norland, K. S.; "Stopped-Flow Turbidimetry for the Characterization of Silver Halide Emulsion Dissolution," *J. Imaging Sci.*, **30**, 243–246 (1986)

Steigerwald, M. L., Alivisatos, A. P., Gibson, J. M., Kortan, R., Muller, A. J., Thayer, A. M., Duncan, T. M., Douglass, D. C., and Brus, L. E.; "Surface Derivatization and Isolation of Semiconductor Cluster Molecules," *J. Am. Chem. Soc.*, **110**(10), 3046–3050 (1988)

Suslina, L. G., Panasyuk, E. I., Konnikov, S. G., and Federov, D. L.; "Exciton Spectra and Band Structure of Zinc Cadmium Sulfide ($Zn_xCd_{1-x}S$) Mixed Crystals. (in Russian)," *Fiz. Tekh. Poluprovodn.*, **10**(10), 1830–1838 (1976)

Tanaka, T. and Iwasaki, M.; "The Multistage Process of Formation of Ultrafine Silver Bromide Particles As Revealed by Multichannel Spectrophotometry," *J. Imaging Sci.*, **29**, 86–92 (1985)

Towey, T. F., Khan-Lodhi, A., and Robinson, B. H.; "Kinetics and Mechanism of Formation of Quantum-sized Cadmium Sulphide Particles in Water–Aerosol-OT–Oil Microemulsions," *J. Chem. Soc., Faraday Trans.*, **86**, 3757–3762 (1990)

Ueno, A., Kakuta, N., Park, K. H., Finlayson, M. F., Bard, A. J., Campion, A., Fox, M. A., Webber, S. E., and White, J. M.; "Silica–Supported ZnS–CdS Mixed Catalysts for Photogenaration of Hydrogen," *J. Phys. Chem.*, **89**(18), 3828–3833 (1985)

Verbeeck, A. and DeSchryver, F. C.; "Fluorescence Quenching in Inverse Micellar Systems: Possibilities and Limitations," *Langmuir*, **3**(4), 494–500 (1987)

von der Osten, W.; "I–VII Compounds" in Landolt–Börnstein, Numerical Data and Functional Relationships in Science and Technology New Series III 17b Semiconductors O. Madelung ed., p. 275–302, Splinger, Berlin (1982)

Wang, Y., Suna, A., Mahler, W., and Kasowski, R.; "PbS in Polymers. From Molecules to Bulk Solids," *J. Chem. Phys.*, **87**(12), 7315-7322 (1987)

Weller, H., Schmidt, H. M, Koch, U., Fojtik, A., Baral, S., Henglein, A., Kunath, W., Weiss, K., and Dieman, E.; "Photochemistry of Colloidal Semiconductors. Onset of Light Absorption As a Function of Size of Extremely Small CdS Particles," *Chem. Phys. Lett.*, **124**(6), 557-560 (1986)

Williams, E. F., Woodberry N. T., and Dixon J. K.; "Purification and Surface Tension Properties of Alkyl Sodium Sulfosuccinates," *J. Colloid Sci.*, **12**, 452-459 (1957)

Yamauchi, H., Ishikawa, T., Kondo, S.; "Surface Characterization of Ultramicro Spherical Particles of Silica Prepared by W/O Microemulsion Method," *Colloid Surf.*, **37**, 71-80 (1989)

Youn, H.-C., Baral, S., and Fendler, J. H.; "Dihexadecyl Phosphate, Vesicle-Stabilized and In Situ Generated Mixed CdS and ZnS Semiconductor Particles. Preparation and Utilization for Photosensitized Charge Separation and Hydrogen Generation," *J. Phys. Chem.*, **92**(22), 6320-6327 (1988)

Zulauf, M. and Eicke, H.-F.; "Inverted Micelles and Microemulsions in the Ternary System H_2O/Aerosol-OT/Isooctane as Studied by Photon Correlation Spectroscopy," *J. Phys. Chem.*, **83**(4), 480-485 (1979)

List of Publications

1. **Hirai, T., Sato, H., and Komasawa, I.**; "Mechanism of Formation of Titanium Dioxide Ultrafine Particles in Reverse Micelles," *Ind. Eng. Chem. Res.*, **32**(12), 3014-3019 (1993)
2. **Hirai, T., Sato, H., and Komasawa, I.**; "Mechanism of Formation of CdS and ZnS Ultrafine Particles in Reverse Micelles," *Ind. Eng. Chem. Res.*, **33**(12), 3262-3266 (1994)
3. **Sato, H., Hirai, T., and Komasawa, I.**; "Mechanism of Formation of Composite CdS-ZnS Ultrafine Particles in Reverse Micelles," *Ind. Eng. Chem. Res.*, **34**(7), 2493-2498 (1995)
4. **Hirai, T., Tsubaki, Y., Sato, H., and Komasawa, I.**; "Mechanism of Formation of Lead Sulfide Ultrafine Particles in Reverse Micellar Systems," *J. Chem. Eng. Japan*, **28**(4), 468-473 (1995)
5. **Sato, H., Hirai, T., and Komasawa, I.**; "Mechanism of Formation of Silver Halide Ultrafine Particles in Reverse Micellar Systems," *J. Chem. Eng. Japan*, **29**(3), - (1996)
6. **Sato, H., Tsubaki, Y., Hirai, T., and Komasawa, I.**; "Mechanism of Formation of Metal Sulfide Ultrafine Particles in Reverse Micelles Using a Gas Injection Method," submitted for publication

Acknowledgment

The author is greatly indebted to Professor Isao Komasawa and Associate Professor Takayuki Hirai (Dept. of Chemical Engineering, Faculty of Engineering Science, Osaka University) for their constant guidance and helpful advice throughout this work. The author is sincerely grateful to Professors Yushi Hirata, Tomoshige Nitta, Korekazu Ueyama, (Faculty of Engineering Science, Osaka University) and Hiroshi Yoneyama (Faculty of Engineering, Osaka University) for a number of valuable comments and criticisms during the completion of this thesis.

The author would like to thank Associate Professor Tadashi Okuyama and Dr. Kunihisa Yoshida for the measurement of absorption spectra using the stopped-flow equipment.

The author is also thankful to the following foreign staff for their valuable discussions and suggestions during their stay at the Department, Professors Marie P. Pileni (Universite P. et M. Curie, France) and Brian H. Robinson (University of East Anglia, U. K.). The author wishes to thank Professor Ryoichi Kuboi and Dr. Izumi Tsuboi for their kind encouragement and also other members at the same laboratory for their friendship. Special thanks are given to following colleagues for their cooperation: Messrs. Takayoshi Matsumoto, Susumu Shiojiri, Yoritaka Tsubaki, Hidekazu Fujimoto, and Jun-ya Mizumoto.

The author gratefully acknowledges the financial support of this work from the Research Fellowships of the Japan Society for the Promotion of Science for Young Scientists.